VISVESVARAYA TECHNOLOGICAL UNIVERSITY
JNANA SANGAMA, BELAGAVI – 590 014

Thesis On

Analysis of Retinopathy Images to Detect the effect of Diabetes on Eye

Submitted in Partial Fulfillment of the Requirements of the award of the Degree of

Doctor of Philosophy in
Computer Science and Engineering

Submitted by

Mr. Ambaji S.Jadhav
USN: 2BL15PEJ01

Under the Guidance/Supervision of

Dr. Pushpa B. Patil

Professor, Department of Computer Science and Engineering

Research Centre

Department of Computer Science and Engineering,
B. L. D. E. A's Vachana Pitamaha Dr. P. G. Halakatti College of
Engineering and Technology,
Vijayapur-586 103, Karnataka, India.

DECLARATION

This is to declare that the thesis work entitled "**Analysis of Retinopathy Images to Detect the effect of Diabetes on Eye"** is carried out by me, **Mr. Ambaji S.Jadhav**, **USN: 2BL15PEJ01** a bonafide student of the Research Centre, Department of Computer Science and Engineering, **B.L.D.E.A's V. P. Dr. P. G. Halakatti College of Engineering & Technology, Vijayapur, Karnataka, India** in partial fulfillment for the award of **DOCTOR OF PHILOSOPHY** in **Computer Science and Engineering** of **Visvesvaraya Technological University, Belagavi**, during the year **2015-21**. To the best of my knowledge and belief, the work reported in the thesis has not been submitted by me for the award of the any degree and is not the repetition of the work carried out by others.

Place: Vijayapur

Date: 14/7/2021

Mr. AMBAJI S.JADHAV

Research Scholar

Department of Computer Science and Engineering,

B.L.D.E.A's V.P. Dr. P. G. Halakatti College of

Engineering & Technology, Vijayapur, Karnataka,

India

Vachana Pitamaha Dr. P. G. Halakatti College of Engineering and Technology, Vijayapur-586 103, Karnataka, India.

Certificate

This is to certify that the thesis work entitled "**Analysis of Retinopathy Images to Detect the effect of Diabetes on Eye**" carried out by, **Mr. Ambaji S. Jadhav** (**USN: 2BL15PEJ01**) a bonafide student of Research Centre, Department of Computer Science and Engineering, **B.L.D.E.A's V. P. Dr.P. G. Halakatti College of Engineering & Technology, Vijayapur, Karnataka, India** in partial fulfillment for the award of **DOCTOR OF PHILOSOPHY** in **Computer Science and Engineering** of the **Visvesvaraya Technological University, Belagavi, during the year 2015-21.** To the best of my knowledge, the work reported in the thesis has not been submitted for the award of any degree or diploma and is not the repetition of the work carried out by others. In my opinion, this thesis is of the standard required for the award of the degree of Ph.D.

Research Guide/Supervisor

Professor Department of Computer Science and Engineering, B.L.D.E.A's V.P. Dr. P. G. Halakatti College of Engineering & Technology, Vijayapur, Karnataka, India

Forwarded by:

Dr.Pushpa B. Patil

Principal,
B.L.D.E.A's. V.P. Dr. P.G.H
College of Engg. & Tech.
VIJAYAPUR-586103.

ACKNOWLEDGEMENTS

Since it is not possible to bring in all the names, though I wish to do so, I place on record my sincere gratitude to each one of them who helped directly or indirectly in completing this thesis work.

<div align="right">Mr. Ambaji S. Jadhav</div>

ABSTRACT

Diabetic Retinopathy (DR) is one of the most occurred diabetic eye diseases that cause serious complication to the eye even to vision loss. The risk of this problem can be completely prevented by means of two fundamental public health interventions such as early diagnosis and treatment. However, the effective screening and diagnosing the DR from the retinal fundus images is a major challenge. In this scenario, the experts and other professional diagnosis teams depend on analyzing the retinal fundus images using the Computer-Aided Diagnosis (CAD) system. The general processing stages of CAD system involves pre-processing, segmentation and classification pertaining to retinal blood vessels or other abnormalities. Various machine learning methods have been developed. Further the recent contribution of deep learning models and its successful performance over the conventional techniques under medical applications have been motivated the researchers for adopting the deep learning models to diagnose the DR. This research work focuses to analyze the retinal fundus images for the effective diagnosis of DR using intelligent techniques. It performs the DR detection in different phases. In the first phase the blood vessel analysis is performed by, image enhancement, filtering and morphological operation. In the filtering, Peak Signal-to-Noise Ratio (PSNR) and Mean Squared Error (MSE) computation is performed on for DRIVE database. Blood vessels are segmented using morphology operation. Feature extraction by DWT and Gray-Level Co-Occurrence Matrix (GLCM) is done and classification by Support Vector Machine (SVM) and distance measures like city block, Spearman, and Minkowski are employed for CHASE_DBI and DRIVE databases. In the second phase, the examination of optic disc, exudates and blood vessels is done. Here, wavelet transform is used for detecting the optic disc using DIARETDB1 dataset, whereas morphological operation, grey level thresholding and Discrete Wavelet Transform (DWT) is used for detecting the exudates and classify the image into normal and abnormal. The third phase of the research work segments and analyses the blood vessels for detecting DR. Initially, the combination of Contrast Limited Adaptive Histogram Equalization (CLAHE) and average filter performs the pre-processing. Further, the optimized Gray level thresholding is used for the blood vessel segmentation and feature extraction techniques like Texture energy Measurement (TEM), Local Binary Pattern (LBP), Shanon's entropy and Kapur's entropy are utilized. The classification of the image is performed by the optimal

trained Neural Network (NN). The developed new algorithm termed as Modified Levy Updated-Dragonfly Algorithm (MLU-DA) enhances the performance of both segmentation and classification to classify the image as normal and abnormal using the High Resolution Fundus (HRF) images. The fourth phase of this research work diagnoses the DR from the retinal fundus images by segmenting and analyzing the retinal abnormalities like haemorrhages, Microaneurysm, soft exudates and hard exudates. After enhancing the contrast of the image by CLAHE, open-close watershed transformation helps to remove the optic disc and Grey Level thresholding helps to remove the blood vessels. Further, the utilization of Top hat transformation followed by Gabor filtering segments the retinal abnormalities. From the segmented abnormalities, LBP, TEM, Shanon's, and Kapur's entropy are extracted as features and carried out the optimal feature selection by proposed Modified Gear and Steering-based Rider Optimization Algorithm (MGS-ROA). Further, the optimized Deep Belief Network (DBN) classifies the image into normal, severe, moderate, and earlier stages of DR, in which MGS-ROA updates the DBN weight. The experiment is carried out for DIARETDB1image datasets. The final contribution of this research work focuses on analyzing the optic disc, blood vessels and retinal abnormalities for diagnosing DR using DIARETDB1 image datasets The open-close watershed transform segments the optic disc, Grey level thresholding segments the blood vessels and top hat transform followed by Gabor filtering segments the abnormalities like haemorrhages, Microaneurysm, soft exudates and hard exudates. Here also, features like LBP, TEM, Shanon's, and Kapur's entropy are extracted from the segmented optic disc, blood vessels, and abnormalities and the proposed Trial-based Bypass Improved Dragonfly Algorithm (TB-DA) is used to carry out the optimal feature selection process The classification of images is done by the hybridization of DBN and NN, in which the TB-DA optimizes weight function of both classifies.

CONTENTS

List of Figures

LIST OF TABLES

List of Abbreviations and symbols

Abbreviation/ Symbol	Description
DR	Diabetic Retinopathy
BDR	Back Ground Diabetic Retinopathy
PDR	Proliferative Diabetic Retinopathy
SDR	Severe Diabetic Retinopathy
CAD	Computer-Aided Diagnosis
DWT	Discrete Wavelet Transform
TEM	Texture Energy Measurement
LBP	Local Binary Pattern
GLCM	Gray Level Co-occurrence Matrix
ONH	Optical Nerve Head
SVM	Support Vector Machine
CLAHE	Contrast Limited Adaptive Histogram Equalization
NN	Neural Network
MLU-DA	Modified Levy Updated-Dragonfly Algorithm
ROA	Rider Optimization Algorithm
MGS-ROA	Modified Gear and Steering-based ROA
DBN	Deep Belief Network
TB-DA	Trial-based Bypass Improved Dragonfly Algorithm
PSNR	Peak Signal to Noise Ratio
MSE	Mean Square Error
SASG	Single Annotations by Single Grader
SAMG	Single Annotations from Multiple Graders
MAV	Multiple Annotations by Voting
DAAD	Double Annotations with Adjudication of Disagreement
PCA	Principal Component Analysis
ROC	Retinopathy Online Challenges
CLEAR-DR	Class-Enhanced Attentive Response Discovery Radiomics
AM-FM	Amplitude Modulation-Frequency Modulation

MIL	Multiple Instance Learning
CNN	Convolutional Neural Network
FOV	Field of View
CCD	Charge Coupled Device
FPR	False Positive Rate
FNR	False Negative Rate
FDR	False Discovery Rate
NPV	Negative Predictive Value
MCC	Mathews Correlation Coefficient
MF	Multi-deviation Fusion
FBG	Fiber Bragg Grating
FCM	Fuzzy-C Means
ANN	Artificial Neural Network
BPNN	Back Propagation Neural Network
ROI	Region of Interest
RBF-NN	Radial Basis Function- Neural Network
LM	Levenberge-Marquardt
LM-NN	Levenberge-Marquardt based Neural Network
DA	Dragonfly Algorithm
WOA	Whale Optimization Algorithm
GWO	Grey Wolf Optimization
PSO	Particle Swarm Optimization
T-PSO	Texture feature based- Particle Swarm Optimization
T-GWO	Texture feature based- Grey Wolf Optimization
T-WOA	Texture feature based- Grey Wolf Optimization
MLUDA-NN	Modified Levy Updated-Dragonfly Algorithm using NN
T-MLUDA-NN	Texture feature based-MLUDA-NN
T-PSO-NN	Texture feature based- Particle Swarm Optimization using NN
T-DA-NN	Texture feature based-Dragonfly Algorithm using NN
T-GWO-NN	Texture feature based- Grey Wolf Optimization using NN
T-LM-NN	Texture feature based- Levenberge-Marquardt- Neural Network
E-MLUDA-NN	Entropy feature based-MLUDA-NN
E-GWO-NN	Entropy feature based- Grey Wolf Optimization using NN
E-LM-NN	Entropy feature based- Levenberge-Marquardt- Neural Network

E-DA-NN	Entropy feature based-Dragonfly Algorithm using NN
BN	Batch Normalization
DNNs	Deep Neural Networks
ELM	Extreme Learning Machine
SKIZ	Skeleton of Influence Zones
OCT	Optical Coherence Tomography
DCNN	Deep Convolutional Neural Network
HCF	Highest Common Factor
GLSZM	Gray Level Size Zone Matrix
MLP-NN	Multi Layer Perceptron -NN
CA	Approximated coefficients
NB	Naïve Bayes
GP	Genetic programming
FP-CSO	Frequent Pattern-Cat Swarm Optimization Algorithm
LFM	Linear Frequency Modulation
CH	Horizontal coefficients
CV	Vertical coefficients
CD	Diagonal coefficients
LTE	Laws Texture Energy
KNN	K-Nearest Neighbors
RBM	Restricted Boltzmann Machine
CD	Contrastive Divergence
CPD	Cumulative Probability Distribution
SIFT	Scale Invariant Feature Transform
HOG	Histogram of Oriented Gradients
M, N	Number of rows and columns of input image respectively
U, V	Number of rows and columns in windows
μI	Mean value of intensity
WIN	Segmented window
SD	Standard deviation
EN	Energy
C	Image used for Dilation
D	Structuring element used
D$_z$	Translation of structuring element
h	Response of matched filter
S	Desired signal
S^H	Conjugate transpose of desired signal
R_v^{-1}	Inverse covariance matrix of the noise

$W_\emptyset(j_0,k)$	Approximation coefficient of DWT
$W_\emptyset(j,k)$	Detailed coefficient of DWT
NG	Number of gray levels.
X,Y	DRIVE database image groups
T^P	True positive
T^N	True negative
F^P	False positive
F^N	False negative
FE_{fea}	Features
nf	Number of features
EF	Error function
Acc	Accuracy
Ne_{dr}	Dragonfly neighbors
Lo	Location of present dragonfly
CN	Count of neighboring dragonfly
Lo_{ni}	Location of ni[th] neighboring dragonfly
$Align_{dr}$	Alignment of dragonfly
Ve_{ni}	Velocity of ni[th] neighboring dragonfly
CC_{dr}	Control cohesion of dragonfly
X_{ni}	ni[th] dragonfly
FL	Location of source of food
DE_{dr}	Distraction towards enemy
E_n	Position of enemy
ΔLo	Step vector
ΔLo_{itr+1}	Movement of dragonfly
ne	Separation of weight of dr[th] dragonfly
Ne_{dr}	Separation of dr[th] dragonfly
$align$	Alignment weight of dr[th] dragonfly
$Align_{dr}$	Alignment of dr[th] dragonfly
af	Food factor of dr[th] dragonfly
AF_{dr}	Food source of dr[th] dragonfly
cc	Weight of cohesion of the dr[th] dragonfly
de	Enemy factor of the dr[th] dragonfly
DE_{dr}	Location of enemy of the dr[th] dragonfly
$\delta 0$	Weight of inertia
Lo_{itr+1}	Updated position of dragonfly
Lo_{itr}	Present position of dragonfly
Pv	Position vector

$, r_2$	Random numbers in the interval [0,1]
ε	Constant
wf	Weight function
Pv_{max}	Maximum pixel value
Pv_{min}	Minimum pixel value
α	Clip parameter
$CPD(bv)$	Cumulative probability distribution
bv	Brightness value
LoT	Level of threshold
UM	Uniformity measure
HG_{im}	Labeled image histogram
nl	Number of labels
$LBP_{PB,RB}$	PB-bit binary number
$, ro_{PB-1}$	Quantized values of PB points
PB	Number of bits in patterns
gr_{CP}	Gray value of center pixel
gr_{CV}	Gray value of PB points
$W5$	Mask for wave detection
$E5$	Mask for edge detection
$S5$	Mask for spot detection
$R5$	Mask for ripple detection
$L5$	Mask for level detection
$p1 \ \& \ q1$	constants
IT	Invariant TEM
Ent_{di}	Normalized histogram
Gv_{di}	Different gray level values
$me \times ne$	Size of ROI
Sha	Scatter density
$Ka_{\beta,\delta}$	Kapur's entropy
β, δ	Coefficients of Kapur's entropy
Acf	Activation function
B_z	Optimal weight
ED	Error difference
ON_{on}	Actual outcome
$Wtr_{Shd}(f)$	Watershed line function
$SP(f)$	Support function
rgm_t	Regional minima
$cbs(rgmt)$	Catchment basin with regional minima
$gds_{hr}(i, gr_t)$	Geodesic distance from point I to group gr

hr	Some pixel points that don't contribute to any influence zone
gr	Group of points
$tdz_{hr}(gr_t)$	SKIZ of gr and hr
$SKIZ_{HR}(gr)$	Points those do not belong to any influence zone
r	Constant in the range [0, 1]
$DZ_{hr}(gr)$	Geodesic distance from hr to gr
σ_u, σ_v	Fixed Gaussian distance along u, v
u_θ , v_θ	Orientation along u,v
θ	Orientation angle
LR_{ts+1}^{BPR}	Location of bypass rider
LR_{ts}	Position of leading rider at time step ts
$\eta \ and \ \xi$	Random values for rider that lies between 0 and rn
$\delta r \ and \beta r$	Random values associated with riders
p , q	Two different riders
cn	Count of coordinates of riders
csl	Coordinate selector
$STR_{p,cs}^{ts}$	Pth rider's steering angle in Csth coordinator
$dstr_P^{ts}$	Distance traveled by Pth rider
off_{ts}	Off time
vlr_P^{ts}	Velocity of rider
gr_P^{ts}	Gear of the Pth rider at time step ts
Spd_P^{gr}	Gear's speed limit of Pth rider
spd_{max}^P	Maximum speed of Pth rider
acc_P^{ts}	Accelerator of Pth rider at ts time step
brk_P^{ts}	Brake of Pth rider at ts time step
$LR_{ts+1}^{ovt}(P, csl)$	Location of Pth rider in csl coordinate selector
$dri_{ts}(P)$	Direction indicator of Pth rider at time step ts
LR_{ts}^{rs}	Relative success rate of Pth rider at time step ts
LR^{ler}	Location of leading rider
$srt_{ts}(P)$	Success rate of Pth rider at time step ts
$LR^{ler}(ler, q)$	Location of leading rider
$ST_{c,d}^{ts}$	Steering angle of Pth rider in qth coordinate
$LR_{ts+1}^{Atk}(p, q)$	Best position of attacker
Ft_P	Fitness function of the present solution
Ft_{max}	Maximum fitness value
$Dstnc$	Distance function
STR_{ts+1}	Updated steering angle
STR_{ts}	Present steering angle
LR_{ts}	Present location of leader

LR_{ts+1}^*	Best position of leader
λ	Noise level
$Pbt(\lambda)$	Probability function of noise
$pstmp$	Pseudo temperature
$nest_e$	Impact of single unit state on global energy
$M_{e,f}$	Weight among the neurons
θ_e	Bias of neurons
$Eng(nest)$	Energy of Boltzman machine
$RP(z_{vs}, z_{hs})$	Probability using function
Pt	Partition function
Wm	Weight matrix
ΔWm	Update of weight matrix
$RP_{z_{hs}}$	Probability for function for hidden layer neuron
Nfp	Count of features
c, d	Two different features
$obf1$	Objective function 1
C^a	Actual result
D^a	Predicted result
MR	Error function
nf^*	Number of optimal features
D^d	The actual output vector of DBN and NN
E^d	Forecasted output vector of DBN and NN
M_{ne}^{nn}	Weight function of NN
M_{ne}^{dbn}	Weight function of DBN

Chapter 1

Introduction

Recently all over the world diabetes has already affected many people's health. The impact of the rapid growth of diabetes leads to many complications. One of the major complications introduced by diabetes is Diabetic Retinopathy (DR). Diabetic Retinopathy is an eye disease that occurs due to the blood vessels associated with the retina are damaged and which results in vision loss [1]. Diabetic Retinopathy creates blindness and sight loss for the age group of 18-65 years.

The DR is categorized into three forms like Background DR (BDR), Profelerative DR (PDR) and Severe DR (SDR). In the BDR stage, the retina arteries may leak and get weakened that forms hemorrhages. The leakage in the normal vessels generally causes edema or swelling, which leads to reduced vision [2]. In the PDR phase, blood circulation difficulties in the retinal regions can cause ischemic or oxygen-deprived. New fragile vessels tend to form in the circulatory system that provides the required oxygen content to the retina and this is called neovascularization. Leakage of blood into the retina and vitreous may cause floaters or spots, besides reducing vision. In the case of the SDR disease phase, the scar tissue and the abnormal vessel growth are continued which leads to cause severe issues like glaucoma, retinal detachment and slowly causes vision loss. In the diabetic population, the screening program has estimated that the results of the population around 1 - 6% ranges have been shown as severe cases [3], though there are fewer available screening resources [4]. The number of cases may increase if screening resources are enhanced. Therefore, an automatic screening scheme helps to solve this resource deficit. The blood vessels in the retina are vulnerable to abnormal glucose metabolism [5]. Recently this metabolic malfunction known as diabetes modifies the retinal vessel structure and functions. Due to these changes in the blood vessels, numerous lesions or injuries are triggered to the retina itself, which are together recognized as DR [6]. The diabetic injuries in the retina have undergone various processes like diagnosis [7], screening and monitoring that overcomes the recent optical health concern, sight loss and blindness. Generally, DR condition begins from diabetes that weakens the retinal blood vessels. These are vulnerable and predominantly considered when the blood vessels are small and delicate [8]. The structural changes in the retina and weakening of retinal blood vessels are also phrased as DR.

1.1 Motivation

The screening of DR is a major problem in the ophthalmology field, for solving this issue the portable fundus cameras are combined with the telemedicine field that gives a bright perspective. Telemedicine is an emerging field for ophthalmologists for performing triage and creating accurate diagnoses in distantly situated patients. Nowadays, artificial intelligence is being used in the medical field for diagnosing many health issues by processing corresponding images. The major advantage obtained by these computer-aided diagnoses (CAD) methods is a decrease in the load of medical experts. For early DR diagnosis and to support specialists, an effective and efficient method is needed for the retinal fundus analysis that uses the computer-aided diagnosis method. However, to attain rapid and consistent computer-aided processing and diagnosis, machine learning applications are employed for the automatic diagnosis of DR fundus images, which is a required and vital task. Based on the recent studies about CAD systems, it is very helpful to enhance the accuracy of the diagnostics for experts that help in reducing the burden of growing workload.

1.2 Retinal Disorders

Abnormalities associated with the eye is categorized into two major classes, the initial one is the eye diseases like glaucoma, conjunctivitis, cataract and blepharitis. The second is classified based on the lifestyle of a person like diabetes, hypertension and arteriosclerosis. The DR condition arises due to diabetes and if it is not treated properly then it may eventually lead to vision loss. Ophthalmologists strongly suggest that early detection of the DR effectively gives the solution for getting the best treatment for this disease. The DR occurs in the population belongs to the three main categories as BDR, PDR, and SDR. These types are explained in the above section. These classes can arise in different forms like Microaneurysms, Haemorrhages and Exudates [9], which are explained below.

Fig.1.1 shows the sample fundus image used for automatic diagnosis of diabetic retinopathy which also contains disease annotations.
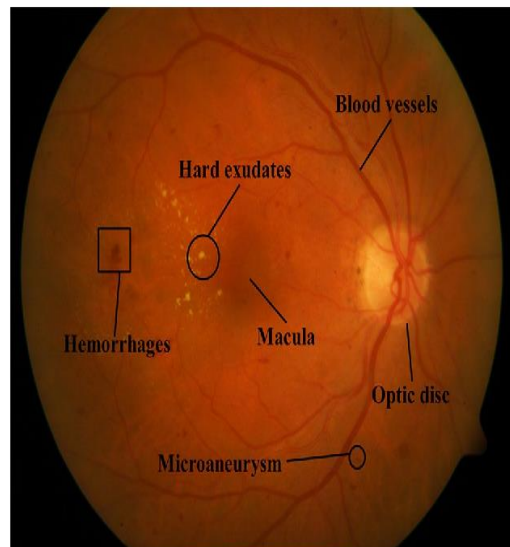
Fig.1.1 Color Fundus image with anatomical structures and disease annotated

1.2.1 Microaneurysms: This is the initial medical abnormality that is observed in the eye. It is visible in seclusion or groups like tiny or dark red spots or appears in the form of small hemorrhages inside the retina that is sensitive to light. The microaneurysms size is ranging from 10 to100 microns, which are circular in shape. Usually, these appear apart from the optic nerve, in which the blood vessels are placed above the complete retina

1.2.2 Haemorrhages: Haemorrhages occur in the retinal deeper layers and these are in a round shape, thus it is called 'blot' or hemorrhages. Hemorrhage is caused because of the bleeding in the blood vessels during the blood flow to entire retinal tissues, which is located on the back portion of the eye. Retinal hemorrhages normally occur at the exterior of the macula that will be unnoticed for a long time.

1.2.3 Exudates: These describe some light injuries found within the retina and they are considered as the exudates. These usually look like white patches and based on the patches, the level of diabetes is found in the person. At the beginning stage of diabetes, the white patches are present in the first quadrant of the image and very little. Therefore, the decisions are made based on the area occupied by the white patches, which is one of the important facts for finding the presence of diabetes. There exist two forms of exudates as hard and soft exudates.

Hard exudate is one type of exudate and it is the major characteristics of DR. The hard exudates can differ in size ranging from small dots to big patches with clear edges. The eye contains blood and fluid, which is made of protein and fat. These proteins and fat will tend to

form the exudates. These deposited fats which formed as exudates cause harm to the visual power by avoiding light from reaching the retina.

Soft exudate is the second type of exudate, which is often named as "cotton wool spots" and these exist usually in the advanced stage of retinopathy. These exudates are the significant features of retinal images along with the variations of blood vessels that are considered for the normal and abnormal retinal images classification process.

1.2.4 Blood Vessels: These are the main components of the retinal structure whose function is to supply nutrients to retinal cells. The blood vessels get weakened and thickened later split into small new vessels like structures because of the diabetes effect.

1.3 Problem Statement

The computational practices play a main role in real-time applications. In recent years, numerous researches on medical-related applications are extremely dependent on computing approaches. Ophthalmology is an important field of the biomedical sector that needs computer-based automated methods for disease identification in individual eyes. Moreover, these automated methods are giving accurate results in less time. Therefore, for various issues, several automated methods have been implemented, which are used in real-time experiments, however, it is complex to attain the universal technique between them. All over the world or mainly in the developed countries, there is a shortage in medical staff due to the huge population, thus the development of an automated method can drastically decrease the physical work concerned in diagnosing retinal images in large quantities. In rural places, an automated system is necessary for the instant diagnosis of retinal images. By using automated diagnosis system results, the ophthalmologist can simply alert the patient concerning the effects of DR difficulty even at a single appointment. Hence, it is absolutely useful to the patient for avoiding the loss of vision.

The diabetes causes many health problems to human being including eye which is one the important organ of human body. So our problem of research looks like this "**Analysis of Retinopathy Images to Detect the Effect of Diabetes on Eye"**

1.4 Research Objectives

The major objective behind this research is to ensure the diagnosis of DR from retinal fundus images of publicly available and live datasets. To accomplish this, the analysis of blood vessels, optic disc and retinal abnormalities play a key role. Even though diverse advancements were there using CAD system for diagnosing DR, more effective contributions have to be developed and this research follows the below objectives as most significant.

1. To develop suitable techniques for "pre-processing and segmentation" methods that help in the classification of retina images accurately.

2. To identify the best approaches for "blood vessel, optic disc and exudates" segmentation that could identify the region of interest correctly.

3. To identify the best approaches for retinal abnormality segmentation from which good features can be extracted that help in getting high classification accuracy

4. To focus on the concept of abnormality segmentation, feature extraction and optimal feature selection to offer better performance in DR detection.

5. To introduce diverse enhancements on meta-heuristic optimization techniques to enhance the "segmentation, optimal feature selection and classification" for DR diagnosis.

1.5 General Architecture of the Proposed System

This section provides a brief discussion about the general architecture for the detection of diabetes' effect on the functioning of the eye. Fig. 1.2 shows the general architecture of detecting the impact of diabetes, which is popularly known as DR.

1.5.1 Databases of Retinal Images

For Diabetic Retinopathy detection there are several standard databases available online, namely DRIVE, STARE, Chase_DB, DIARETDB1, DIARETDB2 and MESSIDOR. Each of these databases has the different number of images including normal case and diseased cases along with the ground truth of the images.

1.5.2 Segmentation

Blood veins segmentation from the retinal images is helpful for early diagnosis of disease progress like hemorrhage, microaneurysm and exudates formation. In the segmentation process, the pre-processed images help to differentiate various retinal parameters. Image segmentation is achieved to extract bright objects that are necessary for the characterization of the images using the optimal grey-level thresholding, statistical morphology procedure, Discrete Wavelet Transform (DWT), watershed transform and Top hat transform are applied. Numerous techniques are available for the segmentation process like the K-means clustering algorithm, simple threshold method, and the "morphological operations such as dilation, erosion, opening, closing, and skeletonization", etc.
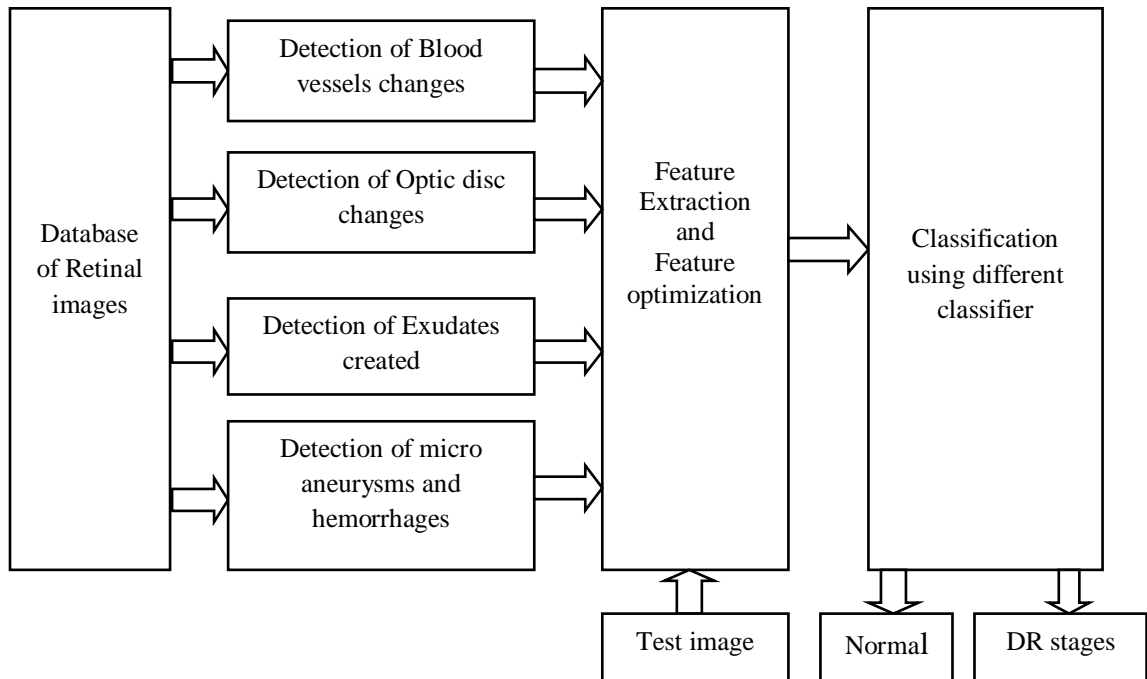
Fig. 1.2: Block diagram for detecting the effect of diabetes on eye

1.5.3 Feature Extraction

Feature extraction is used to gather meaningful information from the retina images. The local or global features may be extracted during this step. The proposed research work employs the properties of "connected components, texture energy measures(TEM), local binary patterns (LBP), entropy, Gray Level Co-occurrence Matrix (GLCM) and Histogram of Oriented Gradients (HOG)" as features for the diabetic detection from retinal forms of images.

1.5.4 Image Classification

The recognition of DR is a complicated multi-class classification issue, in which the decision boundaries are highly nonlinear between normal and abnormal images. Some retinal images are partially overlapped with the other images and the decision boundaries are to be accurately estimated. Based on this estimation, various retinal images are differentiated, which cannot be done by some traditional numerical classification methods. The retinal images of diabetes are classified by machine learning classifiers, however many classifiers need the set of training images, which includes the entire details about all types of the diseased images, but it is complex to contain entire disease cases. Various techniques are used for the classification of images such as random forest, support vector machine, artificial neural network, k-nearest neighbor, deep learning classifiers and hybrid classifiers.

1.6 Challenges in Diabetic Retinopathy

The researchers are showing more interest in automatic DR detection in the medical industry from the retinal fundus images. In the medical field, the research interest is justified by reducing the costs and high potential for new products. Here, there are some challenges.

- **Optic disc boundary detection:** In many of the cases of retina images have exudates whose size and color is closely equal to optic disc size and color, which require enhancement in resolving the optic disc boundaries and it is complex in 2D retinal images due to blurred edges.
- **Varying patterns of blood vessels:** The directions of blood vessels in the retinal structure vary from person to person, it is an anatomical feature. The varying patterns make the extraction of blood vessels a complex task. Each image consists of a varied optic nerve head (ONH) structure. To overcome all these difficulties, there is not a unique technique. Thus, there is a requirement of introducing various effective algorithms for recognizing DR detection and associated structural variations in retinal images.
- **Negligible signs at the mild stage**: At the beginning of diabetes almost no sign of its effect is observed on the retina as microaneurysms start developing at this stage whose appearance is very similar to the background color of the retina. As there is the growth of diabetes mellitus, there will be more demand for screening phases in detecting DR. In public health intercessions, proper treatment is required for reducing the probability of loss of vision.

- **Inconsistency in the result**: The present manual DR screening programs make use of retinal images that relied on talented readers. However, it suffers from inconsistency over sites and is labor-intensive. Therefore, there has been growth in the computerized evaluation of retinal fundus image programming, which mitigates the feasibility of cost. The automated DR diagnosis is an interesting area of research for a longer duration. This is described by minimizing the time as well as the health care costs for the novel solutions in the medical field.

- **Need for good algorithms**: Various effective algorithms must be proposed for the DR identification that is associated with the retinal variations and associated structures. Owing to the increasing growth of diabetes mellitus, the need for the DR screening stages is growing in a very fast manner. The treatment, as well as the early DR detection, is needed for the health intercessions that can avoid the vision loss probabilities.

1.7 Contributions of the Research Work

The main contributions of this thesis are listed below.

- The first contribution of this research is the blood vessels are analyzed based on three steps. From the DIARETDB1 database, the removal of noise, as well as the extraction of blood vessels, is performed. The performance is evaluated with the DRIVE database to reveal the effectiveness of the proposed method. After the segmentation process, feature extraction is accomplished by the DWT and GLCM and the classification is done using the SVM. The developed technique produces better results for CHASE_DBI and DRIVE databases.

  In another approach which is based on the blood vessel, the segmentation and classification are executed by the wavelet transforms and distance measure. The image segmentation is done using two-level DWT with mathematical morphology. The images are classified based on the distance measures values obtained using "city block, Spearman and Minkowski" distance measures using GLCM features.

- The second contribution of this research is the segmentation and examination of the "optic disc, exudates and blood vessels". The detection of the optic disc is done by the wavelet transform and windowing method that divides the segmented image into multiple windows. Standard deviation and energy are computed from each window and the window having the highest energy is detected as optic disc. The detection of exudates is done by

morphological operation and DWT. The method is tested on the DIARETDB1 dataset and it provided better performance

- The third contribution of this research includes the segmentation of blood vessels and other abnormalities to analyze the detection of DR. The images are pre-processed by the combination of "Contrast Limited Adaptive Histogram Equalization (CLAHE)" and average filter. Later the blood vessels are segmented using the optimized gray-level thresholding and the features are extracted by Texture Energy Measure (TEM), Local Binary Pattern (LBP), Shanon's entropy and Kapur's entropy. Later the classification of the images is performed by the optimally trained Neural Network (NN). The proposed algorithm called "Modified Leavy Updated-Dragonfly Algorithm (MLU-DA)" is applied for enhancing the performance of segmentation. Using the DIARETDB1 dataset, the images are classified into abnormal and normal images.

- The fourth contribution of this research is the segmentation of retinal abnormalities from the retinal fundus images. The retinal abnormalities such as hard exudates, soft exudates, hemorrhages and Microaneurysm are segmented for analysis of DR condition. The images are enhanced using CLAHE and the optic disc is eliminated using the open-close watershed transformation and the blood vessels are removed by the grey level thresholding. In the next step, the retinal abnormalities are segmented with the Top hat transformation and Gabor filtering. The features are extracted from the segmented abnormalities using LBP, TEM, Shanon's, and Kapur's entropy. Then the proposed "Modified Gear Steering based Rider Optimization Algorithm (MGS-ROA)" is used for the selection of optimal features. Finally, the classification is done by Deep Belief Network (DBN) for classifying the images into moderate, normal, earlier and severe phases of DR, where the weight function of the DBN is updated by the proposed MGS-ROA. Here, the images from the DIARETDB1 databases are used for experimental evaluation.

- The fifth contribution of this research focuses on the analysis of the optic disc, blood vessels and retinal abnormalities like hard exudates, soft exudates, hemorrhages and Microaneurysm from the DIARETDB1 databases. The segmentation of the optic disc, blood vessels and retinal abnormalities are carried out using the open-close watershed transform, grey-level thresholding and top hat transform with Gabor filtering, respectively. The features are extracted from the segmented blood vessels, optic disc and abnormalities using LBP, Shanon's, and Kapur's entropy and TEM. A new algorithm developed called

"Trial Based Dragonfly Algorithm (TB-DA)" is adopted for the selection of optimal features. The images are classified into four classes by the hybridization of Neural Network (NN) and DBN, where the TB-DA performs optimization in training the classifier. In this work, the performance of the developed method is tested using the DIARETDB1 dataset.

1.8 Organization of the Thesis

The chapters of the thesis are ordered as mentioned below.

Chapter 1 explains the introduction of DR, motivation for this research work, problem statement, objectives of this research, the general architecture of proposed research, challenges in DR detection, thesis contributions and the thesis organizations.

Chapter 2 describes DR detection by Blood vessels segmentation, feature extraction and classification, data sets used, performance measures, their experimental analysis and the summary.

Chapter 3 explains DR detection by Optic Disc and Exudates segmentation and classification based density of exudates as moderate or severe case, their experimental analysis and the summary.

Chapter 4 describes the Modified Levy Updated-Dragonfly Algorithm for optimal thresholding merged with the neural network-based method to the detection of DR, its experimental analysis and the summary.

Chapter 5 discusses the Modified Gear Steering-based Rider Optimization Algorithm for DR detection with optimal feature selection based deep learning classifier, its experimental analysis and the summary.

Chapter 6 analyzes Trial Based-Dragonfly Algorithm on diagnosing DR by "segmenting blood vessels, optic disc and retinal abnormalities", its experimental analysis and the summary.

Chapter 7 concludes the thesis with the summary, major findings of this research and future scope

Chapter 2

Blood Vessel Segmentation and Classification based Approach

In chapter 1 the general technique for DR detection and its complications on the eyes is provided but there is no universal method that gives consistently good results over all the retina images. So for several decades, the diagnosis of DR has always been remaining as a major challenge in the research. The key features used to detect diabetes include optic disc, blood vessels, exudates, microaneurysms and hemorrhages, etc.

2.1 Introduction

In this chapter segmentation of blood vessels is addressed which are the main signs of diabetic retinopathy at the beginning stage. Blood vessels carry nutrients to the retina and transfer the waste generated back but because of diabetic retinopathy swelling of blood vessels begins so segmenting these will have significant information about diabetic retinopathy. Here three approaches have been used to detect DR based on blood vessels changes in the retina images.

The first approach [10] proposed method is composed of three steps. In the first step, the enhancement operation removes the noise and increases the retinal blood vessel's contrast. In the second step, blood vessels are separated by morphological operations. The final step classifies the input images as "normal or abnormal". The experiments are performed on the DRIVE database.

In the second approach [11], three major steps are used. In the first step, pre-processing removes the noises from the retinal images. In the second step known as the filtering step, several filters are applied to retina images and the corresponding PSNR and MSE are calculated. The median filter is effective in removing noise from retina images of DRIVE data set. In the final step, the segmentation is performed with the morphological operation and DWT for the blood vessel extraction. The performance measure is evaluated using DRIVE database to estimate the efficiency of the developed technique.

The third proposed approach [12] uses three steps. In the first step, pre-processing is performed in which the filtering technique improves the appearance of the blood vessels later segmentation of blood vessels is done using morphological operation. The second step involves feature extraction, in which a feature vector is formed by DWT and GLCM features.

In the last step, the SVM classifier is used for classifying the retina image as abnormal or normal. The performance is tested on CHASE_DBI and DRIVE databases concerning sensitivity, specificity and accuracy that yield better results.

2.2 Related Work

In 2019, Xu *et al*. [13] have recommended a new technique that included two discrete procedures from the microaneurysms turnover and the pathological risk factors for the DR detection. To categorize the new, resolved and unchanged microaneurysms, seven pathological features related to the microaneurysms were explored by performing the pattern classification and statistical analysis models. By using Grampian Diabetes Database, the proposed model was evaluated. The outcomes demonstrated that it has achieved the best accuracy. For early detection of DR, a new and non-invasive detection approach was introduced. In 2013, Sopharak *et al*. [14] have introduced effective approaches for detecting fine microaneurysms, specifically from non-dilated pupils. By using mathematical morphology, they are coarsely segmented and with Naive Bayes classifier, fine segmentation was done at the pixel level. Here, a total of 18 microaneurysm features was considered and those were extracted for Naive Bayes classifier. The method is performed well compared to other methods but fails to identify mild cases

In 2019, Li *et al.* [15] have developed automatic deep learning-based models for diagnosing DR. The authors have gathered 13,673 retinal images from 9,598 patients for analyzing these deep learning models in clinical laboratories. By using seven graders as per the quality of the image and DR level, these retinal fundus images were split into six classes. To annotate four types of DR lesions, 757 images with DR were chosen. Therefore, existing deep learning techniques were analyzed using the gathered images based on image classification, object detection and semantic segmentation. Yet, these models performed worst on segmentation and detection of lesions and this was the most challenging thing.

In 2018, Ramos *et al.* [16] have determined a novel approach for the blood vessel detection from the retinal images. With the help of the Low-Pass Radius filter, the noise available in the green channel of RGB image was decreased. On the other hand, for consistent enhancement of both structure and contours of blood vessels, 30-element Gabor filter and Gaussian fractional derivative were employed. Thus, a threshold and a sequence of morphology-based decision rules were subjected to blood vessel isolation and decreased the

occurrence of false-positive pixels. For optic disc detection from the original image, the proposed model has been employed and eliminated it from the result of the threshold. By using the freely accessible DRIVE dataset, the developed model was analyzed for the first manual delineations and test image set. The proposed model provided the best results concerning accuracy and specificity.

In 2019, Wang et al. [17] have estimated the possibility of DR diagnosis and the existence of DR-associated features using a two-step process. Initially, the annotation quality was analyzed in the grading of DR by measuring the variability of inter-grader. The cosine similarity was considered for assessing the inter-grader variability of DR. For this, quadratic weighted Cohen's kappa was utilized. Further, various annotation models such as "single annotations by single grader" (SASG), "single annotations from multiple graders" (SAMG), "multiple annotations by voting" (MAV) and "double annotations with adjudication of disagreement (DAAD)" were compared over the performance of severity prediction using logistic regression. Both severity and features of DR have explored the feasibility of detection based on these comparison outcomes. Hence, a total of 1589 retinal fundus images were graded in the tests. The outcomes have shown that retinal specialists were reliable when compared to normal ophthalmologists during the gradation of both the existence of severity and features of DR.

In 2017, Zhou et al. [18] have presented a novel unsupervised classification technique based on sparse Principle Component Analysis (PCA) for microaneurysms detection. The class imbalance problem was avoided as it has not considered the non-microaneurysms training set. Later, the effective features were chosen because of sparse PCA features that merged the elastic net penalty using PCA together. Consequently, for determining the true microaneurysms from spurious candidates, a single 2T statistic was suggested. The tests were performed on Retinopathy Online Challange (ROC) competition dataset. In 2019, Kumar et al. [19] have addressed a novel interpretable CAD model based on "Class-Enhanced Attentive Respo Discovery Radiomics" (CLEAR-DR) for aiming the clinical decision support for DR. The system has provided a visual interpretation of the decision making procedure for producing best results for grading the disease using the discovered deep radiomic sequencer. The efficiency of the developed CLEAR-DR has been demonstrated that the interpretability of diagnostic grading outcomes was better for DR grading application.

In 2016, Shaik *et al.* [20] have observed the improvement of blood capillary segmentation of the patient who was suffering from diabetes. By using the hybrid morphological reconstruction approach, a hybrid model was introduced as the pre-processing model, whereas the watershed segmentation algorithm was considered post-processing. In 2010, Agurto *et al.* [21] have labeled the usage of "Multidimensional Amplitude Modulation - Frequency Modulation" (AM-FM) techniques in differentiating between pathological and normal retinal fundus images. With the standard images, the proposed model was tested. Exudates, hemorrhages, microaneurysms, normal vessel patterns, neovascularisation on the retina and normal retinal background are the region types. From many scales, "the cumulative distribution functions of instantaneous amplitude, relative instantaneous frequency angle and instantaneous frequency magnitude" were employed as texture feature vectors. To measure the inter structure similarity, distance metrics were employed. The outcomes have proved that a statistical variation based on AM-FM features gives good results.

In 2018, Zhou *et al.* [22] have presented a Deep Multiple Instance Learning (MIL) approach for automatic diagnosis of DR and it achieved a constant enhancement in the DR detection with its lesions. The estimation of patch-level DR estimation was done by a pre-trained CNN. Further, global aggregation performed the classification. Next, an end-to-end multi-scale model was introduced for tackling irregular DR lesions. The datasets such as Messidor and Kaggle were used for analyzing the efficiency of the proposed model to detect DR images. By using connected component-level validation, the proposed model attained the best results in detecting DR lesions on the DIARETDB1 dataset. In 2018, Costa *et al.* [23] have addressed MIL technique for dealing with the leverage of implicit data. The main intuition of the developed model was "joint optimization of the instance encoding and the classification phases of image". Likewise, many pathological images were acquired. The developed model achieved optimal outcomes when differentiated over conventional approaches.

In 2018, Dashtbozorg *et al.* [24] have introduced a novel and reliable approach for microaneurysm detection from retinal images. By using gradient weighting and iterative thresholding approaches, many preliminary microaneurysm candidates were extracted. Later, a new feature set based on local convergence index filters was extracted for shape descriptors and intensity. To discriminate microaneurysms from non-microaneurysm candidates, the collective feature set was given to the "hybrid sampling or boosting classifier". With the help of 6 public datasets that include in the Retinopathy Online Challenge (ROC), the proposed model was evaluated on images using various resolutions and modalities. The results showed

that the developed model achieved optimal outcomes than the other models. In 2016, Seoud *et al*. [25] have suggested a novel model for automatic detection of both "hemorrhages and microaneurysms". The proposed model has intended a novel group of shape features named "dynamic shape features", which doesn't need accurate region segmentation for categorizing the images. To discriminate among the vessel segmentation and lesions, these features denoted the shape growth in image flooding. The proposed model was evaluated for each image and for each lesion with six datasets, which were freely accessible. The outcomes have demonstrated that the suggested model achieved the optimal performance concerning the variability in image resolution, acquisition and quality of the system. Advanced medical imaging techniques enhanced the recognition of different diseases through image analysis by artificial intelligence techinues [113][114]

2.3 Proposed Methodology

In this section approaches for "segmentation and classification" of retinal images based on blood vessels are described.

The variations in the blood vessel structure can be recognized [26][27] by the precise blood vessel extraction from the retinal fundus images. The proposed system of automatic blood vessel segmentation and analysis for the retinal fundus images is shown in Fig. 2.1. This model is used for computing the blood vessel area by segmenting the retinal blood vessels and monitoring the blood vessel variations caused by diabetes.
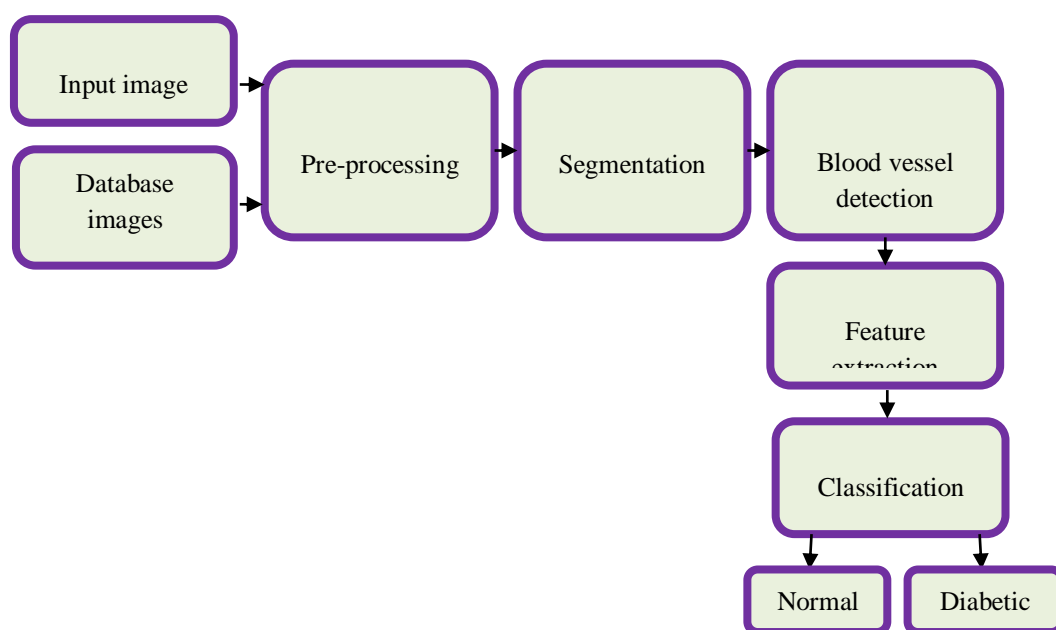
Figure 2.1: Block diagram of the proposed blood vessel analysis

2.3.1 Pre-processing

- **RGB to Gray Conversion:** The conversion of RGB image to the grayscale image is used for minimizing the computational time and the size of the data. The areas are considered to be uniform by resizing the images to some size like 256×256 pixels.

- **Contrast Enhancement:** Low contrast images happen due to non-uniform illumination or poor condition as well as small active range or nonlinearity of the imaging sensor. A good representation of the transformed images is obtained by improving the contrast associated with the images. Here, the contrast enhancement is accomplished by the "Contrast Limited Adaptive Histogram Equalization (CLAHE)".

2.3.2 Segmentation

The number of pixels in the segmented image is affected by the shape and size of the structuring element that is excluded or included from the object in the image. The closing operation is performed by dilation and accompanied by erosion. Dilation thickens or grows the binary image. The dilation operation in the grayscale is used to close the small dark regions and maximize the brighter regions. The dilated objects are minimized to their original shape and size using erosion. The erosion does not react to the dark regions that are closed with the dilation. The closing operation closes the thin dark segmented vessels on a brighter background. The edge detection method receives the input image via a smoothing filter. The outcomes obtained are compared with the image that passes after and before the smoothing filter.

- **Background Exclusion and Thresholding:** This step removes the background from an image such that the foreground objects are viewed clearly. A binary image is produced that contains the pixel value as either 1 or 0.

- **Morphological Closing:** The term $C \bullet D$ represents the closing of the image C using the structuring element D and it is given in Eq. (2.1).

$$C \cdot D = (C \oplus D) \ominus D$$

(2.1)

The morphological closing technique is applied in this step by keeping the disk as the structuring element. The structure element square's size is selected as 10 to transfer small shapes and characters from the foreground to the background color.

In another approach segmentation is accomplished using "discrete wavelet transform and mathematical morphology".

Eq. (2.2) gives coefficients of Discrete Wavelet Transform (DWT).

$$W_\phi(j_0, k) = \frac{1}{\sqrt{m}} \sum_x f(x) \phi_{j_0,k}(x) \tag{2.2}$$

Here, m=0, 1, 2, 3....n , and an arbitrary starting scale is denoted by k. Eq. (2.3) describes the approximate coefficients.

$$W_\phi(j, k) = \frac{1}{\sqrt{m}} \sum_x f(x) \psi_{j,k}(x) \tag{2.3}$$

Where f(x), $\phi_{j_0,k}(x)$ and $\psi_{j,k}$(x) defines the discrete variable functions x=0, 1, 2,.....m-1 and $\phi_{j_0,k}(x)$ defines a member of the set expansion functions and a scaling function is given by $\phi(x)$. Coefficients defined in Eq. (2.2) and Eq. (2.3) are usually called approximation and detailed coefficients respectively.

2.3.3 Feature Extraction

Machine learning classifiers classify the diabetes retinal images, but most of these classifiers need a group of features to train the classifiers. From the given retinal image, extractions of texture features is performed and given below.

- **Contrast:** The variations in the quantification related to the neighboring pixel values are referred to as the contrast. Eq. (2.4) describes the contrast that gives a good feature for representing the image further.

$$Contrast = \sum_{i,j=0}^{NG-1} P_{i,j}{}^2 \tag{2.4}$$

$P_{i,j}$ is element i,j of the normalized symmetrical GLCM and NG is the gray level count.

- **Homogeneity:** The "co-occurrence of matrix values" together with a combination of low and high values present in the image is referred to as the homogeneity and given in Eq. (2.5)

$$Homogeneity = \sum_{i,j=0}^{NG-1} \frac{P_{i,j}}{1 + (i-j)^2} \tag{2.5}$$

- **Entropy:** The information present in the image is evaluated using entropy. The uncertainties present in the intensity distribution of an image are evaluated through entropy as described in Eq. (2.6).

$$Entropy = \sum_{i,j=0}^{NG-1} \ln(P_{i,j})P_{i,j} \qquad (2.6)$$

- **Correlation:** The correlation present in the image linearity is described in Eq. (2.7).

$$Correlation = \sum_{i,j-0}^{NG-1} \frac{P_{ij}(i-\mu)(j-\mu)}{\sigma^2} \qquad (2.7)$$

In the above equation μ, σ represent mean and variance respectively. The image is said to contain a huge amount of linear structure if and only if the correlation is high.

- **Energy:** The local kernels help to generate texture features. For all the image coordinates, the summing and multiplication of pixels with the specific kernel is found. The absolute values are added to the local region for finding the TEM. Eq. (2.8) describes the energy.

$$Energy = \sum_{i,j}^{NG-1} (P_{ij})^2 \qquad (2.8)$$

2.3.4 Classification using Support Vector Machine (SVM)

This is a supervised type of machine learning algorithm for the "classification and regression" tasks. However, this is widely employed in classification efforts. In the SVM classifier, every data item is plotted as a "point in n-dimensional space", here n is the total feature count used where the value of every feature being the meticulous coordinate value. Then, classification is accomplished using the hyperplane which separates the classes very accurately.

2.3.5 Distance Measures

The input image, data matrix of size MXN in which the row vectors are described by $1XM$ such that, $y_1, y_2, \ldots \ldots y_{kr}$. Matrix z is a data matrix of size MxN, in which the row vectors are described by $1XN$ such that $z_1, z_2, \ldots \ldots \ldots z_{kr.}$. Eq. (2.9), Eq. (2.10), and Eq. (2.11)

describes the "city block distance, Minkowski distance and the Spearman distance" that are calculated among the vectors y_{kr} and z_{kr} correspondingly.

$$D = \sum_{kr=1}^{nr} |y_{kr} - z_{kr}| \tag{2.9}$$

$$D = (\sum_{kr=1}^{nr} |y_{kr} - z_{kr}|^{P})^{\frac{1}{P}} \tag{2.10}$$

$$D = \sum_{kr=1}^{nr} (y_{kr} - z_{kr})^2 \tag{2.11}$$

Where kr and nr represent the number of feature vectors

2.4 Datasets Used

There are some data sets available for retina images publicly which are used for testing the algorithms which are developed for the diagnosis of diabetic retinopathy. Some of the data sets used are given below.

2.4.1 DIARETDB1

It is composed of a total of 89 images. Here, 5 images are related to the healthy retina and 84 images are related to the mild and PDR. These are defined by four experts in terms of, "microaneurysms, hemorrhages, hard and soft exudates". These are obtained by a fundus camera with a 50-degree FOV in PNG format.

2.4.2 DRIVE

The DRIVE (Digital Images for Vessel Extraction) represents a publicly available database. It is composed of 40 images. These images were obtained from the DR screening program in the country of the Netherlands. It is composed of 453 subjects from 31 to 86 years of age. It was compressed in a JPG format that is a familiar practice in the screening programs. The 7 images consist of pathology such as, "exudates hemorrhages and pigment epithelium changes". The images are captured by a Canon CR5 non-mydriatic 3-CCD camera at an angle of 45 degrees FOV. Every image is shot in 786x584 pixel format. These images were categorized into testing and training set with 20 images in each. A well-reputed

ophthalmologist trained the observers. 14 images of the training group were segmented by the first observer and the 6 images were segmented by the second observer. The segmentation of the test group occurred twice which resulted in groups X and Y. the group X was segmented by the first two observers and a third observer segmented the group Y.

2.4.3 STARE

It is composed of a total of 20 images. Here, 10 images are composed of pathology. The digitized slides are shot by a TRV-50 fundus camera at an angle of 35 degrees FOV. It was digitized in 605x700 pixel format. The diameter of the FOV is around 650x500 pixels. The entire images are segmented manually by two observers.

2.4.4 DIARETDB0

It is composed of 130 retinal images. Here, 20 images are normal and 110 images are composed of several DR symptoms.

2.4.5 Chase_DB

The dataset contains 28 eye fundus images. The first 8 images are used for training and the remaining 20 for testing. Out of 28 images, 6 have pathology

2.4.6 Messidor

The dataset has 1200 eye fundus color images of the posterior pole of the eye. The Messidor database was acquired by 3 ophthalmologic departments using a color video 3CCD camera 800 images were acquired with pupil dilation (one drop of Tropicamide) and 400 without dilation.

2.5 Performance Measures

In our work, the performance is analyzed based on the following metrics.

i. **Accuracy:** "It is a ratio of the observation of exactly predicted to the whole observations".

$$Acc = \frac{T^P + T^N}{T^P + T^N + F^P + F^N}$$

(2.11)

"Where T^P is true positive, T^N is true negative, F^P false positive and F^N is false Negative"

ii. **Sensitivity:** "It measures the number of true positives, which are recognized exactly".

$$Sens = \frac{T^P}{T^P + F^N}$$

(2.12)

iii. **Specificity:** "It measures the number of true negatives, which are determined precisely".

$$Spec = \frac{T^N}{T^N + F^P}$$

(2.13)

iv. **Precision**: "It is the ratio of positive observations that are predicted exactly to the total number of observations that are positively predicted."

$$\Pr ec = \frac{T^P}{T^P + F^P}$$

(2.14)

vi) **False Positive Rate:** "It is the ratio of the count of false-positive predictions to the entire count of negative predictions".

$$FPR = \frac{F^P}{F^P + T^N}$$

(2.15)

vii) **False Negative Rate:** "It is the proportion of positives which yield negative test outcomes with the test".

$$FNR = \frac{F^N}{F^N + T^P}$$

(2.16)

viii) **Negavie Predictive Value:** "It is the probability that subjects with a negative screening test truly don't have the disease".

$$NPV = \frac{F^N}{F^N + T^N}$$

(2.17)

ix) **False Discovery Rate:** "It is the number of false positives in all of the rejected hypotheses".

$$FDR = \frac{F^P}{F^P + T^P}$$

(2.18)

x) **F1 score:** "It is defined as the harmonic mean between precision and recall. It is used as a statistical measure to rate performance"

$$F1 = \frac{Sens \times \mathrm{Pr}\,ec}{\mathrm{Pr}\,ec + Sens} \qquad (2.19)$$

xi)   Mathew Correlation Coefficient: "It is a correlation coefficient computed by four values".

$$MCC = \frac{T^P \times T^N - F^P \times F^N}{\sqrt{\left(T^P + F^P\right)\left(T^P + F^N\right)\left(T^N + F^P\right)\left(T^N + F^N\right)}} \qquad (2.20)$$

2.6 Results and Discussion

The patient's data in the medical analysis is classified into two classes as to whether the disease is present or not. Specificity and sensitivity measures assess the diagnosis classification. Sensitivity finds the percentage of images from the database that are accurately identified with diabetes. Specificity finds the percentage of images from the database that are correctly identified as non-diabetic images. Fig.2.2 shows different stages of retinal disease.

The testing of sample fundus retina images and their extracted blood vessels from the related input images are shown in Fig. 2.3 and 2.4. The input retinal images classify the test image as non-diabetic or diabetic that represents the separated blood vessels. Moreover, based on the calculated areas of the blood vessels, the retinal fundus images are classified as either diabetic or non-diabetic.

| (a) Mild | (b) Moderate | (c) Severe |
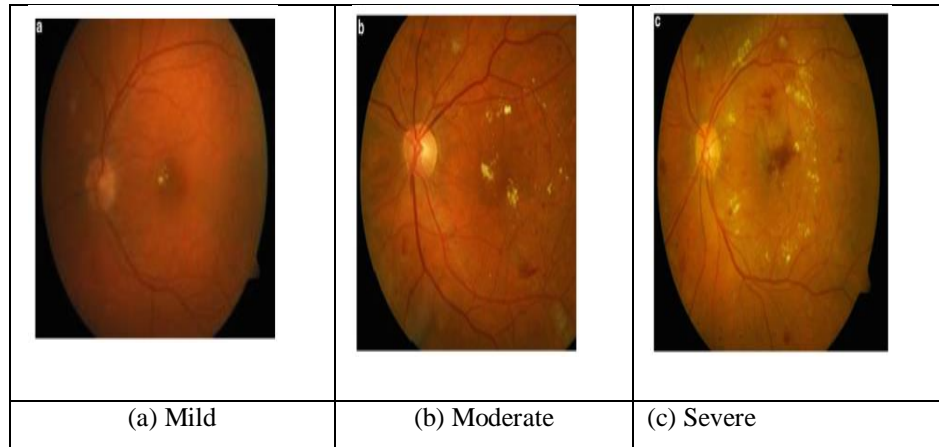
Fig. 2.2: Stages of diabetic progression

Image 1	Image 2	Image 3	Image 4
(a) Input			
(b) Extracted blood vessels			
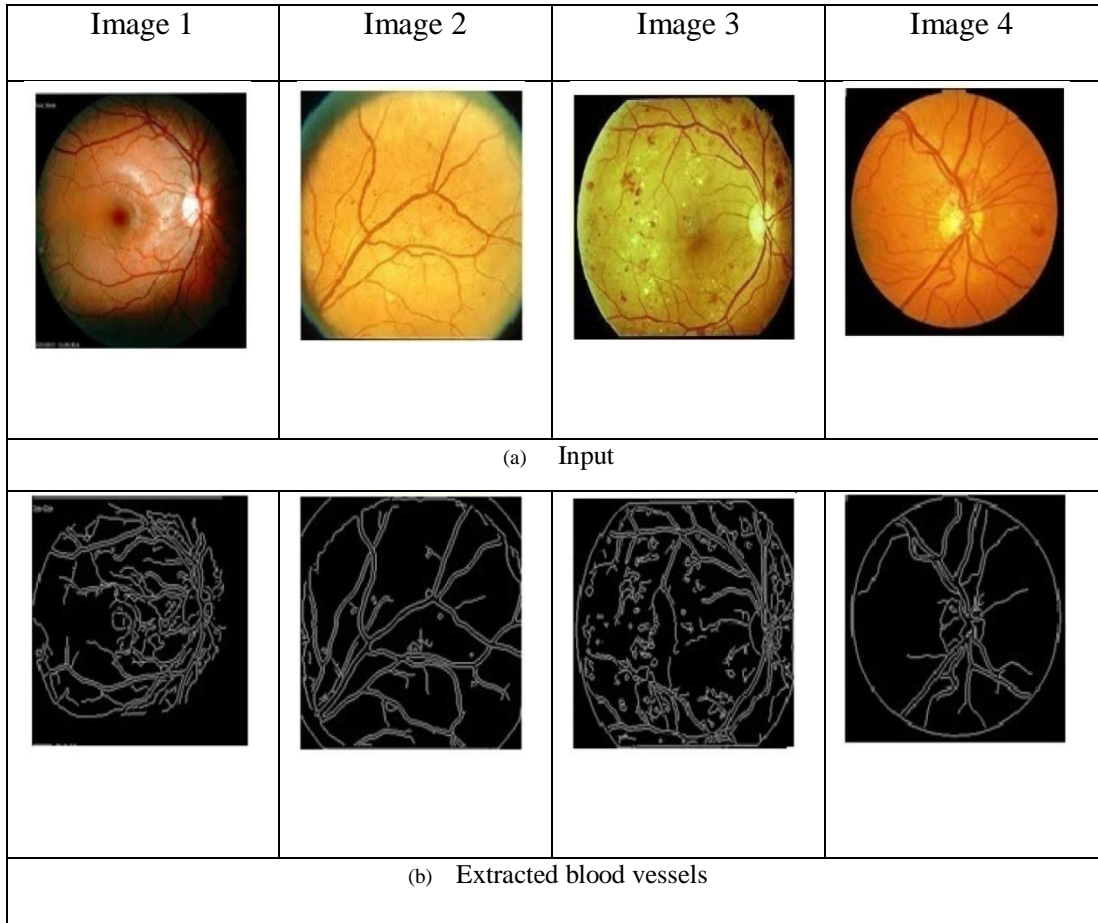
Fig. 2.3: Input retina images and blood vessels extracted from input images

(a)) retinal fundus images	(b) segmented blood vessels
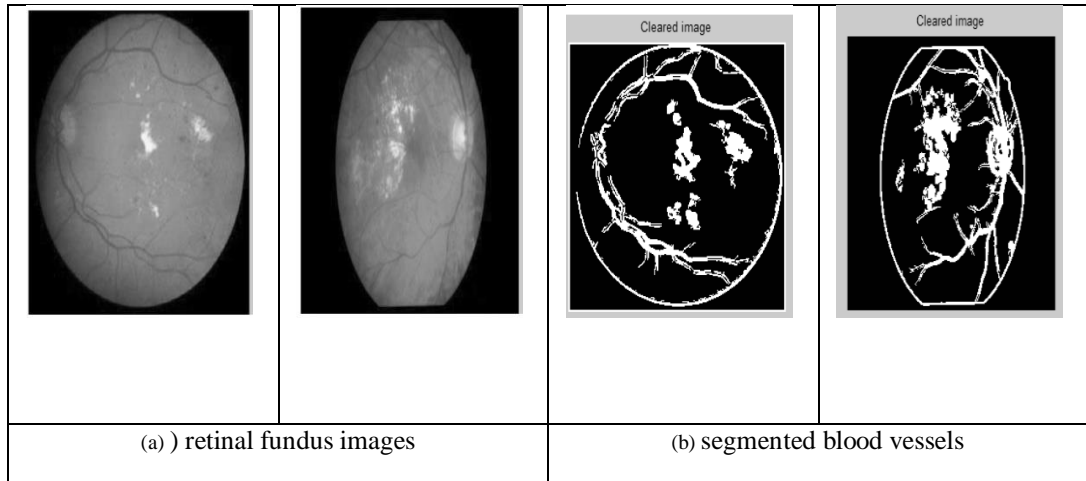
Fig. 2.4: Results of blood vessel detection

By keeping the manual labeled dataset as a reference, the specificity, sensitivity and accuracy values obtained are 0.666, 1.000 and 0.923 on the CHASE_DBI and DRIVE data set, which obtained better results than the existing unsupervised and supervised algorithms as given in Table 2.1.

Table 2.1: Performance analysis of developed blood vessel evaluation using two datasets

Performance measures	CHASE_DBI database			DRIVE database				
	Methods			Methods				
	Azzopardi [28]	Fraz *et al.* [29]	Proposed method	Deepa *al.*[30]	Gao *et al.* [31]	Mendinca *et al.* [32]	Santosh *et al.* [33]	Proposed method
Specificity	94.85	97.10	**91.00**	36.40	25.00	97.60	83.52	**66.60**
Sensitivity	78.96	72.20	**100.00**	87.40	88.00	73.40	64.77	**100.00**
Accuracy	92.80	94.50	**82.60**	95.00	94.00	94.60	89.72	**92.30**

The classification yield slightly different accuracy [34] on a different database. Blood vessel segmentation results obtained in terms of pixels is tabulated in Table 2.2. The distance measures utilized in the approach are described with distance values are given in Table 2.3. The outcomes of retinal image classification using the DIARETDBI database accuracy are given in Table 2.4.

Table 2.2: Extracted blood vessel pixels comparison using the developed technique and manual segmentation

Test images (DRIVE DB)	Obtained number of pixels	Count of pixels (manual or first observer)	Percentage difference
Image 1	41220	38419	7.2
Image 2	42135	38457	9.41
Image 3	47056	38480	22.23
Image 4	39344	38514	2.14
Image 5	36061	38480	6.28
Image 6	39812	38501	3.40
Image 7	42811	38404	11.41
Image 8	48020	38429	24.91

Image 9	41351	38470	7.41
Image 10	30674	38463	20.20
Image 11	39879	38460	3.61
Image 12	43155	38458	12.21
Image 13	33769	38448	12.15
Image 14	43779	38421	13.91
Image 15	39596	38410	3.01
Image 16	37434	38481	2.72
Image 17	44873	38414	16.80
Image 18	37618	38434	0.47
Image 19	38036	38461	1.10
Image 20	38130	38414	0.71

Table 2.3: Comparison of the performance of the distance measure

Reference images	Count of images in the database	Type of image	Number of test images	Average distance (city block)	Average distance (Minkowski)	Average distance (Spearman)
Normal	10	Mild	10	0. 2240	0.0637	0.0190
		Severe	10	0.5540	0.1341	0.0364
		Normal	10	0.1500	0.6180	0.0170
		Moderate	10	0.3140	0.0851	0.0209

Table 2.4: Comparison of classification accuracy for various methods

Methods	Classification accuracy (in percentage)
Niemeijer *et al.* [35]	80
Iyer *et al.* [36]	70
Proposed Method	**91.10**

2.7 Summary

Three approaches are used for blood vessel segmentation. In the third approach for blood vessel analysis, the blood vessel detection accuracy improved from 82.60% to 92.30%. The enhancement and morphological operation of the first approach removed the noise and extracted the blood vessels from the DRIVE database. The second approach performed the pre-processing, filtering and segmentation for extracting the blood vessels. The performance was evaluated with the DRIVE database to reveal the effectiveness of the proposed method. Three steps were induced in the third approach. In the first step, pre-processing enhanced the appearance of the blood vessels by computing the PSNR and MSE. Next, the appearance of blood vessels was enhanced by several filters. The next step performed feature extraction to extract the features using DWT and GLCM. Further, SVM is adopted to classify the condition of the image in the last step. The proposed method is tested on databases CHASE_DBI and DRIVE yielded better performance by the proposed technique in terms of measures like "sensitivity, specificity and accuracy".

Chapter 3

Optic Disc and Exudates Segmentation based Approach

In chapter 2, blood vessels segmentation and classification of the retina as a diabetic or non-diabetic is performed however for more accurate classification of the retina only changes in blood vessels details are not sufficient. So it is necessary to consider some more features of the retina like optic disc changes and exudates creations, those can provide more needful information for the classification of retinal disease.

3.1 Introduction

In this chapter two approaches are developed, first one is proposed to identify and separate the optic disc [37] from the retinal fundus RGB image using the wavelet transform. This method produces a detection accuracy of around 95% on the DIARETDB1 and DRIVE datasets. In the second approach, exudates detection [38] is performed using morphological operation and DWT for classifying the human retina as diabetic or normal. The proposed methods provide good results over the existing methods.

3.2 Related Work

In 2012, Antal and Hajdu [39] have presented an ensemble-based model for enhancing the detection of microaneurysm. The combination of internal components of microaneurysm detectors such as candidate extractors and pre-processing approaches was done and the output of this is applied to many classifiers. For microaneurysm detection, the proposed model was analyzed in an online competition, in which this model was presently ranked as very good, and also on two other datasets. As microaneurysm detection was decisive in DR gradation and the developed approach was tested on the Messidor dataset. In 2017, Pires *et al*. [40] have directly trained the classifier for lesion detection. For the retinal images such as Fisher vector and BossaNova, additional novelties were the use of existing mid-level features. These features extended the conventional Bag of Visual Words and enhanced the compound classification task accuracy. For direct referral, the suggested model was performing well.

In 2018, Kar and Maity [41] have analyzed lesion detection and neovascularisation in an integrated model for DR gradation. From the sub-sample measurements compressed sensing and imaging were done. To extract and classify the thin and thick vessels, the blind evaluation of the multi-deviation fusion (MF) scale and fuzzy entropy maximization was

performed. For detecting neovascularisation, the mutual information among the tortuosity and vessel density of thin vessels was maximized in 2D. The results were merged for DR gradation in the usual platform. In 2016, Olafsdottir *et al.* [42] have investigated the occurrence and seriousness of retinopathy observed in diabetes cohorts detected by monitoring when compared over the existing healthcare system. For the screening process total of 257 diabetic patients are considered, 151 were screened by CAD system and 106 by traditional healthcare system were involved. By using fundus photography, retinopathy was analyzed. To grade the images, "the modified Airlie House usage of Early Treatment Retinopathy Study protocol" was employed. From diagnosing diabetes until the eye examination, averages of clinically gathered body mass index values, Fiber Bragg Grating (FBG) and blood pressure were calculated. During the examination, peripheral neuropathy, blood chemistry and smoking habits were evaluated. By improving the severity grade of retinopathy as resultant, similar outcomes were found. For screening-detected diabetes cohort when compared over clinically detected cohort, the cumulative retinopathy occurrence was majorly less in 10 years people's follow-up. The occurrence of DR and improving the seriousness of DR among the patients with screening-diagnosed diabetes is less than those who had detected their diabetes by traditional healthcare system were considered. The early DR diagnosis reduced the pre-diagnostic time spent with hyperglycemia.

For automatic hard exudates detection in DR with fuzzy logic and morphological segmentation, a new method was introduced by Basha and Prasad [43]. Because of the color similarity within the "blood vessels, exudates and optic disc", the introduced algorithm produces some false detection. Khan et al. [44] presented a method for improving the exudates by fuzzy morphology was explained, in which the color retinal image is changed into a greyscale image. The boundaries of the exudates were enhanced by the fuzzy morphological closing operation. To acquire the enhanced image, the final image is included with the actual image in the last phase. During the clinical tests, these enhanced images produced the best results. A new model for detecting exudates by local contrast enhancement and color normalization is introduced in Das et al. [45]. Here, NN and Fuzzy-C Means (FCM) have been developed. Even though this notion works well in "LUV color space (L stands for luminance, whereas U and V represent chromaticity values of color images)", the detection accuracy is very less in non-uniform illumination. Chakraborty et al.[46] introduced an automatic approach to detect exudates from retinal images. In [47] a method to detect exudates from the less brightness digital images which belong to DR, the FCM clustering

approach was employed. Once the contrast enhancement pre-processing is done, the features such as "standard deviation on intensity, count of edge pixels, intensity and hue" are extracted for delivering as input parameters for coarse segmentation by the FCM clustering approach.

In 2013, Ranamuka and Meegama [48] have suggested a method based on morphological image processing for detecting hard exudates from DR retinal fundus images. Here fuzzy logic was used. In the initial step, the exudates were recognized by mathematical morphology which involved the optic disc elimination. Consequently, by using an adaptive fuzzy logic algorithm, hard exudates were extracted by using the RGB values for forming "fuzzy sets and membership functions". In each exudate, the output of the fuzzy for the entire pixels was computed to the given input set for RGB channels of the pixels in an exudate. As per the region of hard exudates, the fuzzy output was calculated. One of the most significant effects of DR is loss of vision [49] [50] [51]. In Korea, as there is a significant growth in diabetes mellitus, more Korean people infect by this disease in the future [52]. The occurrence of DR in Korea has been reported as 44.4 people from 1000 people in 1998. In 2013, the occurrence of DR has reported more than 56 people per year in 1000 persons [53] [54]. However, as the research persons varied, it is complex for comparing figures from the two reports in a direct format. In the past decade, the enhancements in DR screening also resulted in the best DR detection when the occurrence of DR increases among the people.

3.3. Proposed Methodology

Optic disc and exudates detection from retina image helps in the detection of severity for diabetic retinopathy. As both optic disc and exudates are bright lesions, during the segmentation process they lead to the wrong detection. In this method, discrete wavelet transform is applied to detect spatial density to differentiate among exudates and optic disc.

3.3.1 Pre-processing

Pre-processing has the main role in image segmentation since the distribution of brightness present in the image leads to differences during the selection of the threshold. In general, pre-processing is referred to as the contrast-enhancing, filtering, reading and resizing of images. Each database images have various sizes and therefore the input images have been resized to around 256×256.

The unwanted noises are removed by the filtering process. The image Ip_{im} is applied with an averaging filter of about 5×5 size to the pixels containing the weight of numerical value equal to one. To make the process of thresholding simpler, it is necessary to attain uniform illumination across an image using adaptive histogram equalization.

The block diagram of the proposed model is presented in Fig. 3.1.
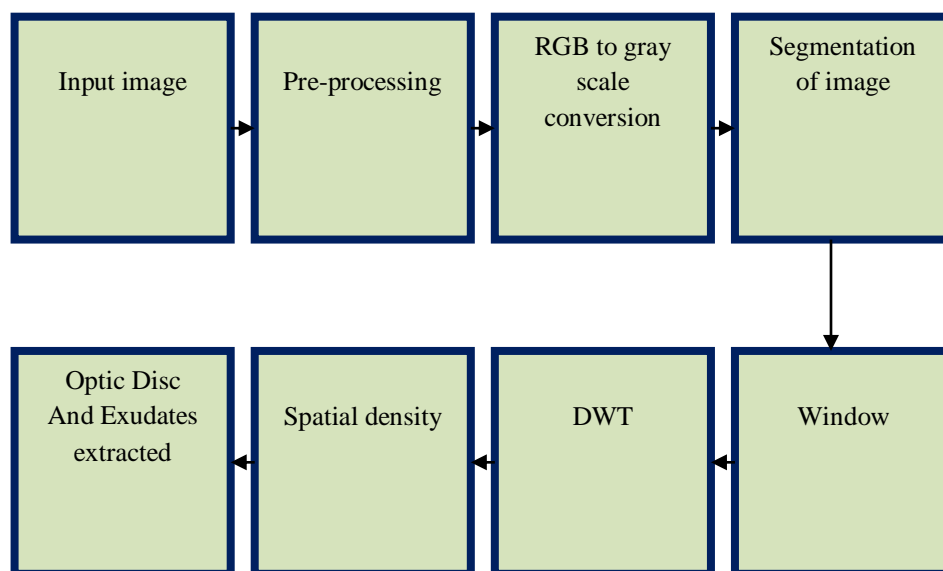
Fig. 3.1: Block diagram of the proposed optic disc and exudates detection framework

Conversion of the color image to gray scale: The processing of color images in a direct manner leads to take high complexity and therefore it is necessary to perform the grayscale conversion. In gray scale, one sample is represented by eight pixels called intensity information that may help to reduce complexity.

3.3.2 Blood Vessel Segmentation

Blood vessels present in the retinal images are segmented using mathematical morphology and wavelet transform. With the help of the thresholding method, the exudates and optic disc are segmented using Eq.(3.1).

$$C \oplus D = \bigcup_{d \in D} C_d \tag{3.1}$$

Where C and D represent the image to be dilated and structuring elements respectively. $\oplus$ is dilation operator and C_d is the translation of C by d.

The erosion operator is used to exclude the pixels present in the object boundaries to the background pixels using Eq.(3.2).

$$C \ominus D = \{Z \in E | \boldsymbol{D}_z \in C\}$$

(3.2)

Where E is Euclidean space and D_z is the translation of D by the vector z. Θ is erosion operator.

The noisy and bright pixels are available along the optic nerve's contour. The vessels are extracted from the fundus images to gather the noise into one connected object. Eq. (3.3) describes the matched filter used for extracting the vessels.

$$h = \frac{1}{\sqrt{S^H R_v^{-1}}} R_v^{-1} S$$

(3.3)

Where S and S^H represent desired signal and conjugate transpose of the desired signal respectively. R_v^{-1} represents inverse covariance matrix of the noise.

- **Detection of Optic Disc and Exudates:** The objects having less intensity background are minimized to return the objects in an undisturbed format. Owing to the color, the fundus image is composed of more data and therefore, it is transformed to a gray scale image having less content of data for processing further. In the next step, the image is segmented using a suitable threshold value, which returns the binary image as an output having bright objects. It is divided into several partitions known as windows. The window size is chosen appropriately. The spatial density is calculated by employing two-level DWT. The standard deviation and energy are calculated for all the window content. The optic disc is detected by the window having the highest standard deviation and energy. In some cases, two windows might contain higher standard deviation and energy then the optic disc is displayed by merging these two windows into one. The detected area may be composed of exudates and optic disc. Since the optic disc's area is more than that of the exudates, it is removed employing the area thresholding-based method. Since the erosion follows dilation, the morphological closing operation is accomplished on the eroded image to detect the exudates.

3.3.3 Segmentation of Optic Disc and Exudate

The thresholding of the image is represented as in Eq. (3.4), in which $Ip_{im}(i, j)$ represents the input image with pixels coordinates i and j.

$$Threshold = \begin{cases} 1; & \text{if } Ip_{im}(i,j) > LoT \\ 0; & \text{otherwise} \end{cases} \qquad (3.4)$$

Where *LoT* represents the threshold value of intensity.

The standard deviation and energy are called the spatial density, which is obtained by applying DWT to the windowed image. The spatial density is calculated as follows. The input retinal image is represented by Ip_{im}, a window is represented by $WIN \in Ip_{im}$, and its size is denoted by $U \times V$. The DWT coefficients are calculated by applying the two levels. The windows are chosen to counterpart with the optic disc area. The Ip_{im} retinal image is divided into several windows.

The algorithm of the proposed technique is provided in Algorithm 3.1.

Algorithm 3.1: Optic Disc and Eexudates detection
Input: Color fundus image

1. Perform the grayscale conversion from RGB image
    2. Perform adaptive histogram equalization for equal illumination
    3. Do mathematical morphology-based blood vessel segmentation
    4. Remove the blood vessels from the image
    5. Perform optic disc and exudates segmentation by a thresholding technique
    6. Divide the segmented image into multiple windows and apply DWT
    7. Identify the optic disc location
    8. Remove the optic disc by area thresholding to extract the exudates
    9. Display optic disc and exudates using features like standard deviation, mean and energy

Output: Retinal image classification based on the optic disc and exudates existence

For each window, the DWT coefficients are calculated and then the standard deviation and energy of those coefficients are computed as in Eq. (3.5) and Eq. (3.6).

The optic disc can be found from the segmented image area by calculating the following parameters.

$$EN = \frac{1}{U \times V} \sum_{i=1}^{U} \sum_{j=1}^{V} |WIN(i,j)| \qquad (3.5)$$

$$SD = \left[\frac{1}{U \times V} \sum_{i=1}^{U} \sum_{j=1}^{V} \left(WIN(i,j) - \mu I \right)^2 \right] \qquad (3.6)$$

Where i and j represent image coordinates, MXN represent the size of the image, μI represents the mean value of intensity, SD and EN represent standard deviation and energy vectors of the window WIN respectively and UXV represent the size of each window.

The final image displays the optic disc and exudates separately in the segmented retinal fundus images

3.4 Results and Discussions

The proposed technique is tested using the DIARETDB1 data set. The optic disc images are identified from the remaining parameters. The performance of the developed technique is calculated with sensitivity and specificity. The fraction of the pixels that are classified accurately is represented by sensitivity. The fraction of pixels that are wrongly classified as optic disc represents the specificity. Eq. (2.2) and Eq. (2.3) in section 2.5 of Chapter 2, describe the two parameters. In this analysis, 89 fundus images from the DIARETDB1 data set are tested and the outcomes are shown in Fig.3.2 and Fig.3.3, and performance of the method in terms of specificity and sensitivity is tabulated in Table 3.1

| (a)Input image | (b)Blood vessel segmented image | (c) Optic disc and exudates segmented image | (d) Sample windowed images |
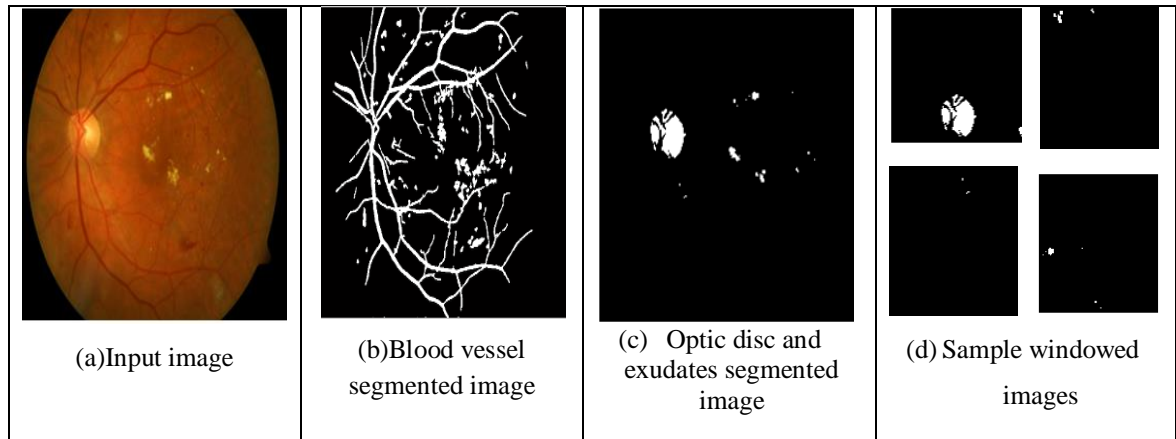
Fig.3.2 Segmentation of optic disc and exudates
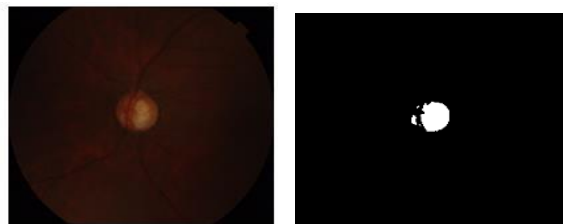
Fig. 3.3 Segmentation of optic disc

Table 3.1: Segmentation performance on STARE and DRIVE database for optic disc Detection

Method	TNF value (Specificity)	TPF value (Sensitivity)
Ahmed [55]	100%	94.74%
Walter [56]	100%	92.74%
Wavelet transform (Proposed)	100%	95%

3.5 Summary

In this chapter, the methodology has been utilized for DR detection and analysis of the optic disc and exudates. A new technique is proposed in the methodology using morphological operation and DWT to separate the optic disc from exudates with the help of windowing and wavelet transform technique increased detection accuracy from 92.74% to 95% on the DIARETDB1 datasets.

Chapter 4

Modified Levy Updated-Dragonfly Algorithm-based Approach

Chapter 3 provides segmentation of blood vessels, optic disc and exudates which help in detecting diabetic retinopathy, which is more effective for moderate and severe cases. In mild cases of diabetic retinopathy, accurate segmentation of blood vessels from the retina is the most important thing since the DR starts at blood vessels only. For accurate classification, efficient features extraction from segmented images plays a crucial role in classification accuracy.

4.1 Introduction

The DR diagnosis in the early stage is complex and also the identification approach is taking more time even for experienced specialists. In recent days, for the recognition of diverse diseases and progress examination, intelligent disease detection approaches are employed. Consequently, intelligent learning approaches are designed based on the computer-aided diagnosis method for the effective diagnose of DR using the benchmark dataset. The proposed DR diagnostic method based on modified Leavy updated dragonfly algorithm with neural network [57] is composed of four steps as "(a) Image Pre-processing, (b) Blood Vessel Segmentation, (c) Feature Extraction and (d) Classification". In the beginning, for pre-processing stage, the average filter and CLAHE are used. For the segmentation process, the execution of blood vessel segmentation is done by the optimized grey-level thresholding for segmenting the proper region of interest. After extracting the blood vessels, feature extraction is accomplished by the approaches like "local binary pattern (LBP), texture energy measure (TEM)" and two entropy computations such as Kapur's entropy and Shanon's entropy. Later, the gathered features are applied to a neural network (NN) classifier using an optimized training algorithm. This proposed algorithm called "Modified Levy Updated-Dragonfly Algorithm" is used for obtaining the optimal value of grey level thresholding and training of neural network in an optimal way. This algorithm enhances the accuracy of segmentation and decreases the error among the forecasted and real results of the NN. Lastly, this classification accuracy shows the effectiveness of the proposed DR detection method.

4.2 Related Work

In 2019, Chakraborty *et al*. [58] have labeled a supervised learning algorithm with Artificial Neural Network (ANN) for obtaining the best results in detecting DR. The features that were extracted from the input retinal images were subjected to the ANN-oriented classifier. By assessing many attributes of the existing ANN, the customized ANN was designed for enhancing the accuracy of the proposed model. ANN employed here was feed-forward Back Propagation Neural Network (BPNN). It has been confirmed that the developed approach provided the best outcomes in DR detection. In 2019, Leeza and Farooq [59] have suggested an improved automated model for detecting the severity of DR. This was dictionary-based and pre-processing methods where post-processing is not included. The proposed model combined the pathological representation of an explicit image into a learning outline. To calculate the descriptive features, points of interest were detected. For generating the dictionary, these features were grouped. Later, pooling and coding were subjected to compact the feature representation. To categorize the images into five classes such as mild, severe PDR, NPDR, moderate and normal. The method includes radial basis kernel SVM and NN as classifiers. Thus, the developed algorithm has provided good outcomes in detecting DR when compared to conventional algorithms.

In 2014, Franklin and Rajan [60] have introduced an algorithm for detecting the presence of exudates automatically, which was useful for the specialists in diagnosis and development of DR. By using their high grey-level variations, exudates were usually detected, which were employed by ANN by giving "size, texture, shape and color as the features". Using the DIARETDB1 dataset, the characteristics of the developed model were validated. The outcomes have proven that the proposed model was performing well in detecting DR. In 2011, Marin *et al*. [61] have introduced a new supervised learning algorithm for the blood vessel detection from the retinal fundus images. For pixel classification, this algorithm has employed NN, whereas, for pixel representation, 7-D vector consisted of "gray-level and moment invariants-based features" were computed. By using "STARE and DRIVE datasets", the proposed model was assessed. The results have proven that the proposed model was accurate for detecting vessels using STARE database images.

In 2018, Amin *et al*. [62] have recommended an automatic technique for "DR detection and classification". To improve the ROI, a local contrast improvement model was employed on grayscale images. For the accurate lesions region segmentation, an adaptive thresholding

approach with mathematical morphology was employed. Next, the "statistical and geometrical features" were joined for the best classification. By using E-aphtha, DIARETDB1, local datasets and MESSIDOR, the developed method was evaluated. In 2020, Kumar *et al*. [63] have offered an automatic model for early diagnosis by enhanced segmentation approaches for "blood vessels and optic disc". The early symptoms of DR are hemorrhages, red lesions and microaneurysms. For detecting hemorrhages and microaneurysms, improved models were proposed that were used for early diagnosis of DR. The developed DR detection model has included five phases like "pre-processing, blood vessel detection, fovea localization, optic disc segmentation, feature extraction and classification". To perform pre-processing and detecting blood vessels, mathematical morphology operation was employed, whereas for optic disc segmentation, watershed transform was utilized. The major intuition was to introduce enhanced segmentation approaches for "optic disc and blood vessels". For disease classification, Radial Basis Function Neural Network (RBF-NN) was used. Moreover, the RBF-NN was trained using the microaneurysms and hemorrhages features. Therefore, the accuracy of the developed model was analyzed based on specificity and sensitivity.

By using the K-means clustering algorithm, [64] introduced a novel approach for hard exudate detection. From the analysis, the sensitivity of the introduced model is high. During image acquisition, the developed model has little false detection because of artifacts and less contrast.

Osareh et al. [65] introduced an exudates detection system via the local contrast enhancement and color normalization. The implementation of neural networks, as well as the fuzzy C-means clustering, also took place. But the technique functioned only on LUV color space and the accuracy of detection was less for the non-uniform illumination. Akara et al. [66] described the exudates detection by an automatic technique for detecting the exudates having low contrast digital images with the help of an FCM clustering technique. Contrast enhancement preprocessing was subjected to four features as, "intensity, the standard deviation on intensity, hue and many edge pixels". These were revealed as input to the coarse segmentation by the FCM clustering technique. Rajput and Patil addressed a technique for the hard exudates detection [67] with the help of the k-means clustering algorithm. The sensitivity also showed better results. Yet, this suffered from false detection because of the very less artifacts and contrast in the image acquisition process.

A three-layered perceptron structure [68] namely "single output layer, single input layer and single hidden layer NN" is employed. Moreover, 243 neurons are considered as input, in which one neuron is considered as output and 50 hidden neurons. Here, a scaled conjugate gradient method was employed for detection. When an NN classifier is employed then the network output lies between 0 and 1.

4.3 Proposed Methodology

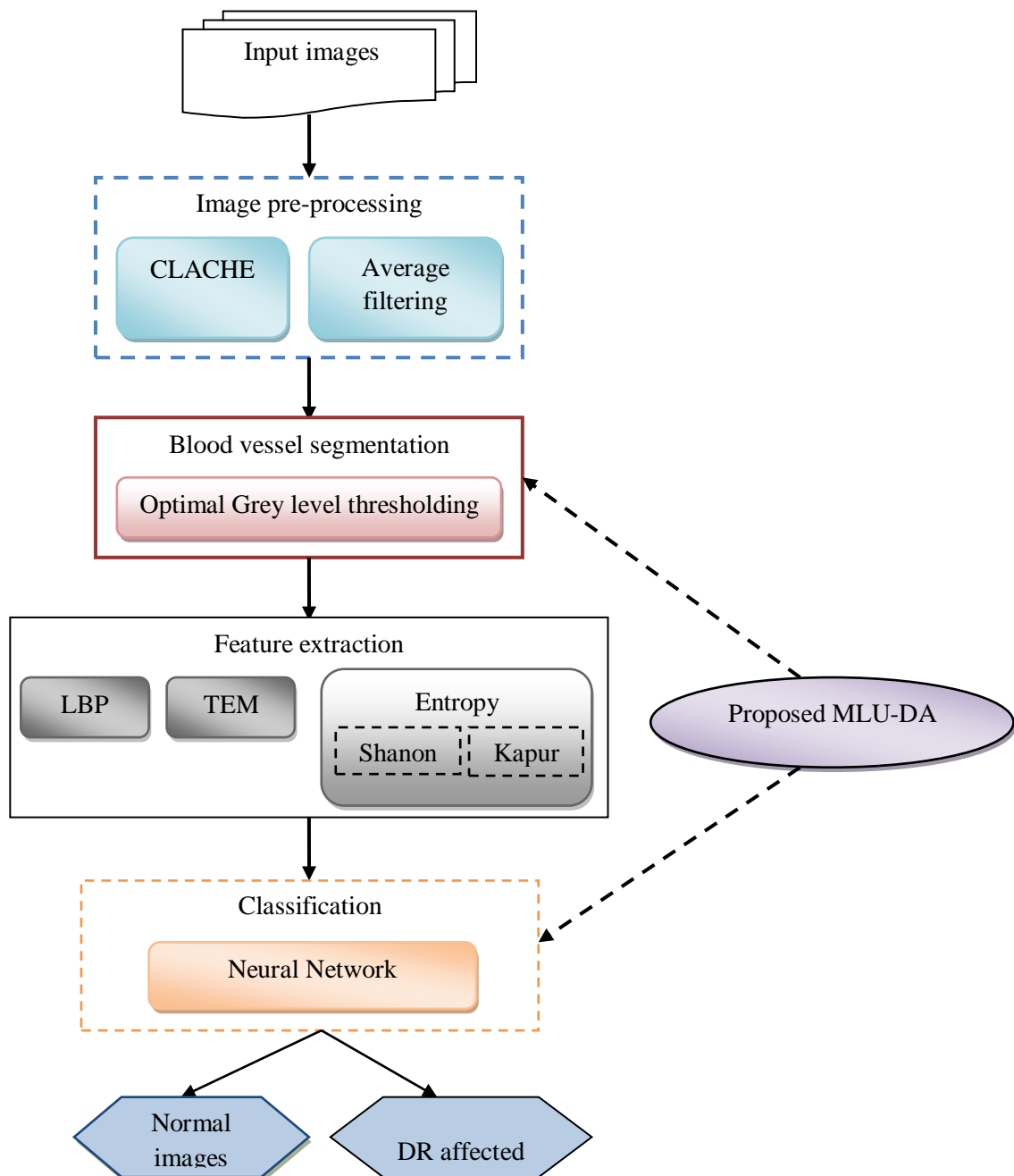The block diagram representation of the proposed DR detection model is given in Fig. 4.1.

Fig. 4.1: Block diagram representation of proposed DR detection method

In this, the DR detection model is presented for classifying the normal images and DR-affected images from various retinal images. These images are taken as the input images that are generally used for eye-related disease detection by the image processing approaches.

This DR diagnostic model is composed of four phases like "Image Pre-processing, Blood Vessel Segmentation, Feature Extraction and Classification". At the initial process, the input images are pre-processed using the average filter and CLAHE. To improve the local contrast, the CLAHE method is used, after applying the CLAHE the average filtering eliminates the noise from the input images that support protecting the sharp features. The pre-processed images are further employed for segmenting the blood vessels that is accomplished by a few processes. By using the grey-level thresholding method, the "contrast-enhanced and the filtered images" are thresholded. The key points such as K_1 and K_2 are extracted from the "contrast-enhanced images and the filtered images" using SIFT method respectively. The key points K_1 and K_2 with two images are differenced and thus subjected for grey level thresholding. To obtain the blood vessel segmented image, the key points extracted images and the enhanced images are combined. After segmenting the blood vessels the features are extracted by feature extraction processes like LBP, TEM and Entropy. The texture characteristics are described using the LBP method, the energy available in the region is found using TEM and the entropy like Shannon and Kapur metrics are applied to measure entropy. For the categorization of "normal images and abnormal images", the combined features are further applied to the NN-based classifier. The proposed DR detection model mainly relies on the two stages like classification and segmentation. The novel meta-heuristic algorithm is proposed for the classification and segmentation stages, which is known as "Modified Leavy Updated Dragonfly Algorithm (MLU-DA)". In the segmentation stage, the proposed MLU-DA is applied for the optimization of levels of thresholding in the Grey level thresholding method. This optimization is done for the accuracy maximization within the "ground truth and segmented images". The training Levenberg–Marquardt (LM) method is substituted using the suggested MLU-DA in the NN-based classification process, where the weight of NN using the proposed MLU-DA is updated for minimizing the classification error. Therefore in the "segmentation and classification" process, the developed MLU-DA is very reliable and robust for improving the DR diagnostic system. Here the labels are correctly assigned to the retinal fundus images for categorizing the normal and DR affected images having more accuracy.

Consider the input image is represented as Ip_{im} for DR detection, the contrast-enhanced image using CLAHE approach is denoted as Ip_{CLAHE}, the blood vessel segmented image is represented as Ip_{seg}, the average filtered image is termed as Ip_{filt}, and from the segmented blood vessels, the entire features extracted are termed as FE_{fea}, where $fea=1,2,\cdots,nf$, here the number of features are termed as nf.

4.3.1 Pre-processing

The input images are subjected to the pre-processing stage, where it is done by CLAHE and average filtering methods.

- **Contrast Limited Adaptive Histogram Equalization (CLAHE)**

CLAHE is utilized for improving the image contrast and it is providing the optimal equalization in terms of the highest entropy and also limits the image brightness. CLAHE is implemented by the following sequential processes such as splitting of each input image into the same size including 8×8 blocks of contextual regions that are in a non-overlapping manner, each image will be combined to the neighborhood of 64 pixels. Secondly, for each contextual region, compute the intensity histogram. Thirdly, the clip boundaries are assigned for clipping the histograms and it is fixed as the least optimal value that is represented as the threshold parameter for adapting the image brightness effectively. Further, change each histogram by selecting the transformation functions. The modification of each histogram is done by the boundary of the preset clip limit. The mathematical representation is depicted in Eq. (4.1).

$$Pv = \left[Pv_{\max} - Pv_{\min}\right] * CPD(bv) + Pv_{\min} \tag{4.1}$$

Here, the estimated pixel value is defined as Pv, where the maximum pixel value and the minimum pixel value are represented as $Pv_{\max}$ and $Pv_{\min}$ respectively, the brightness level is represented as bv and the cumulative probability distribution is shown as $CPD(bv)$. Modify the gray level for exponential distribution based on Eq. (4.2).

$$Pv = Pv_{\min} - \left(\frac{1}{\alpha}\right) * \ln\left[1 - CPD(bv)\right] \tag{4.2}$$

In Eq. (4.2), the clip parameter is indicated as α. CLAHE technique is efficient because of the ability to work on tiny image parts that are known as tiles other than the whole image. It improves the brightness of every tile, thus enables the matching of each histogram output

region with the histogram stated via the distribution type. Finally, with the help of the bilinear interpolation method, the neighboring tiles are joined and the grayscale values are altered. The CLAHE pre-processed images are termed as Ip_{CLAHE} that is given to the average filter for filtering operation.

- **Average Filtering:** The pattern of the target pixel is improved by the average filtering method, after this, the average is taken for all the pixel values. The image feature aids to examine the image shape and size. The average filtering for an image Ip_{CLAHE} is represented in Eq. (4.3).

$$Ip_{filt} = \frac{1}{S \times T} \sum Ip_{CLAHE}(i, j) \tag{4.3}$$

Where $S \times T$ is the size of the mask.

4.3.2. Blood Vessel Segmentation

After pre-processing the images are given to the process of segmentation. The below steps are considered for segmenting the blood vessels. Initially, the SIFT [69] operation is applied for the pre-processed images like Ip_{CLAHE} and Ip_{filt} get two images along with their key points. Moreover, by using the optimized grey-level thresholding the variation among these two images along with their two groups of key points are found. Later, a morphological operation referred to as area opening is applied for the elimination of the small pixels. After applying the "optimized grey-level thresholding and morphological operation", the subtraction is performed among Ip_{CLAHE} and Ip_{filt}. Finally, the final segmented image is obtained by combining the two images.

The gray level thresholding approach segments the blood vessels that are based on the conviction about the image that has a bimodal histogram. Thus a simple method is developed for object extraction. For this operation, the level of threshold is employed that is considered as *LoT* for dividing the modes. The representation of the threshold value for an image is mentioned in Eq. (4.4), which leads to a binary image.

$$Ip_{thresh} = \begin{cases} 1 & if \ Ip(i, j) > LoT \\ 0 & if \ Ip(i, j) \leq LoT \end{cases} \tag{4.4}$$

In the above equation, the pixel along with the intensity value 1 of the image is the same as the objects and 0 is the same to the background. The proposed segmentation process is based

on the optimization of the threshold level LoT by using the proposed modified levy updated dragonfly algorithm that affects achieving better segmentation accuracy. Therefore the segmented image is obtained and it is represented as Ip_{seg}.

The proposed DR detection model mainly focuses on two sections like segmentation and classification. The accuracy of the segmentation should be maximized and minimal detection error should be achieved. Initially the accuracy among the "segmented blood vessels and the ground truth image" is maximized. To attain the above-mentioned objective function, the modification is done in the grey level thresholding, where the proposed MLU-DA is employed for controlling the levels of thresholding.

The objective function is formulated in Eq. (4.5).

$$Obj1 = Max(Acc) \tag{4.5}$$

The accuracy is termed as Acc that is given in Eq. (2.1), of section 2.5.

The second objective is reducing the detection error. This is done by the error variation among detected outcomes and the actual outcome. It is given in in Eq. (4.6)

$$Obj2 = Min(EF) \tag{4.6}$$

Where, EF is the error function.

The proposed MLU-DA is utilized for optimizing the segmentation and classification phases and the solution encoding for the above stages is given in Fig.4.2. Here, the thresholding levels are optimized in the grey level thresholding-based segmentation phase. Here the level is denoted as Le in the range of [-20, 20]. The weights are updated by the proposed MLU-DA in the neural network classifier.
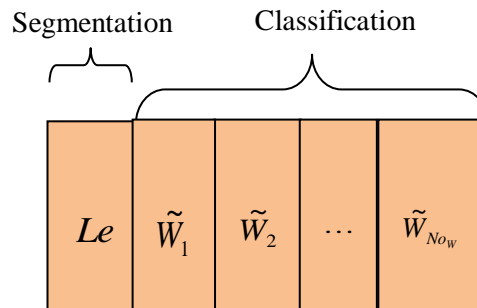

Fig. 4.2: Solution encoding for the developed DR detection method in the classification and segmentation

4.3.3 Feature Extraction

The segmented blood vessels are given for the feature extraction process that is carried out by three methods like "Local Binary Pattern, Texture Energy Measure and Entropy".

i) Local Binary Pattern(LBP)

Local Binary Pattern [70] is effectively used for several applications since texture features are significant due to the strong and efficient texture descriptor. The image pixels are labeled by the LBP operator using the neighborhood thresholding of every pixel among the middle value, thus the result is obtained in binary number form. A descriptor is considered by the labeled image histogram $Ip_{seg}(i, j)$ that is given in Eq. (4.7).

$$HG_{im} = \sum_{i,j} In(Ip_{seg}(i, j) = im), im = 0, \cdots, nl - 1 \tag{4.7}$$

The number of labels is represented as nl that is given by the LBP operator and if A is true then $In(A) = 1$, and if A is false then the value of $In(A)$ is 0. A uniformity measure (UM) is described based on Eq. (4.8), for obtaining a rotation-invariant uniform pattern by considering a PB-bit binary number as $LBP_{PB,RB}$, where $(ro_{PB-1}, ro_{PB-2}, \cdots, ro_1, ro_0)$ Here, the values are ≤ 2 in Eq. (4.9).

$$UM(LBP_{PB,RB}) = |ro_{PB-1} - ro_0| + \sum_{PB=1}^{PB-1} |ro_{PB} - ro_{PB-1}| \tag{4.8}$$

$$LBP_{PB,RB} = \begin{cases} \sum_{pb=0}^{PB-1} Ip(gr_{cp} - gr_{cv}) & \text{if } UM(LBP_{PB,RB}) \leq 2 \end{cases} \tag{4.9}$$

Here, the gray value is termed as gr_{cp}, and the gray value of PB points is denoted as gr_{cv}, $pb = 0, \cdots, PB - 1$. The circles are selected with several radii over the center pixels by using LBP and also a multi-scale examination is executed. After that, LBP images are divided for each scale. "Energy and entropy" of the LBP image are built around a diverse count of pixels that are used as feature descriptors.

ii) Texture Energy Meausure(TEM)

For calculating the TEM, Law's mask [71] is considered for the better performance on texture descriptor that is used for various applications. The energy presented in the filter regions are estimated based on the alterations of texture energy pleaded to the image. Further, all masks are obtained from 1-D vector five pixels lengths like $W5, E5, S5, R5, and L5$ that are

represented as the wave, edge, spot, ripple and level, respectively. From the segmented image Ip_{seg}, the texture data is extracted by the convolution of images with 2D mask. If the filter is used as $L5$ and $E5$ the abtained texture image depends on the Eq. (4.10)

$$Text_{L5E5} = Ip_{seg}(i, j) \otimes L5E5 \qquad (4.10)$$

To normalize the contrast of the residual texture images $Text(i, j)$, the texture image $Text_{L5L5}$ is used; this is given in Eq. (4.11).

$$Nor\,(Text_{(i,j)}) = \frac{Text_{(i,j)}}{Text_{(i,j)^{L5E5}}} \qquad (4.11)$$

The results are moved to the TEM filter, which contains the moving non-linear window average of total values as defined in Eq. (4.12).

$$TEM_{(i,j)} = \sum_{p1=-7}^{7} \sum_{q1=-7}^{7} \left| Tex_{(i+p1, j+q1)} \right| \qquad (4.12)$$

An invariant TEM is denoted as IT that is obtained by combining the entire 25 TEM descriptors and $p1$ and $q1$ are constants. IT is given in Eq. (4.13).

$$IT_{E5L5} = \frac{TEM_{E5L5} + TEM_{L5E5}}{2} \qquad (4.13)$$

iii) Entropy

Generally, entropy is defined as "the uncertainty associated with the randomness". For the proposed DR detection model there are two entropy approaches considered that are Shannon and Kapur entropy. Consider the segmented image as $Ip_{seg}(i, j)$ with different gray values Gv_{di}, where ($G_{V_{di}} = 0,1,2......AL-1$). The normalized histogram is defined for a particular area of interest with the size $(me \times ne)$ that is given in Eq. (4.14).

$$Ent_{di} = \frac{Gv_{di}}{me \times ne} \qquad (4.14)$$

Furthermore, Shannon entropy is formulated in Eq. (4.15), where Ent_{di} represents different entropy values. Kapur entropy contains an additional dynamic range over a broadcasting rule range and this is applied for the evaluation of scatter density and regularity.

$$Sha = -\sum_{di=0}^{AL-1} Ent_{di} \log_2(Ent_{di}) \qquad (4.15)$$

Kapur's entropy is given in Eq. (4.16).

$$Ka_{\beta,\delta} = \frac{1}{\delta - \beta} \log_2 \frac{\sum_{di=0}^{AL-1} Ent_{di}^{\beta}}{\sum_{di=0}^{AL-1} Ent_{di}^{\delta}} \qquad (4.16)$$

Here, the coefficients are represented as $\beta \, and \, \delta$ where $\beta \neq \delta$. Therefore, the grouping of three features sets like "LBP, TEM and entropy" is defined as FE_{fea}, in which $fea = 1,2,\cdots,nf$, and the count of features is termed as nf.

4.4 Dragonfly Algorithm (DA)

The DA is inspired by the behavior of swarms in nature either in dynamic or static nature. The swarm entities are fighting against enemies for getting their food. By using the conventional DA, the positions are updated based on the important factors like "Cohesion, alignment, separation, attraction and distraction" that are inspired by the dragonfly behavior. The division of dr^{th} dragonfly is built its neighbors as Ne_{dr} that is given in Eq. (4.17).

$$Ne_{dr} = -\sum_{ni=1}^{CN}(Lo - Lo_{ni}) \qquad (4.17)$$

Here, the location of the present individual is termed as Lo the count of neighboring individuals is represented as CN and the location of ni^{th} the neighboring individual is denoted as Lo_{ni}. Subsequently, alignment is calculated by Eq. (4.18).

$$Align_{dr} = \frac{\sum_{ni=1}^{CN} Ve_{ni}}{CN} \qquad (4.18)$$

In Eq. (4.18), Ve_{ni} is the velocity of ni^{th} the neighbouring individual. Likewise, the control cohesion of ni^{th} the dragonfly CC_{dr} is described in Eq. (4.19). The attraction in the direction of food is computed based on the Eq. (4.20).

$$CC_{dr} = \frac{\sum_{ni=1}^{CN} X_{ni}}{CN} - Lo \qquad (4.19)$$

$$AF_{dr} = FL - Lo \qquad (4.20)$$

Here, the location of source of food is referred to as FL and Lo is the location of present individual. The distraction towards the enemy is measured using Eq. (4.21).

$$DE_{dr} = En + Lo \qquad (4.21)$$

In Eq. (4.22), the position of the enemy is specified as En. For updating the positions of dragonflies, two vectors are taken such as step(ΔLo) and position (Lo) vectors. Moreover, the movement of each dragonfly is described using the concept of particle swarm optimization [72] and step vector that is calculated based on Eq. (4.22).

$$\Delta Lo_{itr+1} = (neNe_{dr} + alignAlign_{dr} + ccCC_{dr} + afAF_{dr} + deDE_{dr}) + \delta \bullet \Delta Lo_{itr} \qquad (4.22)$$

Here, the current iteration is denoted as itr the separation weight and the separation of dr^{th} individuals are termed as ne and Ne_{dr} respectively. The alignment weight and the alignment of dr^{th} individuals are denoted as $align$ and $Align_{dr}$ respectively. The food factor and the food source of dr^{th} the dragonfly are termed as af and AF_{dr} respectively. "The weight of cohesion, the cohesion of dr^{th} individual, the enemy factor, the location of an enemy of the dr^{th} individual and the weight of inertia" are represented as cc, CC_{dr}, de, DE_{dr} and δ, respectively. Eq. (4.22) describes the step vector. The position vector is measured using Eq. (4.23).

$$Lo_{itr+1} = Lo_{itr} + \Delta Lo_{itr+1} \qquad (4.23)$$

Eq. (4.24) describes the updated location of the dragonfly. Moreover at the moment, by using Eq. (4.25), Eq. (4.26), Eq. (4.27), and Eq. (4.28), the dragonflies are updated.

$$Lo_{itr+1} = Lo_{itr} + Levy(pv) \times Lo_{itr} \qquad (4.24)$$

$$Levy(pv) = 0.01 \times \frac{r_1 \times \phi}{|r_2|^{\frac{1}{pv}}} \qquad (4.25)$$

Here, the random numbers are termed as r_1 and r_2 in the interval of [0, 1], and the location vector is shown as pv and ϕ is the direction of movement of a dragonfly.

The Euclidean distance is calculated between all the dragonflies for establishing the neighborhood of an individual dragonfly and the values like Lo and ΔLo are updated. The conventional DA algorithm is given in Algorithm 4.1.

Algorithm 4.1: Pseudo code of conventional DA
Input: Image pixels weight function of NN
1. Initialize X and ΔX
2. while the final state is not fulfilled
3. Update source of enemy & food
4. Update the terms δ, se, al, co, af, and de
5. Calculate Se, Al, Co, AF, and DE
6. Update the neighbor's radius
7. if a dragonfly is composed of at least one neighboring dragonfly
8. Update velocity vector by Eq. (4.23)
9. Update position vector by Eq. (4.24)
10. Else
11. Update position vector by Eq. (4.25)
12. end if
13. Confirm the updated solution by fitness evaluation
14. end while
Output: Optimized threshold value and weight functions of NN

- **Modified Levy Updated Dragonfly Algorithm:** The conventional DA also has limitations such as unbalanced exploitation and exploration, and premature convergence. To develop and implement the performance of conventional DA and an effective system, the phases like segmentation and classification are improved using the proposed modified algorithm called MLU-DA. As an improvement, the levy update based on Eq. (4.25) is replaced using the new formula Eq. (4.26).

$$Lo_{itr+1} = wf \times Lo_{itr} + af\left(FL - Lo_{itr+1}\right) \tag{4.26}$$

Here, the weight function is referred to as wf. For the proposed MLU-DA algorithm, this new updating rule offers better convergence. The algorithm of the suggested MLU-DA is given in Algorithm 4.2.

Algorithm 4.2: Pseudocode of proposed MLU-DA
Input: Image pixels and weight function of NN

1. Initialize X and ΔX

2. while (the final condition is not satisfied)

3. Update source of enemy & food

4. Update the terms δ, se, al, co, af, and de

5. Calculate Se, Al, Co, AF, and DE

6. Update the neighbours radius

7. if a dragonfly is composed of at least one neighbouring dragonfly

8. Update velocity vector by Eq. (4.24)

9. Update position vector by Eq. (4.25)

10. Else

11. Update position vector by Eq. (4.26).

12. end if

13. Confirm the updated solution by fitness evaluation

14. end while

Output: Optimized threshold value and Optimized weight function of NN

4.5. Classification using Optimized Neural Network

The "normal and abnormal images" are categorized based on the NN classifier where the input is given as FE_{fea}. Because of the flexibility of NN [73], it is suitable for classification in various applications. A modification is done in the training of NN this is given in Fig. 4.3.
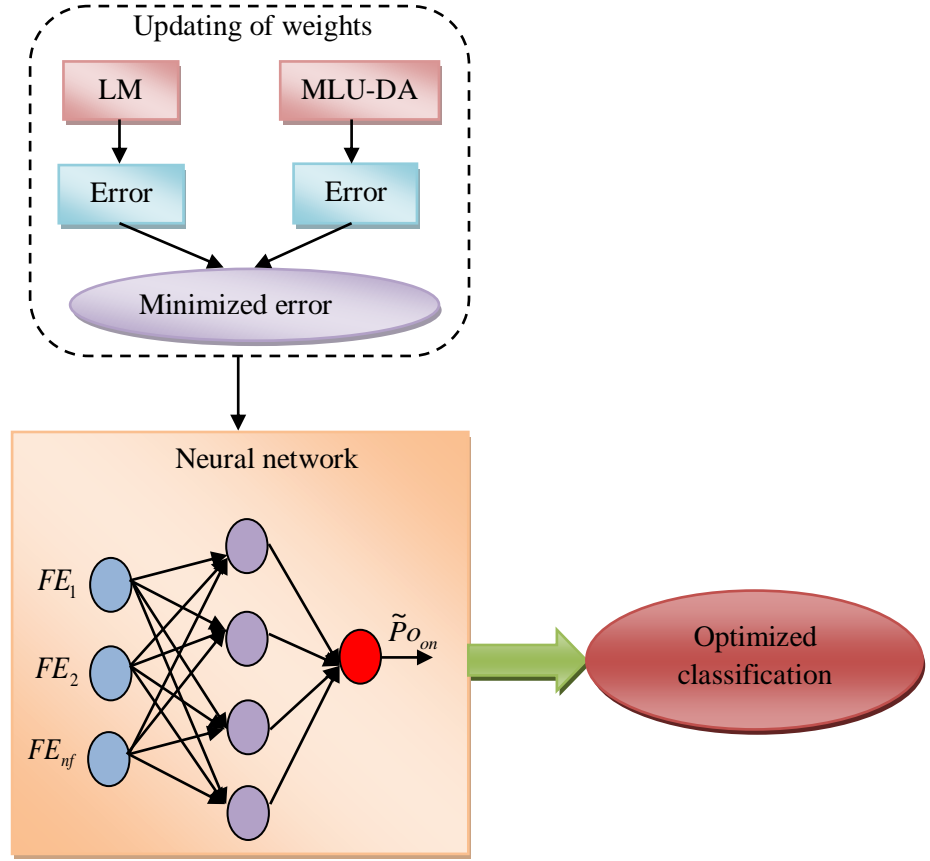
Fig. 4.3: Updating of weights in NN using proposed MLU-DA

The error difference is calculated among the predicted outcome and the actual outcome that must be reduced using the weight optimization by proposed MLU-DA.
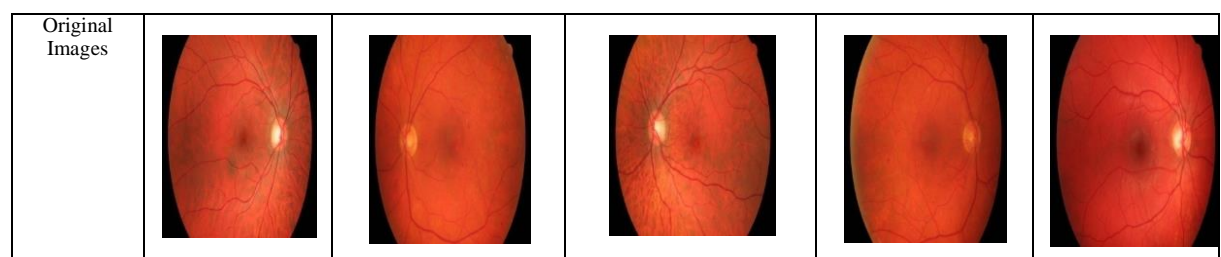
4.6 Results and Discussions

The developed DR diagnosis model is developed in MATLAB 2018a, and the results are obtained by conducting simulations. The dataset was collected from "https://www5.cs.fau.de/research/data/fundus-images/:" for the experimentation. Here, the experiments were conducted by considering the count of iteration as 100 and the population size as 50. The segmentation was analyzed by comparing the proposed MLU-DA with conventional methods like WOA [74], GWO [75], DA and PSO-oriented gray-level thresholding. The performance of the classification was evaluated with the individual and combined features (LBP + TEM + Entropy). Additionally, the standard LM-NN was contrasted with the optimally trained NN for evaluating the performance. Various performance metrics are examined to show the characteristics of the suggested MLU-DA-based segmentation and classification that are "Accuracy, Sensitivity, Specificity, Precision, FPR, FNR, NPV, FDR, F1 score and MCC".

Here, the performance is analyzed based on the performance metrics like, "Accuracy, Sensitivity, Precision, False positive rate, False negative rate, Negative predictive value, False discovery rate, F1 score and Mathew correlation coefficient" which are explained with mathematical representation in section 2.5 of chapter 2.

- **Analysis of Segmentation**

The segmentation analysis is improved by the gray level thresholding. The characteristics of the optimized segmentation is estimated by differentiating the proposed MLU-DA-oriented gray-level thresholding with the traditional optimization algorithms such as "PSO, GWO, WOA, and DA-based thresholding", hence the results of the segmented images are given in Fig.4.4 and the performance metrics evaluation is given in Table 4.1. Various performance metrics are evaluated to demonstrate the characteristics of the segmentation analysis. The accuracy of the segmentation analysis on developed MLU-DA is improved than the existing algorithms. It is 0.178% improved than traditional gray-level thresholding and 0.183% improved than PSO and GWO and 0.19% improved than WOA and DA-based thresholding respectively, which is tabulated in Table 4.1. For the proposed MLU-DA, the precision is 1.22% enhanced than traditional gray-level thresholding, 1.27% enhanced than GWO and WOA based gray-level thresholding, 1.21% enhanced than PSO-based gray-level thresholding and 1.22% enhanced than DA-oriented gray-level thresholding. The sensitivity is calculated for the proposed MLU-DA algorithm that shows better results than the conventional methods. It is 13.9% superior to existing gray-level thresholding, 14.2% advanced than PSO-based gray-level thresholding, 15% better than GWO and WOA-oriented gray-level thresholding and 14.6% progressed than DA-oriented gray-level thresholding. Likewise, the other performance measures are also evaluated and show the enhanced performance for the proposed segmentation method. These results are used to validate the consequences of the optimized thresholding on segmenting the blood vessels. Hence, the results are proved that the performance of the proposed segmentation using the developed MLU-DA algorithm is efficient.
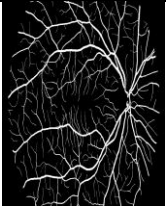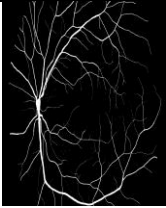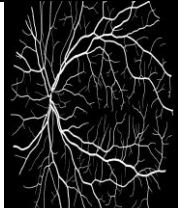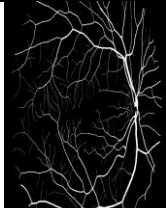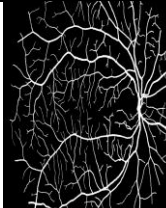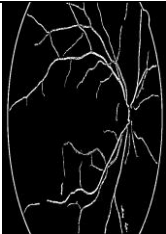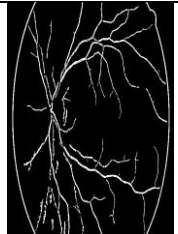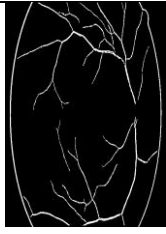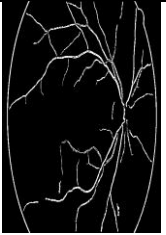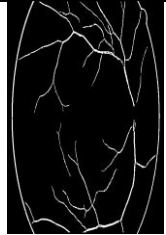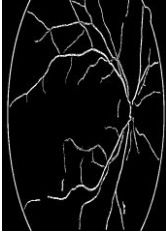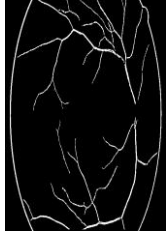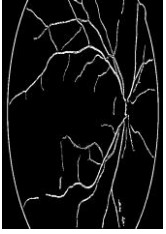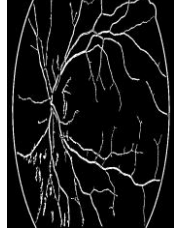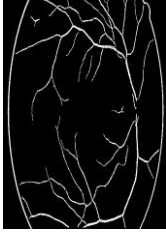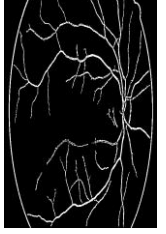
	(a)	(b)	(c)	(d)	(e)
Ground Truth Images					
Segmented Results					
Traditional gray level thresholding					
PSO-oriented gray level thresholding					
GWO-based gray level thresholding					
WOA-oriented gray level thresholding					
DA-based gray level thresholding					
MLU-DA oriented gray level thresholding					

Fig. 4.4: Experimental outcomes for pre-processing and segmentation for DR detection

Table 4.1: Analysis of the developed blood vessel segmentation by optimized and standard gray level thresholding

Performance Measures	Traditional gray level thresholding	PSO-oriented gray level thresholding [72]	GWO- based gray level thresholding [75]	WOA-oriented gray level thresholding [74]	DA- based gray level thresholding [110]	MLU-DA oriented gray level thresholding (Proposed)
MCC	0.5145	0.5136	0.5119	0.5119	0.5127	**0.5473**
F1-Score	0.5371	0.5362	0.5341	0.5341	0.5351	**0.5759**
FDR	0.3421	0.3422	0.3418	0.3418	0.3421	**0.3502**
NPV	0.9792	0.9793	0.9795	0.9795	0.9794	**0.9755**
FNR	0.5460	0.5474	0.5505	0.5505	0.5489	**0.4827**
FPR	0.0207	0.0206	0.0205	0.0205	0.0206	**0.0244**
Precision	0.6578	0.6577	0.6581	0.6581	0.6578	**0.6497**
Specificity	0.9792	0.9793	0.9795	0.9795	0.9794	**0.9755**
Sensitivity	0.4539	0.4525	0.4494	0.4494	0.4510	**0.5172**
Accuracy	0.9368	0.9368	0.9367	0.9367	0.9367	**0.9385**

- **Analysis of Texture Feature**

The texture analysis is done to show the characteristics of the grouping of "LBP and TEM". The performance is compared with the proposed joined features with the individual features of a conventional algorithms-based NN classifier. The analysis of the performance of texture is depicted in Fig. 4.5, and in Table 4.2, the overall performance analysis for the texture analysis is shown, by comparing various performance metrics. The accuracy of the joined-MLUDA-NN is higher while compared to the other individual features when the exact classification of the labels is done at the desired learning percentages. For the learning percentage at 90%, the accuracy of the joined-MLUDA-NN is 62%, 100% and 53.8%, progressed than T-MLUDA-NN, T-PSO-NN and T-DA-NN respectively, which is given in Fig. 4.5. (a). Better sensitivity is attained for the entire learning percentages for the proposed combined-MLUDA-NN. It is 15.2% and 8.88% surpassed than T-GWO-NN and -MLUDA-NN respectively, with consideration of the learning percentage as 50%. For the suggested combined-MLUDA-NN, the specificity performance is enhanced for accurately identifying the true negative that is 42.8% and 11.1% enhanced than T-PSO-NN and T-MLUDA-NN, respectively for the learning percentage as 70% and this is given in Fig. 4.5(c). Likewise, better precision is obtained for combined-MLUDA-NN for all the learning percentages that is 65% superior to T-GWO-NN, 100% better than T-PSO-NN and T-MLUDA-NN, and 66.6%

advanced than T-DA-NN. Correspondingly, the performance of the FDR and FPR is minimized for the proposed combined-MLUDA-NN when considering entire learning percentages. The FNR is calculated for the learning percentage as 20% and the better performance is obtained for the proposed combined-MLUDA-NN. Form Fig. 4.5 (f), it is 66.6% and 50% superior to T-GWO-NN and T-MLUDA-NN respectively for the learning percentage 20. For the proposed joined-MLUDA-NN, the NPV is obtained better for all the learning percentages when compared to the individual features. It is 75%, 100%, and 33.3% more than T-PSO-NN, T-DA-NN and T-MLUDA-NN respectively for the learning percentage at 90% that is given Fig. 4.5 (g). From Table 4.4, the overall performance is measured by analyzing various performance measures and it proves the better performance for the proposed combined-MLUDA-NN method. The accuracy of the proposed joined-MLUDA-NN is 7.69%, 16.6%, 3.70% and 12% improved than T-DA-NN, T-MLUDA-NN, T-LM-NN and T-GWO-NN and T-PSO-NN respectively. Similarly, for the proposed joined-MLUDA-NN method, the precision is improved than individual features. It is 16.6%, 7.69%, 6.67% and 8.88% progressed than T-MLUDA-NN, T-DA-NN, T-LM-NN and T-PSO-NN and T-GWO-NN respectively. Therefore it is established that the recommended joined-MLUDA-NN model performance is higher than the conventional methods that are considered from the tabular format and graphical representation.
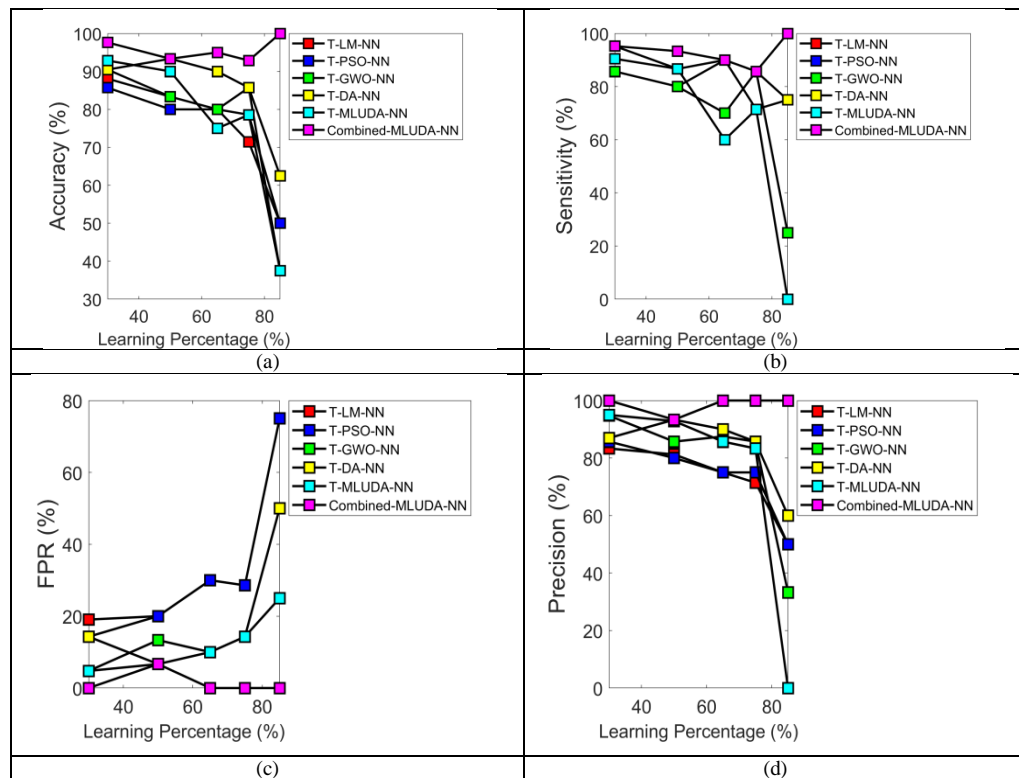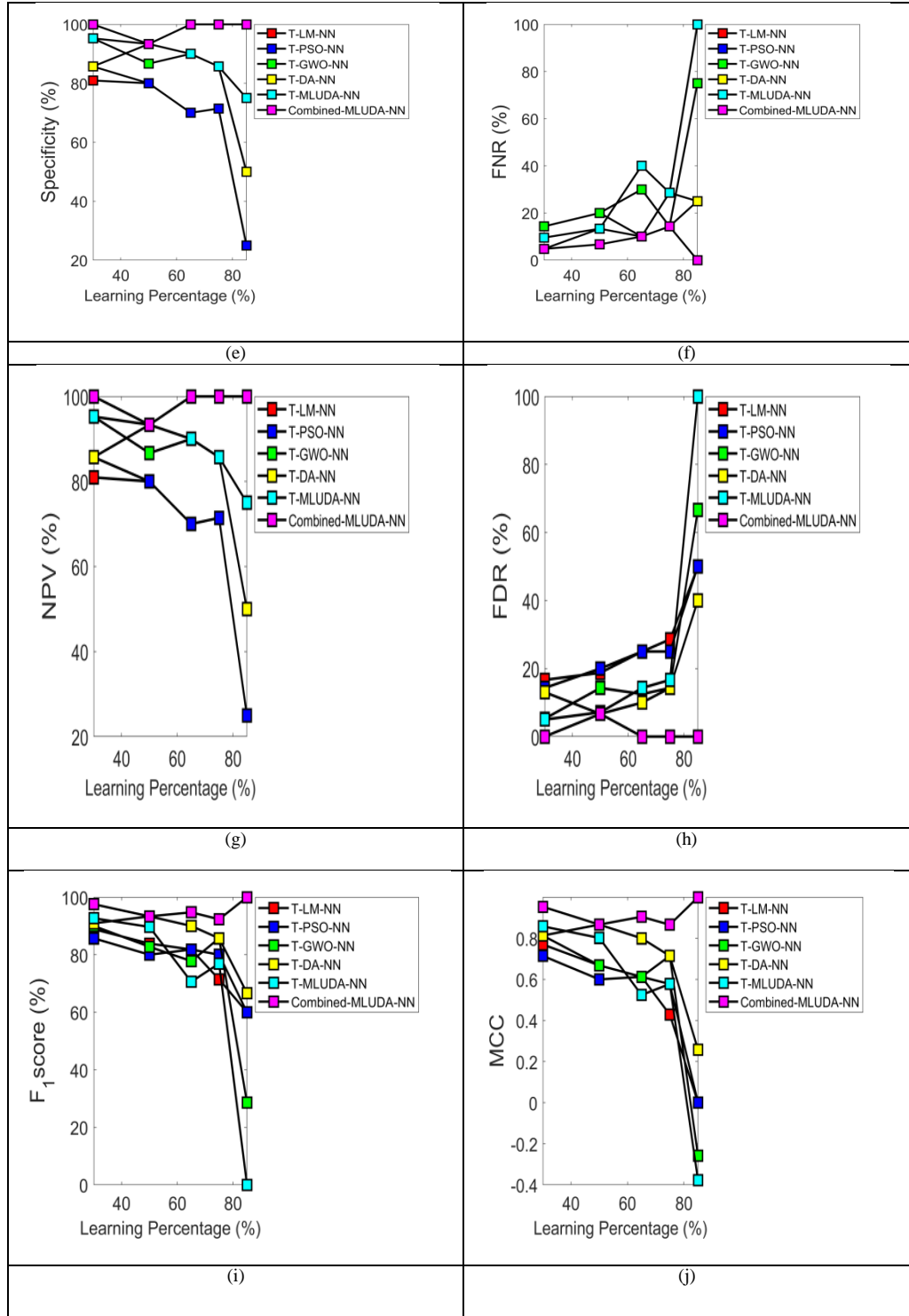
Fig. 4.5: Texture-oriented feature extraction analysis by analysing performance measures "(a) Accuracy, (b) Sensitivity, (c) Specificity, (d) Precision, (e) FPR, (f) FNR, (g) NPV, (h) FDR, (i) F1 score, and (j) MCC"

Table 4.2: Texture feature analysis for joint features and also with optimal trained NN

Performance Measures	T-MLUDA-NN	T-DA-NN [110]	T-GWO-NN [75]	T-PSO-NN [72]	T-LM-NN [73]	Combined-MLUDA-NN (Proposed)
MCC	0.6000	0.7333	0.6681	0.6681	0.8165	**0.8666**
F1-Score	0.8000	0.8666	0.8275	0.8275	0.8888	**0.9333**
FDR	0.2000	0.1333	0.1428	0.1428	0.0000	**0.0666**
NPV	0.8000	0.8666	0.8666	0.8666	1.0000	**0.9333**
FNR	0.2000	0.1333	0.2000	0.2000	0.2000	**0.0666**
FPR	0.2000	0.1333	0.1333	0.1333	0.0000	**0.0666**
Precision	0.8000	0.8666	0.8571	0.8571	1.0000	**0.9333**
Specificity	0.8000	0.8666	0.8666	0.8666	1.0000	**0.9333**
Sensitivity	0.8000	0.8666	0.8000	0.8000	0.8000	**0.9333**
Accuracy	0.8000	0.8666	0.8333	0.8333	0.9000	**0.9333**

- **Analysis of Entropy Feature**

The entropy features are analyzed by comparing the proposed combined-MLUDA-NN model with the conventional optimization-based NN classifier using the various performance metrics that are depicted in Fig. 4.6 and Table 4.3. The learning percentage is considered as 20% for the proposed combined-MLUDA-NN, the accuracy is advanced than conventional methods. It is 11.3%, 5.37%, 8.88% and 2.08% better than E-MLUDA-NN, E-PSO-NN, E-GWO-NN and E-DA-NN respectively. Similarly, the suggested combined-MLUDA-NN model is showing the improved characteristics for the entire measures when differentiated to various conventional methods.
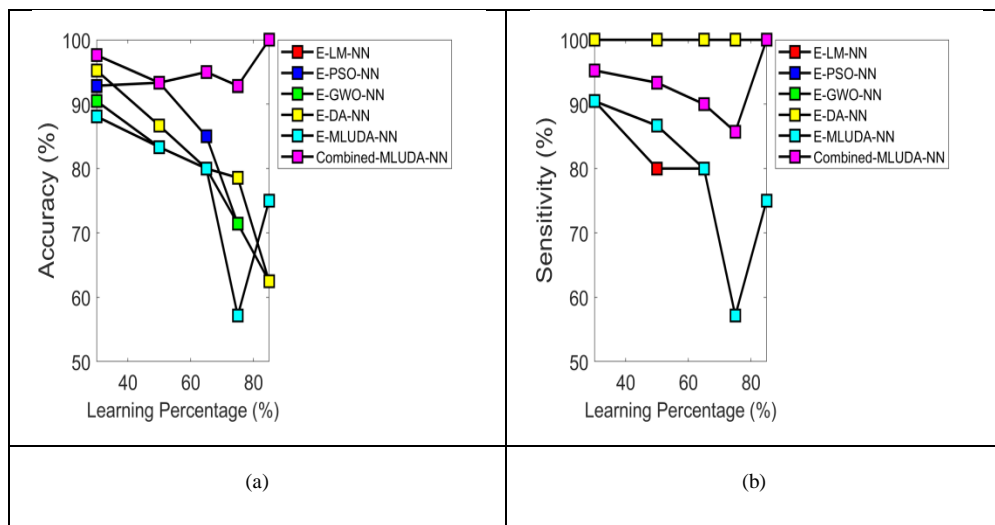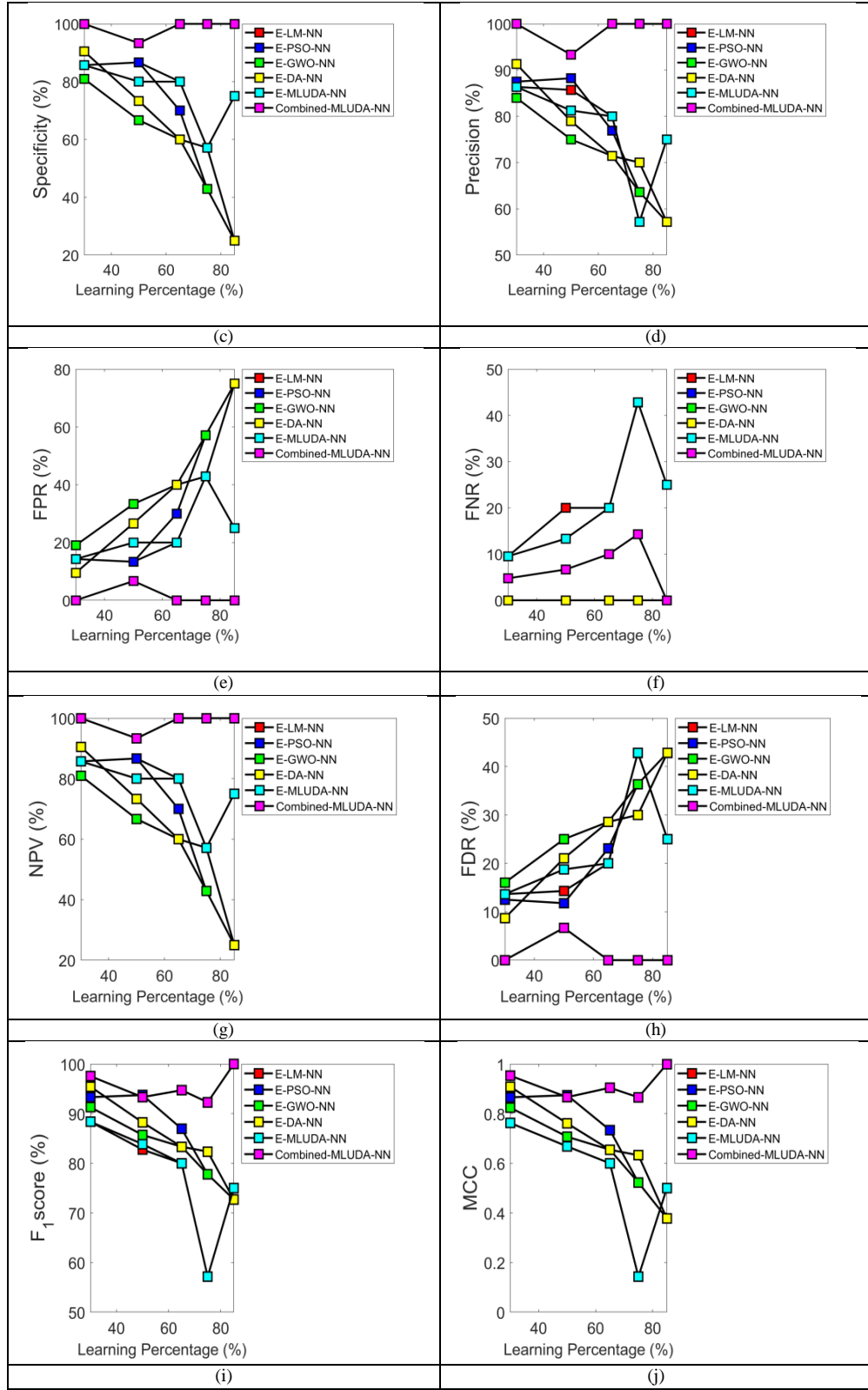
Fig. 4.6: Entropy-oriented feature extraction analysis by analyzing the performance metrics

"(a) Accuracy, (b) Sensitivity, (c) Specificity, (d) Precision, (e) FPR, (f) FNR, (g) NPV, (h) FDR, (i) F1 score, and (j) MCC"

Table 4.3: Feature analysis of entropy-based combined features with optimally trained NN

Performance Measures	E-MLUDA-NN	E-GWO-NN [75]	E-PSO-NN [72]	E-LM-NN [73]	E-DA-NN [110]	Combined-MLUDA-NN (Proposed)
MCC	0.6681	0.8165	0.6681	0.8165	0.7333	**0.8666**
F1-Score	0.8387	0.8888	0.8275	0.8888	0.8666	**0.9333**
FDR	0.1875	0.0000	0.1428	0.0000	0.1333	**0.0666**
NPV	0.8000	1.0000	0.8666	1.0000	0.8666	**0.9333**
FNR	0.1333	0.2000	0.2000	0.2000	0.1333	**0.0666**
FPR	0.2000	0.0000	0.1333	0.0000	0.1333	**0.0666**
Precision	0.8125	1.0000	0.8571	1.0000	0.8666	**0.9333**
Specificity	0.8000	1.0000	0.8666	1.0000	0.8666	**0.9333**
Sensitivity	0.8666	0.8000	0.8000	0.8000	0.8666	**0.9333**
Accuracy	0.8333	0.9000	0.8333	0.9000	0.8666	**0.9333**

- **Analysis of Classification**

For the proposed MLUDA-NN algorithm, the overall performance is analyzed by comparing the conventional algorithms based on trained NN and the performance representation is given in Fig. 4.7 and Table 4.4. The performance metrics are evaluated for the proposed MLUDA-NN algorithm analysis that is differentiated from the traditional algorithms like PSO-NN, DA-NN, GWO-NN and LM-NN, which is producing better results. Therefore, from the analysis, the proposed MLUDA-NN method is more effective for DR detection.
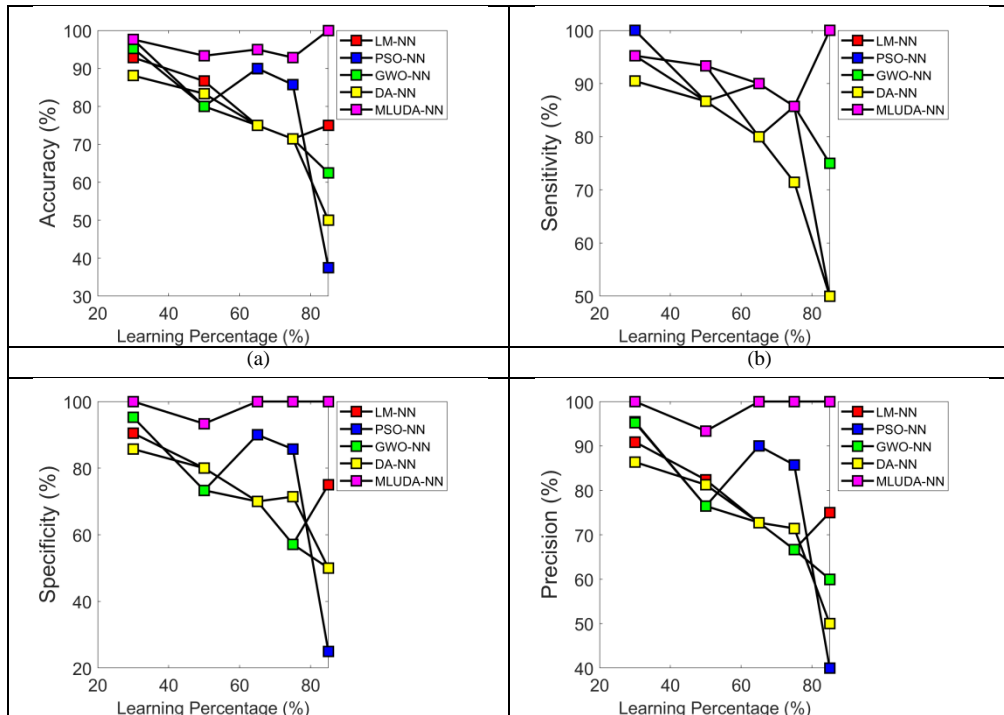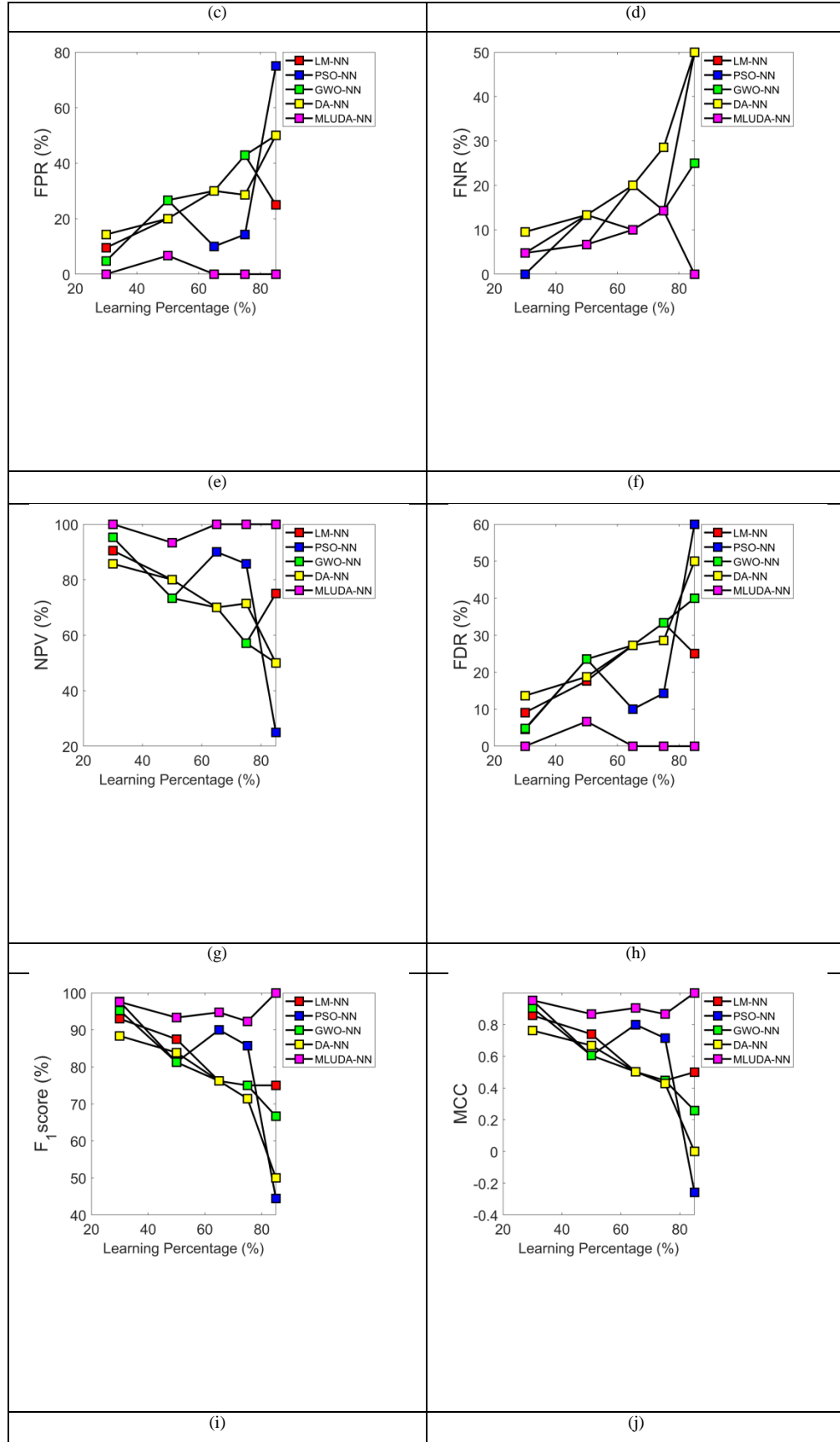
Fig. 4.7: Performance analysis with respect to Learning Percentage "(a) Accuracy, (b) Sensitivity, (c) Specificity, (d) Precision, (e) FPR, (f) FNR, (g) NPV, (h) FDR, (i) F1 score, and (j) MCC"

Table 4.4: Overall performance analysis

Performance Measures	DA-NN [110]	GWO-NN[75]	PSO-NN[72]	LM-NN [73]	MLUDA-NN (Proposed)
MCC	0.6000	0.6000	0.6000	0.6054	**0.8666**
F1-Score	0.8000	0.8000	0.8000	0.8125	**0.9333**
FDR	0.2000	0.2000	0.2000	0.2352	**0.0666**
NPV	0.8000	0.8000	0.8000	0.7333	**0.9333**
FNR	0.2000	0.2000	0.2000	0.1333	**0.0666**
FPR	0.2000	0.2000	0.2000	0.2666	**0.0666**
Precision	0.8000	0.8000	0.8000	0.7647	**0.9333**
Specificity	0.8000	0.8000	0.8000	0.7333	**0.9333**
Sensitivity	0.8000	0.8000	0.8000	0.8666	**0.9333**
Accuracy	0.8000	0.8000	0.8000	0.8000	**0.9333**

4.7 Summary

This chapter has offered a newly developed system for early DR detection and diagnosis. At first, the retinal fundus images are taken for the input of pre-processing stage. The enhancement is done for the images using the "CLAHE and average filter methods". Further, the improved images are given to the blood vessel segmentation technique where the segmentation is executed by the optimized grey-level thresholding. In the feature extraction phase, the features are extracted from the blood vessels by using "LBP, TEM and entropy". Later the collected features were subjected to a classification by considering the NN classifier using the optimized training algorithm. The optimal level of the threshold was generated in the "grey level thresholding and NN training algorithm" by the proposed MLU-DA algorithm. The proposed algorithm performance is compared over the conventional algorithms to demonstrate the overall accuracy of the suggested model. Here the overall accuracy of the proposed MLU-DA algorithm is 16.6% improved than traditional classifiers. Moreover, the precision is 22% higher than LM-NN, 16.6% superior to DA-NN, PSO-NN and GWO-NN.

Chapter 5

Modified Gear and Steering-based Rider Optimization Approach

In Chapter 4 an automatic DR detection model by using the retinal abnormality like blood vessels with the help of a neural network classifier is discussed. In that retina, images are classified as normal and abnormal cases but it is necessary to classify all the cases of DR from mild to severe. The neural network-based approach of classification is suitable when feature vector size is optimum. The classification process becomes slower when a large set of features are used. So feature optimization is required to remove high correlation between features and increase the accuracy of classification.

5.1 Introduction

This chapter focuses on the selection of features extracted from input image using an optimization algorithm that reduces the correlation between features using modified gear steering-based rider optimization algorithm that reduces feature vector size and enhances classifier accuracy. The same optimization algorithm optimizes the weight function of the Deep Belief Network (DBN) classifier. The proposed DR detection model [76] includes "pre-processing, optic disc removal, blood vessel removal, abnormality segmentation, feature extraction, optimal feature selection and classification". In the initial step, the input image is given to pre-processing phase, in which CLAHE is applied for enhancing the brightness of the image. By using open-close watershed transformation, the elimination of optic disc is done. Later, for segmenting and removing the blood vessels, grey-level thresholding is performed. In the next step, the abnormality segmentation is accomplished by "Gabor filtering and Top hat transformation". During feature extraction, features like "TEM, Shannon's entropy, LBP and Kapur's entropy" are extracted. As the feature vector length is found to be large, the process of feature selection is done, where unique features are selected with less correlation. Later, the image is classified into four classes such as "earlier, normal, moderate or severe stages" by optimized DBN. With the help of the proposed meta-heuristic algorithm named "Modified gear steering based Rider Optimization Algorithm (MGS-ROA)", the optimal feature selection and the process of weight update in DBN is done. At the end, experimental evaluation is done to verify the reliable and stable performance of the developed model on the DIARETDB1 data set when compared to conventional models.

5.2 Related Work

For detecting exudates using NN, a method was described by [77] and attained more accuracy by testing with 30 images. A multilayer perceptron NN approach is introduced in [78]. The size, edge strength, texture features and color of candidate lesions are derived and given as inputs to this model. Gerald et al. [79] introduced three-layered perceptron architecture such as, "single input layer, single hidden layer and single output layer neural network". The input was composed of 243 neurons, 50 hidden neurons, and the output was composed of a single neuron. It also employed the scaled conjugate gradient technique. If the NN classifier was utilized, then the range of the network's output lies between 0 to 1. Jayakumari et al.[80] explained a technique for the exudates detection by NN and attained 90% accuracy with 30 images.

In 2018, Sangeetha and Maheswari [81] have introduced the segmentation of blood vessels and retinal image extraction using "thresholding, adaptive histogram equalization, morphological processing and edge detection". To detect DR automatically, a network was introduced using Convolutional Neural Network (CNN) for precise classification of its stages. This network was trained on the freely accessible datasets namely DIARETDB1_v1, DRIVE, and DIARETDB2 using a high-end Graphics Processing Unit (GPU). In addition to this, the images acquired from Aravind Eye Hospital were also used for assessing efficiency. Thus, it has been verified that the suggested CNN achieved the optimal accuracy in diagnosing DR effectively. In 2018, Wan *et al.* [82] have recommended CNN-oriented DR detection for finding an automated model for the classification of retinal images. This approach has 3 steps such as detection, segmentation and classification. By combining "hyper-parameter tuning and transfer learning", the analysis on "VggNet, ResNet, AlexNet and GoogleNet" was done for performing the classification of DR images. For training these approaches, Kaggle dataset was used. The outcomes have proved that the proposed model has the best accuracy of CNNs and transfer learning for the classification of DR images.

In 2019, Hemanth *et al.* [83] have offered histogram equalization and CLAHE techniques for performing image processing for improving the brightness of the image. Later, the classifier CNN was used for performing classification. By using 400 retinal images of MESSIDOR dataset, the developed model was assessed. For detecting DR, the appropriate image processing model and deep learning approaches were employed. In 2019, Zeng *et al.* [84] have trained CNN with Siamese like structure using a transfer learning approach. In order to

perform prediction, the developed method has used binocular retinal images as input and their correlation was learned. Accuracy of 0.951 was acquired using the developed model with the training group of 28104 images and the testing group of 7024 images. This was more than the conventional monocular approach. It was trained for verifying the efficiency of the binocular model and analyzed on 10% validation set. The outcomes have demonstrated that the suggested model attained more kappa scores.

In 2019, Qummar *et al*. [85] have proffered different computer vision-oriented approaches for automatic detection of DR and its features from retinal fundus images. Yet, these approaches were not capable of encoding the underlying complex features and classified several stages of DR by obtaining less accuracy. Here, the public Kaggle dataset was employed from the retinal images for training an ensemble of five CNN methods for encoding rich features and enhanced the classification for various DR stages. The test results have proved that the proposed method accurately detected entire phases of DR. In 2019, Sun [86] has presented two-fold approaches for detecting DR effectively. CNN approach was applied to 1-D unrelated datasets. For gradient dispersion prevention, CNN was merged with the Batch Normalization (BN) layer. An adaptive learning rate model was merged and optimized the proposed system. The tests have revealed that the proposed model has obtained the best training and testing accuracy.

In 2019 Gao *et al*. [87] have developed an automatic DR detection model and offered better suggestions to the patients who were suffering from DR. By giving proper treatment to the patients, a dataset of DR retinal fundus images was used. With this dataset, Deep CNN was trained for severity gradation of DR fundus images. For a four-degree classification task during the experiment, more accuracy was obtained. During the clinical evaluation in many hospitals, the developed model attained a more consistent rate. In 2020, Gazhal *et al*. [88] have recommended CAD model for diagnosing NPDR using CNNs. For Optical Coherence Tomography (OCT) imaging modality, the developed model was introduced. Here, the analysis of all deployment aspects of the developed model was done for the pre-processing phase. Later extracting input retinal features for training CNN using the principles of transfer learning is done. Optimization of CNN is done for merging the features efficiently. This process was done by exploring many situations in the system setup. Later, the best one was selected from the outcomes that shown to be two pre-trained CNNs based models, where the first CNN was uniquely given using the patches of the nasal retina and the next one using the

patches of the temporal retina. The outcomes have demonstrated that the suggested transfer learning-based CAD model achieved optimal accuracy.

In 2020, Ayhan *et al.* [89] have described an instinctive model based on test-time data augmentation is done to quantify the uncertainty in the diagnosis of existing DNN for DR detection. It has revealed that the derived uncertainty measure was well-calibrated, which helped the physicians to analyze the diagnosis procedure. This resulted in the process of the combined uncertainty treatment in DNN-based diagnostic models. In 2020, Zago *et al.* [90] have modeled a lesion localization approach with a deep network patch-based model. The major aim was to decrease the complications of the method by enhancing its performance. For selecting the training patches, efficient processes that included two CNN models were designed, thus the challenging examples were provided special attention in the training procedure. The decision of DR was subjected to the first image by using the region labeling without using special training. By using the benchmark DIARETDB1 dataset, the introduced model was trained. It has been experimented on many datasets without any alteration in the designed methodology.

In 2019, Nazir *et al.* [91] have suggested a novel model for accurate detection of several DR phases by improving the research on content-based image retrieval. The fundus images were denoted using the new Tetragonal Local Octa-Pattern (T-LOP) features for attaining the performance which is close to the manual examination process for huge datasets, which were categorized by Extreme Learning Machine (ELM). The developed model was compared over conventional models for justifying the importance of the model consisting of deep learning-oriented models using four datasets of varying lengths. The test outcomes have confirmed the effectiveness of the DR detection model for serving as a best solution to offer accurate details of DR severity efficiently

5.3 Proposed Methodology

The proposed model consists of recognition of abnormality region, feature extraction from the region, optimization of features and classification. The present chapter aims in detecting the DR condition automatically. Many eye-related diseases, which cause blindness, are "glaucoma, age-related macular degeneration and DR". Image processing is done for detecting eye infections efficiently that is helpful for ophthalmologists for screening the patients and performing clinical analysis. By evaluating the retinal abnormalities like soft

exudates, haemorrhages, hard exudates and microaneurysms, it is possible to identify the retinal diseases. Fig. 5.1 shows the block diagram of the proposed DR detection model.
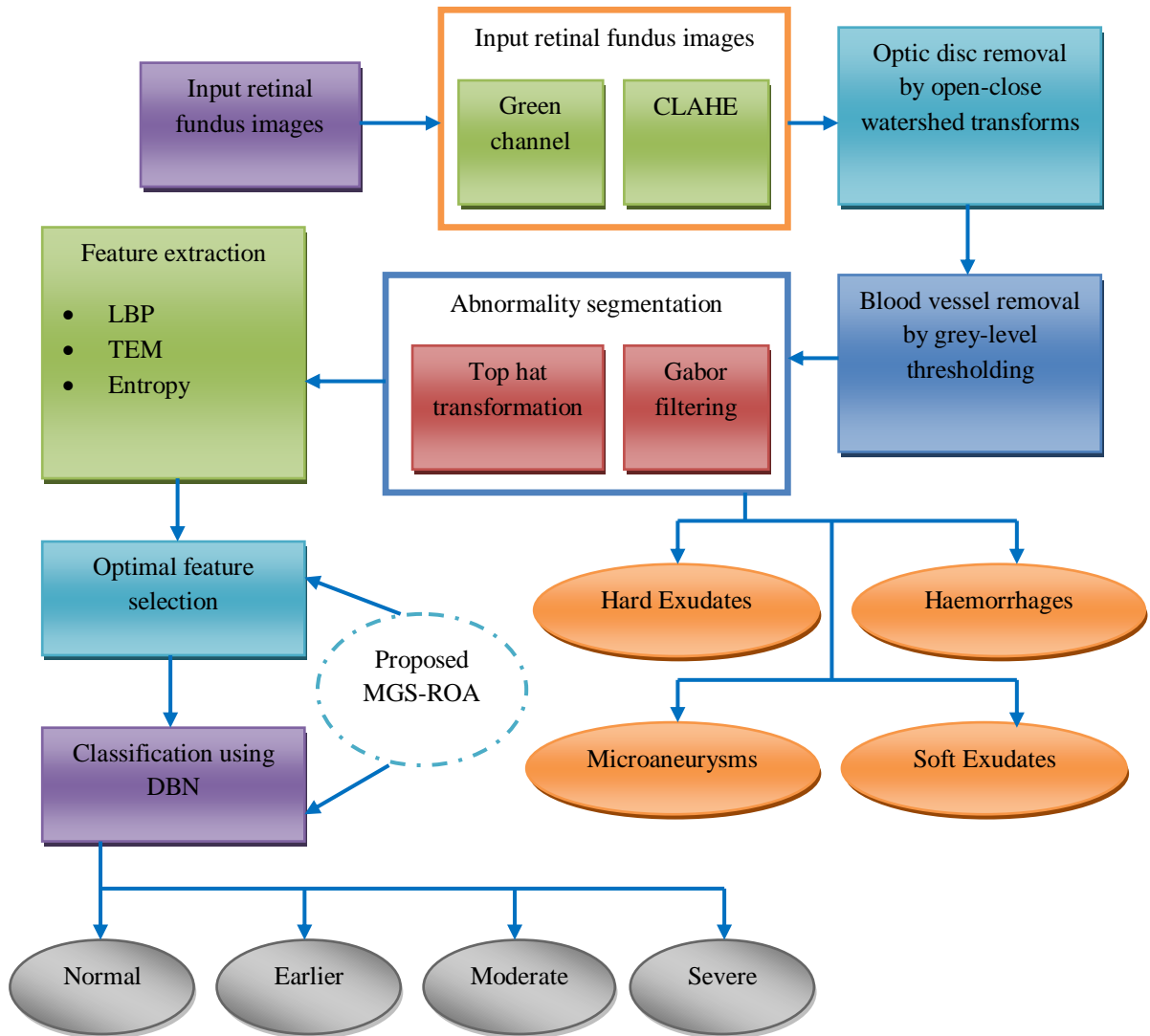
Fig. 5.1 Developed architecture of DR detection method

Initially, the retinal image is subjected to pre-processing phase, where green channel content is obtained and then CLAHE is performed for image enhancement. By using open-close watershed transformation, the segmentation and elimination of optic disc are performed. To split the touching objects available in an image, watershed transform is employed that identifies "catchment basins and watershed ridge lines" in an image by considering it as a surface. By using grey-level thresholding, blood vessels are segmented and removed. The features such as "Shannon's entropy, LBP, TEM and Kapur's entropy" are extracted in the feature extraction phase for further processing. "Shannon's and Kapur's entropy" describes the expected data value existing in an image. LBP is employed for the texture feature

extraction of an image and TEM is employed for finding the energy. As the size of the feature vector tends to be high, the process of feature selection is accomplished, which chooses the individual features with minimum correlation. For selecting the individual features, optimal feature selection is done in the proposed method. To accomplish the feature selection process, an enhanced meta-heuristic algorithm known as, "modified gear steering based rider optimization algorithm (MGS-ROA)" is employed. Further, the optimally selected features using developed MGS-ROA are applied to an optimized classifier named DBN to detect DR. Here, the weights for DBN are tuned by the proposed MGS-ROA algorithm. The major intent of the optimized DR detection is to decrease the correlation of the "chosen features and reduce the error". Therefore, the final classification method provides the result concerning the diagnosis of DR as severe, moderate, earlier and normal states.

Consider Ip_{im} as input retinal fundus image. The term Ip_{pro} represents the pre-processed retinal fundus image. The optic disc removal image is denoted as Ip_{odr}, and the blood vessel removal image is denoted as Ip_{bvr}. In the next step, the term Ip_{abn} denotes the abnormality segmented image. From the segmented abnormalities, the input features are given by Ip_{fea}, in which $fea = 1, 2, \cdots, nf$, and the count of features are denoted as nf. The optimal feature selection is denoted as Ip_{fea}^{*}, in which $fea = 1, 2, \cdots, nf^{*}$, where nf^{*} is the count of optimal features.

5.3.1 Pre-processing

The pre-processing of the retinal images is done by extracting green channel content from retina image and applying "Contrast Limited Adaptive Histogram Equalization (CLAHE)".

Green Channel Extraction: RGB image includes three channels such as, "red, green and blue" here green channel is extracted which contains significant details. The input images have less contrast. After green channel extraction, the abnormalities are observed clearly as it has more contrast.

"Contrast Limited Adaptive Histogram Equalization" [92], the contrast enhancement of the image by CLAHE is described in Section 4.3.1. Therefore, the final pre-processed image is given by Ip_{pro}, which is used for optic disc segmentation and extraction.

5.3.2 Segmentation of Retinal Abnormalities

Once the pre-processing is done, open-close watershed transformation [93] is performed for segmenting the optic disc. At first, the image is given for segmentation. Once the image is read, the structuring element of that particular image is defined. "Morphological dilation followed by opening-closing" is done to the structured element. Later, the markers of the background are computed and those images are applied to watershed transformation. In the later step, the process is subjected for performing quantitative analysis. To tackle the dark and bright elements, an open-close or close-open watershed method is used. The mathematical formulation of morphological image opening on Ip_{pro} using a structuring element D is denoted in Eq. (2.1) of section. 2.3, in chapter 2 and closing is shown in Eq. (5.1).

$$Ip_{pre} \circ D = \left(Ip_{pre} \Theta D\right) \oplus D \tag{5.1}$$

Where '$\circ$' is the morphological image opening operator.

The watershed line is a function that combines a set of points of a function, which doesn't belong to any other catchment basin and the corresponding equation is denoted in Eq. (5.2).

$$Wtr_{shd}(f) = sp(f) \cap \left[\bigcup_t (cbs(rgm_t))\right]^o \tag{5.2}$$

Where $sp(f)$ is the support function, rgm_t is the regional minima, $cbs(rgm_t)$ is catchment basin with regional minima and t represents a catchment basin. Skeleton by Influence Zones (SKIZ) is computed by analyzing the distance transformation over foreground image

Once the watershed ridgelines are computed, the image's intensity is modified by reconstructing morphological operations, thus it has regional minima in the required locations. Therefore, the resultant image is defined as Ip_{odr}, which is employed for future processing.

In this model, the segmentation of blood vessels is accomplished by the grey level thresholding, which is extracted based on the method used in Chapter 4, Section 4.3.2, and the final image is defined as Ip_{bvr}.

Here, the abnormality segmentation is accomplished by Top hat transformation and Gabor filtering mechanisms.

Top Hat Transform [94]: This is defined as the variance among "image opening and the actual image". Here, the main intent is to light the objects on dark background, which improves the image's brightness. In addition, the top hat transform of the segmented image Ip_{bvr} is denoted in Eq. (5.3). Here, the structuring element is given by D.

$$T(Ip_{bvr}) = Ip_{bvr} - (Ip_{bvr} \circ D) \tag{5.3}$$

Gabor Filtering [95]: It is generated from two components called Gaussian and sinusoidal. It has the ability to associate the optimal representation of "spatial domain and the orientation direction". Once the segmentation of abnormalities is performed, the image is represented as Ip_{abn} and it is further subjected to extract the features.

5.3.3 Feature Extraction

The features such as "LBP, TEM, Shannon's and Kapur's entropy" are extracted and the description of each feature extraction is given in Section 4.3.3, of Chapter 4. The size of the feature vector becomes large so it should be optimized to minimize the correlation between features and speed up the classification process. From the input features Ip_{fea}, the optimal features are selected using the proposed algorithm named MGS-ROA. The optimally selected features are denoted as Ip_{fea}^{*}.

5.3.4 Modified Gear Steering based-Rider Optimization Algorithm (MGS-ROA)

In a conventional rider optimization algorithm (ROA) [96], a group of riders is considered who move towards the same target to be the winner of the race. In this situation, a local minimum is prohibited by small local neighborhood, which is controlled by the attacker. However, fast convergence rate is obtained by many global neighborhoods and this is done by the overtaker. Instead of having some advantages, this model is frequently stuck in resolving the various optimization problems. In conventional ROA, the update process of the bypass rider's location is done by Eq. (5.4). The location of the bypass rider is given by LR_{ts+1}^{BpR} and the position of the leading rider at ts time steps is given by LR_{ts}. Further, the random values of riders that lies in between 0 and rn is given by η and ξ, whereas the random values that are ranging from 0 and 1 is given by β and δ. The riders are indicated by p and q with the term cn indicating the count of coordinates.

$$LR_{ts+1}^{BpR} = \delta[LR_{ts}(\eta, p) * \beta(q) + LR_{ts}(\xi, q) * [1 - \beta(q)]] \tag{5.4}$$

Moreover, the update process of the follower is given by Eq. (5.5). Here, the term LR^{ler} denotes the position of the rider and the term csl represents the co-ordinate selector. The pth rider's steering angle in Cs^{th} co-ordinate is given by $STR_{p,Cs}^{ts}$, and the term $dstn_p^{ts}$ indicates the distance traveled by p^{th} rider. This is measured by the product of the rider's velocity with the inverse rate of off time, which is expressed in Eq. (5.6), in which the off time is defined as off_{ts} ler is leading rider location and the velocity of the rider vlr_p^{ts} is denoted in Eq. (5.7).

$$LR_{ts+1}^{Flw}(p,csl) = LR^{ler}(ler,csl) + \left[\cos\left(STR_{p,Cs}^{ts}\right) * LR^{ler}(ler,csl) * dstn_p^{ts}\right] \qquad (5.5)$$

$$dstn_p^{ts} = vlr_p^{ts} * \left(\frac{1}{off_{ts}}\right) \qquad (5.6)$$

$$vlr_p^{ts} = \frac{1}{3}\left[gr_p^{ts} * spd_p^{gr} + spd_{\max}^{p} * acc_p^{ts} + \left(1 - brk_p^{ts}\right) * spd_{\max}^{p}\right] \qquad (5.7)$$

In the above equation the gear of the Pth rider at ts time step is given by gr_p^{ts}, the gear's speed limit of Pth rider is given by spd_p^{gr}, the brake and accelerator of pth rider are denoted as brk_p^{ts} and acc_p^{ts}, respectively. The overtaker is updated based on three factors such as "direction indicator, co-ordinate selector and relative success rate", the respective equation is denoted in Eq. (5.8).

$$LR_{ts+1}^{Ovt}(p,csl) = LR_{ts}(p,csl) + \left[dri_{ts}(p) * LR^{ler}(ler,csl)\right] \qquad (5.8)$$

In the above equation, the location of pth rider in csl co-ordinate selector is shown by $LR_{ts+1}^{Ovt}(p,csl)$, the term $dri_{ts}(p)$ denotes the direction indicator of pth rider at ts time. By using the relative success rate, the direction is measured and it is denoted in Eq. (5.9) based on Eq. (5.10). Here, the relative successive rate of pth rider is given by $Rls_{ts}^{rs}(p)$ at ts time steps and the success rate of pth rider at time ts is denoted as $srt_{ts}(p)$.

$$dri_{ts}(p) = \left[\frac{2}{1 - \log\left(Rls_{ts}^{rs}(p)\right)}\right] - 1 \qquad (5.9)$$

$$Rls_{ts}^{rs}(p) = \frac{srt_{ts}(p)}{\max_{p=1}^{rs} srt_{ts}(p)} \tag{5.10}$$

In addition, the attacker's update process is represented in Eq. (5.11). Here, the position of the leading rider is denoted as $LR^{ler}(ler, q)$, and the term $STR_{p,q}^{ts}$ denotes the steering angle of pth rider in q^{th} co-ordinate is given by $STR_{p,q}^{ts}$.

$$LR_{ts+1}^{Atk}(p, q) = LR^{ler}(ler, q) + \left[\cos\left(STR_{p,q}^{ts}\right) * LR^{ler}(ler, q)\right] + dstn_p^{ts} \tag{5.11}$$

As an improvement, the developed MGS-ROA modifies the update process of steering angle and gear for improving the performance of the conventional ROA. This can be defined based on the fitness function of the present solution Ft_P, in which the maximum fitness value is given by $Ft_{\max}$. The gear gr_p^{ts} is updated based on maximum gear value i.e., 5 when $Ft_P < Ft_{MAX}$ and the update of steering angle is done using Eq. (5.12). Consequently, the gear gr_p^{ts} is updated based on the minimum gear value i.e., 1, whereas the update of steering angle is done by Eq. (5.13). Here, the distance function is denoted as *Distn* and it is expressed in Eq. (5.14).

$$STR_{ts+1} = STR_{ts} + Dstnc \tag{5.12}$$

$$STR_{ts+1} = STR_{ts} - Dstnc \tag{5.13}$$

$$Distn = \frac{abs\left(LR_{ts+1}^* - LR_{ts}\right)}{\max\left(LR_{ts+1}^*\right)} \tag{5.14}$$

In Eq. (5.14), the best position of the leader is given by LR_{ts+1}^*, whereas the present location of the leader is given by LR_{ts}. The pseudo code of the developed MGS-ROA is depicted in Algorithm 5.1.

Algorithm 5.1: Proposed MGS-ROA

Input: Image pixels, feature vectors and weight function of DBN

1   Random rider location initialization rg_{ts}

2   Population initialization

3   Rider parameter declaration such as steering angle STR, gear gr, accelerator acc and brake br

4   Determine success rate sur_{it}

5   **while** $\left(it < Ti_{off} \right)$

6   **for** $c = 1\,to\,RN$

7   By pass rider's location is updated by Eq. (5.4)

8   Follower's location is updated by Eq. (5.5)

9   Overtaker's location is updated by Eq. (5.8)

10 Attacker's location is updated by Eq. (5.11)

11 Based on sur_{it} rank the riders

12 Riders are selected based on maximum sur_{it} as the leading rider

13 Update ST, ge, acc, and br

14 If $F_C < F_{MAX}$

15 If $ge_c^{it} = 5$

16 $ge_c^{it+1} = ge_c^{it}$

17 Else

18 $ge_c^{it+1} = ge_c^{it} + 1$

19 End if

20 Steering angle is updated using Eq. (5.12)

21 Else

22 If $ge_c^{it} = 1$

23 $ge_c^{it+1} = ge_c^{it}$

24 Else

25 $ge_c^{it+1} = ge_c^{it} - 1$

26 End if

27 Update the steering angle using Eq. (5.13)

28 End if

29 return RG^{Ler}

30 **end for**

31 $it = it + 1$

32 **end while**

Output: Optimized threshold, feature vector and weight functions of DBN

5.3.5 Optimized Deep Belief Network for Classification

For effective detection of DR, an optimally trained Deep Belief Network is employed. Deep Belief Network (DBN) [97] includes two types of NN's namely Restricted Boltzmann Machines (RBMs) and Belief Networks. DBN is an unsupervised learning algorithm, apart from backpropagation NNs and perceptron. DBN consists of many layers, in which every layer consists of visible neurons and hidden neurons in the input and the output layer, respectively. To achieve best outcomes, Boltzmann machines are considered as the building blocks of DBN.

The major intuition of Boltzmann network approach is to define the input patterns accurately as per Boltzmann distribution. With the help of the gradient descend model, the Boltzmann energy is used during training to define the least possible energy of the method to the given input. The major cause of this is the associations between the "visible and hidden neurons", which makes the neuron states to rely on each other.

During the calculation of energy difference, RBM is not relied on "visible and hidden neurons". This training is done by the unsupervised learning algorithm. By encoding the input data's probability distribution [98] into the parameters of weight, RBM is learned. RBM permits the probability using the energy function. With the help of the proposed model, the time used by RBM for achieving the association is quite complex, thus contrastive divergence (CD) is used. This produces faster convergence rate during the system distribution.

In the proposed DR detection model, the DBN training is performed by MGS-ROA and RBM for error minimization. For detecting DR automatically, two objective models are considered. The first objective is to minimize the correlation among the features and the other objective is to reduce the error difference among the real and the predicted output of DBN classification. At first, the features need to be chosen such that the correlation among the features must be lesser. It has the probability of defining more accuracy when the correlation among the features is minimum. The correlation among the two features c and d are denoted in Eq. (5.15), here the count of feature pairs is denoted as NfP_e. Therefore, the first objective is to minimize the correlation among the features as shown in Eq. (5.16).

$$Crltn = \frac{NfP\sum cd - \sum c \sum d}{\left(\sqrt{NfP\sum c^2 - (\sum c)^2}\right) - \left(NfP\sum d^2 - (\sum d)^2\right)} \qquad (5.15)$$

$$Obf1 = Min(Crltn) \qquad (5.16)$$

The original resultant vector of DBN is represented as C^a, whereas the predicted result is given by D^a. In Eq. (5.17), the error function between the predicted and the actual result is represented. Objective function that is used to minimize the error is shown in Eq. (5.18).

$$MR = C^a - D^a \qquad (5.17)$$

$$Obf1 = Min(MR) \qquad (5.16)$$

By using the developed MGS-ROA, the objective model is acquired, thus the best detection accuracy is attained. In order to select the optimal features and weight optimization in DBN classification, the developed MGS-ROA is employed. Fig. 5.2 shows the solution encoding for optimal feature selection, whereas Fig. 5.3 gives the solution encoding of optimized weight in DBN classifier.
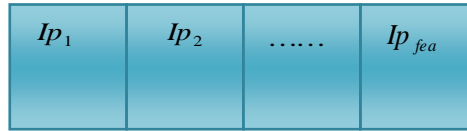
Fig. 5.2: Optimal feature selection in solution pattern
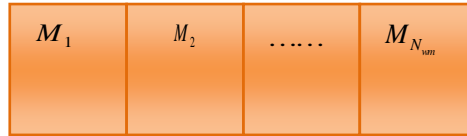
Fig. 5.3: DBN weight update in solution pattern

5.4 Results and Discussions
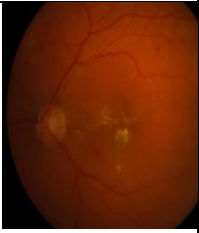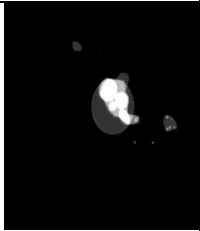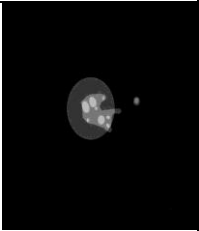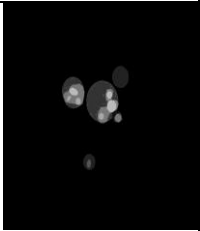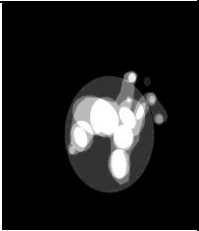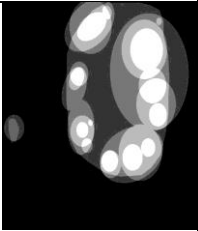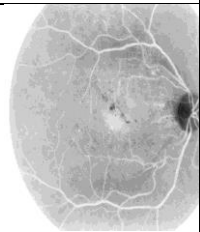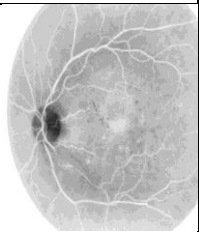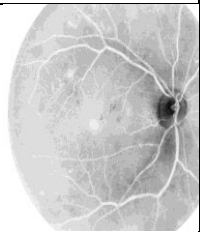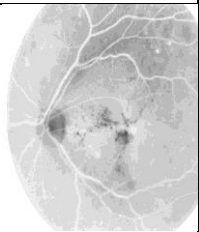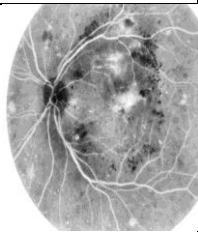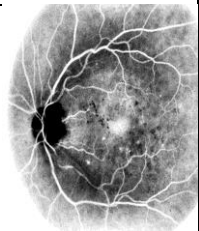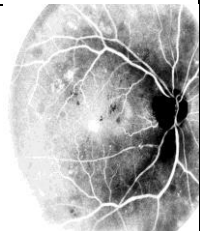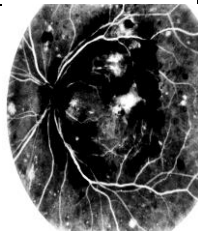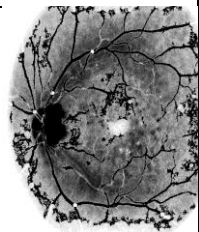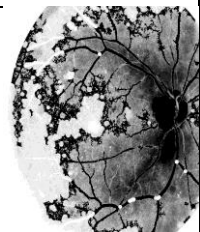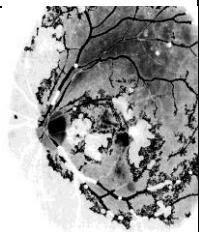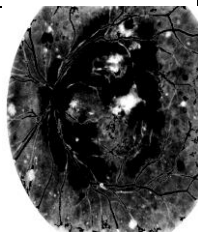
The experimental details and outcomes obtained by this method are discussed in the following steps.

The proposed DR detection model is developed using MATLAB 2018a, and the analysis is carried out. The dataset named DIARETDB1 is employed for performing the experiment that is composed of 89 color fundus images for analyzing the proposed model. From the retinal images, the specialists have marked the regions belonging to "hard exudates, microaneurysms, soft exudates and hemorrhages". The population size for assessing the feature selection is considered as 10, whereas the maximum count of iterations is fixed to 100. The performance of the proposed MGS-ROA-based DBN is compared over traditional "PSO-DBN, GWO-DBN, WOA-DBN, and ROA-DBN" concerning the evaluation metrics

like "accuracy, sensitivity, specificity, precision, FPR, FNR, NPV, FDR, F1-score, and MCC". Here, the ten performance measures are employed for the experiment and the evaluation of each measure is explained in Chapter 2, Section 2.5.

- **Analysis of Segmentation**

The segmentation outcomes of "pre-processing, removal of optic disc and blood vessel and abnormality segmentation" are depicted in Fig. 5.4.

	Image 1	Image 2	Image 3	Image 4	Image 5
Original Image					
Ground Truth Images					
Pre-processing Images					
Optic disc removal Images					
Blood Vessels removal Images					

Segmented Images					
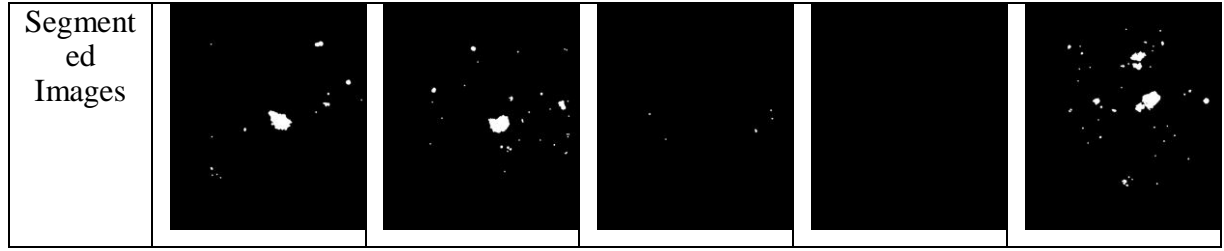
Fig. 5.4: Experimental outcomes of retinal image processing phases

- **Analysis of Performance Measures**

The analysis of the introduced MGS-ROA-DBN and the conventional meta-heuristic-oriented DBN algorithms in terms of the learning percentage is shown in Figure 5.5. The accuracy of the labeled MGS-ROA-DBN is attaining the best detection accuracy over existing algorithms at any of the learning percentages. In Fig. 5.5 (a), the accuracy of the suggested MGS-ROA-DBN is 6.6% better than PSO-DBN and 2.1% superior to WOA-DBN when considering the learning percentage as 45%. The specificity of the enhanced MGS-ROA-DBN is computed efficiently compared to traditional algorithms when considering any of the learning percentages and it is given in Fig. 5.5 (c). At learning percentage 100, the specificity of the proposed MGS-ROA-DBN is 6.8% more than GWO-DBN, 3.3% more than ROA-DBN, 16.2% enhanced than PSO-DBN, 12.7% enhanced than DBN and 9.4% enhanced than WOA-DBN. In Fig. 5.5 (d), the precision of the developed MGS-ROA-DBN has accurately defined the positive values from the entire values. At learning percentage 45, the precision of the recommended MGS-ROA-DBN is 16.2% better than PSO-DBN and 4.4% better than WOA-DBN. The NPV of the implemented MGS-ROA-DBN from Fig. 5.5 (g) is 4.2% improved than WOA-DBN, 3.1% advanced than ROA-DBN, 10.1% advanced than PSO-DBN and 8.8% advanced than DBN at learning percentage 65. The MCC of the presented MGS-ROA-DBN at learning percentage 50 is 8.2% and 27.7% progressed than WOA-DBN and PSO-DBN from Fig. 5.5 (j). Therefore, the results have shown that the offered MGS-ROA-DBN is attaining the best detection accuracy in detecting retinal fundus images. In Table 5.1, the analysis of the implemented MGS-ROA-DBN and the existing algorithms is tabulated. The accuracy of the suggested MGS-ROA-DBN is accurately detecting DR when compared to other algorithms. It is 5.1% superior to GWO-DBN, 2.5% superior to ROA-DBN, 10.8% superior to WOA-DBN, and 13.8% superior to PSO-DBN. The precision of the suggested MGS-ROA-DBN is exactly determined by the positive values from the whole values. Thus, it is 26.6% superior to WOA-DBN, 5.5% enhanced than ROA-DBN, 35.7% surpassed than PSO-DBN and 11.7% surpassed than GWO-DBN. In next level, the NPV of the developed

MGS-ROA-DBN is 1.6% enhanced than ROA-DBN, 6.7% enhanced than WOA-DBN, 3.2% enhanced than GWO-DBN and 8.6% more than PSO-DBN. From the above results, it is shown that the introduced MGS-ROA-DBN is performing well in DR detection.

(a)

(b)

(c)

(d)
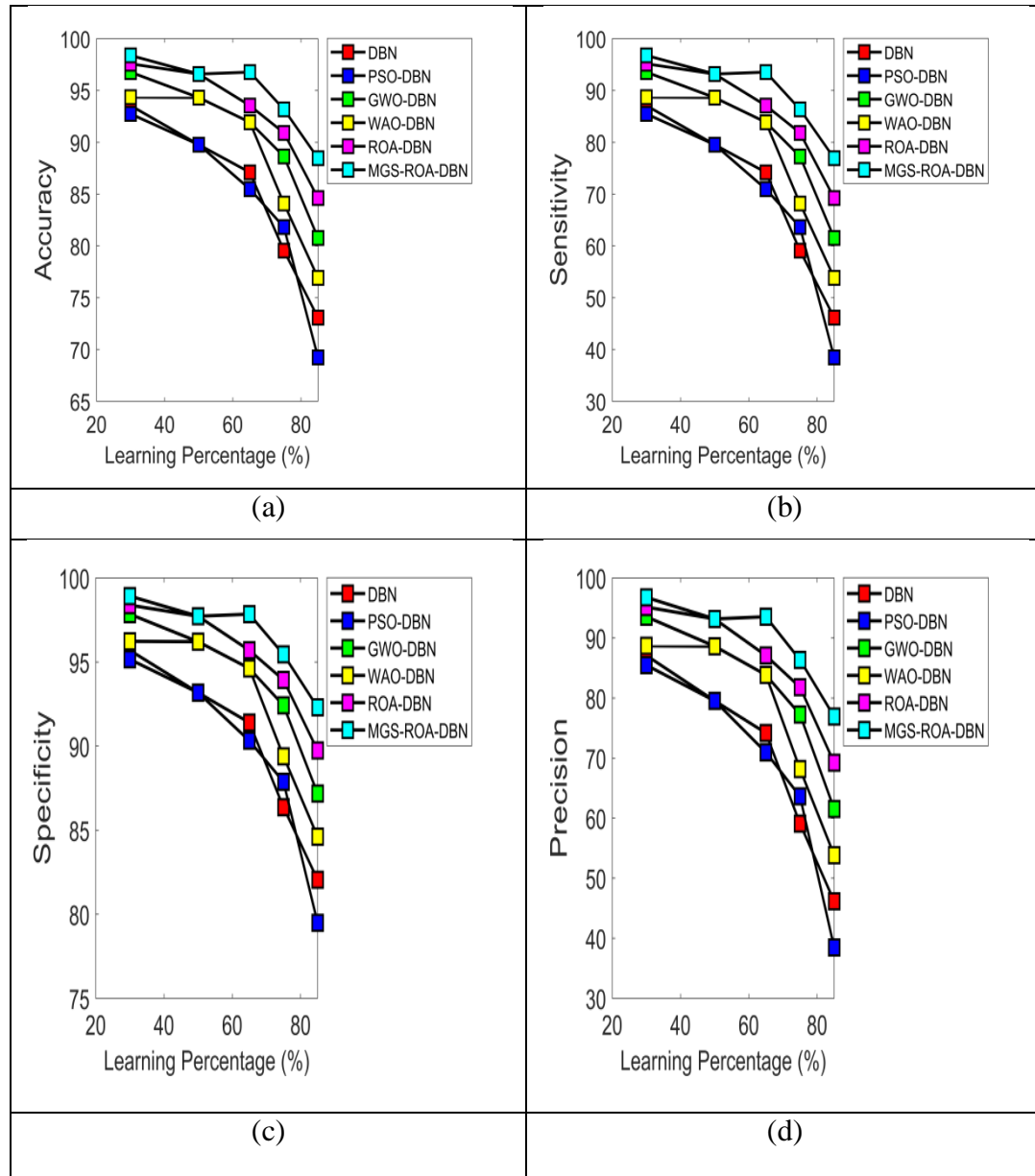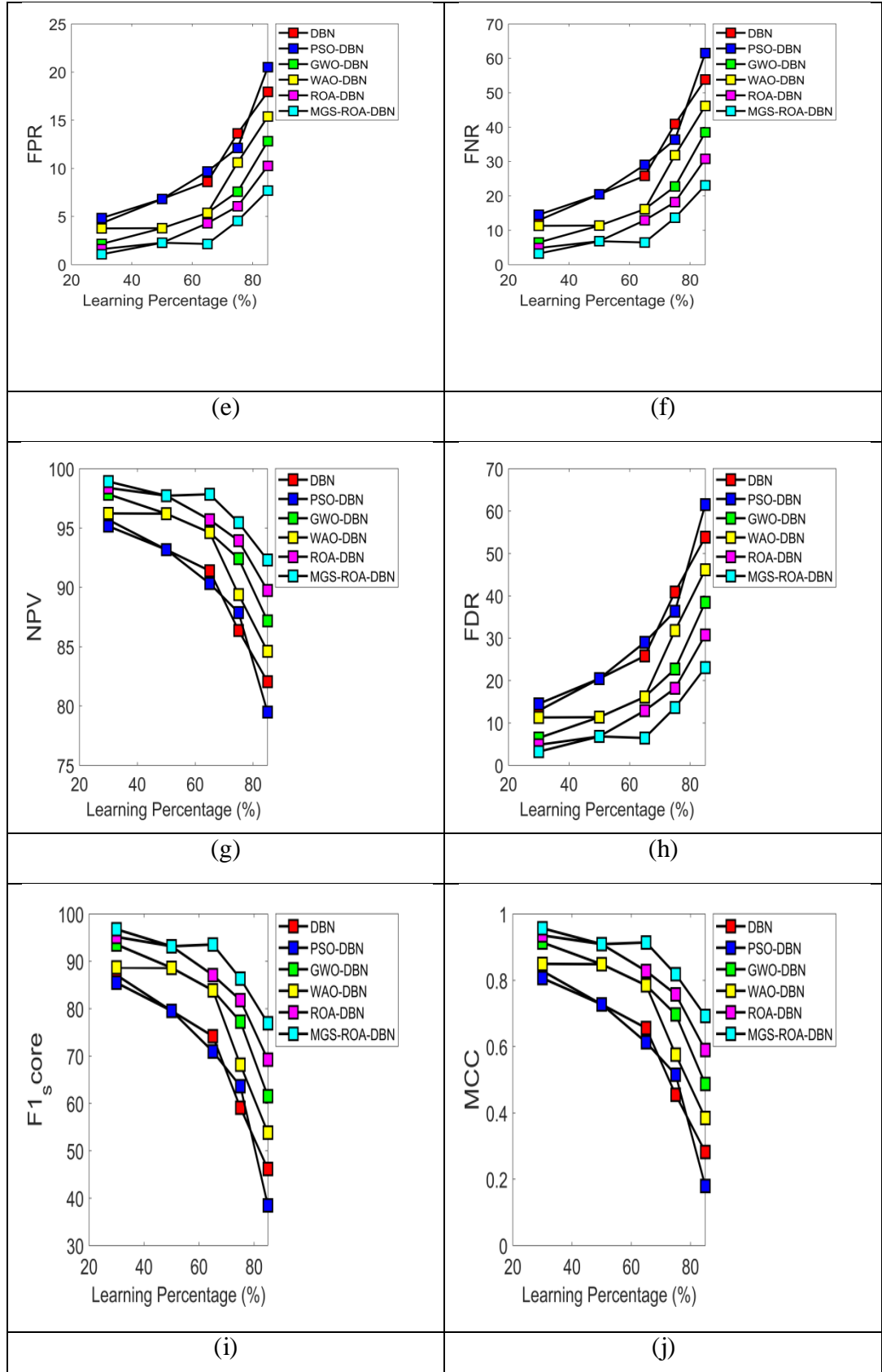
Figure 5.5: Performance analysis of developed and traditional heuristic algorithms for DR detection with consideration of "(a) accuracy, (b) sensitivity, (c) specificity, (d) precision, (e) FPR, (f) FNR, (g) NPV, (h) FDR, (i) F1-score, and (j) MCC"

Table 5.1 Overall performance analysis of the developed and traditional algorithms for detecting DR

Performance Measures	ROA-DBN [96]	PSO-DBN [72]	GWO-DBN [75]	WOA-DBN [74]	MGS-ROA-DBN (Proposed)
MCC	0.7575	0.5151	0.6969	0.5757	**0.8181**
F1-score	0.8181	0.6363	0.7727	0.6818	**0.8636**
FDR	0.1818	0.3636	0.2272	0.3181	**0.1363**
NPV	0.9393	0.8787	0.9242	0.8939	**0.9545**
FNR	0.1818	0.3636	0.2272	0.3181	**0.1363**
FPR	0.0606	0.1212	0.0757	0.1060	**0.0454**
Precision	0.8181	0.6363	0.7727	0.6818	**0.8636**
Specificity	0.9393	0.8787	0.9242	0.8939	**0.9545**
Sensitivity	0.8181	0.6363	0.7727	0.6818	**0.8636**
Accuracy	0.9090	0.8181	0.8863	0.8409	**0.9318**

- **Analysis on Different Classifiers**

Table 5.2 shows the performance of the proposed MGS-ROA-DBN and conventional machine learning algorithms. From Table, the accuracy of the developed MGS-ROA-DBN accurately defined the positive values. The accuracy of the improved MGS-ROA-DBN is 32.2% surpassed than KNN, 17.1% surpassed than SVM and DBN and 30.1% surpassed than NN. In addition, the precision of the presented MGS-ROA-DBN is exactly described by the positive values from the entire values. It is 52.6% more than KNN, 46.1% more than SVM as well as DBN and 55.4% progressed than NN. Therefore, it is confirmed that the developed MGS-ROA-DBN is performing well in DR detection.

Table 5.2: Overall algorithmic analysis of the developed and existing machine learning algorithms.

Performance Measures	SVM [112]	KNN [111]	NN [73]	DBN [97]	MGS-ROA-DBN (Proposed)
MCC	0.4545	0.2121	0.1294	0.4545	**0.8181**
F1-score	0.5909	0.4090	0.2857	0.5909	**0.8636**
FDR	0.4090	0.5909	0.6153	0.4090	**0.1363**
NPV	0.8636	0.8030	0.8787	0.8636	**0.9545**
FNR	0.4090	0.5909	0.7727	0.4090	**0.1363**
FPR	0.1363	0.1969	0.1212	0.1363	**0.0454**
Precision	0.5909	0.4090	0.3846	0.5909	**0.8636**
Specificity	0.8636	0.8030	0.8787	0.8636	**0.9545**
Sensitivity	0.5909	0.4090	0.2272	0.5909	**0.8636**
Accuracy	0.7954	0.7045	0.7159	0.7954	**0.9318**

5.5 Summary

This chapter has introduced a new method named MGS-ROA-DBN to implement the automatic detection of DR by analyzing the abnormalities of the retina like "microaneurysms, hemorrhages, hard and soft exudates". The proposed DR detection model has included "pre-processing, optic disc removal, blood vessel removal, segmentation of abnormalities and classification". In the initial step, the retinal fundus image is given as input to the pre-processing phase, in which the "green channel conversion and CLAHE" is done for enhancing the brightness of the image. Next, the optic disc is eradicated by open-close watershed transformation. Further, the blood vessels are segmented and eliminated using grey-level thresholding. Once the blood vessels are removed, the abnormality segmentation is accomplished using "top-hat transformation and Gabor filtering". The features like "LBP, TEM, Shannon's and Kapur's entropy" are extracted. Further, the feature vector is found to be large, thus the optimal feature selection is done for selecting the unique features with minimum correlation. Later, the image classification is done into four classes namely earlier, normal, severe and moderate stages by a DBN-based classification algorithm. From the analysis, it is proven that the accuracy of the developed MGS-ROA-DBN is 30.1% superior to NN, 32.2% superior to KNN and 17.1% superior to SVM and DBN. Thus, it is cleared from the above results that the proposed MGS-ROA-DBN is performing well in DR detection.

Chapter 6

Trial-based Bypass Improved Dragonfly Algorithm Approach

In Chapter 5, the focus is on detection of DR through segmenting retinal abnormalities, feature extraction, selection of features from extracted features and classification using improved gear steering based rider optimization algorithm. Rider optimization algorithm reduces feature vector size and improves classification accuracy. Furthermore effective feature optimization algorithm can still reduce the correlation in feature vector significantly and in turn, increases the speed and accuracy of DR detection.

6.1 Introduction

This chapter intends to introduce a novel approach using a proposed algorithm "Trial based Bypss improved Dragonfly Algorithm (TB-DA)" for feature optimization and classification in DR detection [99] by performing three analyses based on the "optic disc, blood vessels and abnormalities of the retina". At first, the pre-processing phases such as green channel conversion and CLAHE are done for enhancing the brightness of the image. Later, the segmentation process begins with the segmentation of the optic disc, which is done by open-close watershed transform. Next, the segmentation of blood vessels is done by grey level thresholding. By using "top-hat transformation and Gabor filtering", the abnormalities such as "microaneurysms, hemorrhages, hard and soft exudates" are segmented. The features such as "LBP, TEM, and Shannon's and Kapur's entropy" are extracted from the segmented images and further, it is subjected to optimal feature selection. It is done by the proposed "Trial-based Bypass Improved Dragonfly Algorithm (TB-DA)". These optimally chosen features are given to a hybrid machine learning algorithm which is formed by combining "NN and DBN". As an improvement, the same TB-DA algorithm is employed for improving the training of a hybrid classifier that results in the classification of "normal, mild, moderate or severe images" on the basis of the abnormality level.

6.2 Related Work

In 2019, Xuechen *et al*. [100] have aimed in providing an OCT image-oriented detection approach for automatic detection in an early stage, which included both grades 1 and 0. It has helped the specialists by giving treatment and evaluation, decreasing the loss of vision rate by allowing accurate and timely detection. Here, a new deep learning network named

OCTD_Net was introduced and analyzed for detecting DR in an early stage. From the actual OCT image, one of the networks layer extracted features of the retina and the other extracted retinal layer information. By the developed network, the analysis of the retinal layers and the features learned suggested that the grade 1 DR patients can be presented using major alterations in the thickness and certain retinal layers reflection. However, grade 0 DR patients do not have major alterations. The heat maps of the trained network also recommended that patients with early DR have shown various textures around the zones of the ellipsoid and myoid, photoreceptor outer segments and inner nuclear layers that must receive more attention for early detection of DR.

In 2020, Wang *et al*. [101] have developed a novel model for detecting hemorrhages with "Deep Convolutional Neural Network (DCNN) and multi-feature joint representation". In this methodology, a novel optimized mathematical morphological model was introduced, which initially segmented hemorrhage candidates precisely. Later, each candidate was classified by combined features on the basis of deep features combined with the Highest Common Factor (HCF) that was developed using ridge regression-oriented feature fusion. For constructing HCF, this model has used "multi-space-based intensity features, GLCM-based texture descriptor, Gray Level Size Zone Matrix (GLSZM)-based texture descriptor and geometric features" were used. The DCNN was used for automatic learning the deep information of hemorrhages. Thus for recognizing the true hemorrhages between candidates, a random forest classifier was used. By considering two standard datasets, the developed model was analyzed. The results have shown that the presented model was appropriate for clinical applications based on clinical images from a local hospital. The introduced model combined the conventional HCFs and deep learning features from DCNN for hemorrhages detection. Further, the developed feature selection and combined model decreased the feature dimension and enhanced the detection accuracy of hemorrhages

Sundararaj et al. [102] have addressed a MLP NN method that identified the exudates availability in the fundus images. The inputs were derived from "color, size, the strength of edge and texture features" associated with the candidate lesions.

By using SVM and Naive Bayes (NB) classifiers, the research on "feature selection and classification" of exudates is developed in [103]. Initially, NB was subjected to the training set that included 15 features, which were extracted from equal count of negative examples and every positive illustration of exudates pixels. For eliminating features from the classifier,

feature selection was done on Naive Bayes approach. Later, both SVM and NB classifiers were compared to a baseline nearest neighbor classifier with the optimal feature set from both the classifiers. The results have been confirmed that SVM and NB are performing well when compared over nearest neighbor classifiers.

In 2018, Kar and Maity [104] have suggested a novel and automatic lesion detection model that involved pre-processing, vessel extraction, removal of optic disc, candidate lesion detection and post-processing. Initially, the "blood vessels and optic disc" were conquered for facilitating more processing. The curvelet-oriented edge enhancement accomplishment was used for split the dark lesions. By using an optimally designed wideband pass filter, the contrast among the "bright lesions and background" was improved. Later, the maximization of "Laplacian of Gaussian response and matched filter response" was done. To define the best values for the fuzzy function parameters, DE algorithm was utilized, which determined the candidate region threshold for segmentation. Further, morphology-based post-processing was subjected for excluding the false detection of candidate pixels. The simulations were performed on various public datasets for analyzing the proposed model.

In 2020, Usman and Almejalli [105] have addressed a new technique for microaneurysms detection from the retinal fundus images automatically. For evolving a mathematical expression, the developed model employed genetic programming (GP) and a group of 28 chosen features from the pre-processed images. The optimal expression was evolved by generating a stepwise enhancement procedure through the bilinearization of fitness scores. For real-world applications, the best expression was later employed as a classifier. By using three datasets that are publicly available, the test outcomes validated the usefulness of the developed model.

In 2020, Roshini *et al*. [106] have labeled an automatic DR detection model that included three phases like "image pre-processing, blood vessel segmentation and classification". In pre-processing, the conversion of RGB to "Lab and contrast enhancement" was done. This contrast enhancement was performed by histogram equalization. In the next step the segmentation process included thresholding the contrast-enhanced and filtered images.The thresholding include keypoints of filtered images and contrast-enhanced images and summing both the thresholded binary images. By the developed average filtering model, the filtering of an image was accomplished, in which the filter coefficients were tuned using the suggested Fitness Probability-based Cat Swarm Optimization (FP-CSO). Later, Deep CNN was used for

classification, where the improvement was used on the Convolutional layer that was optimally produced by the developed FP-CSO algorithm. As the traditional CSO algorithm was relied on the fitness probability in the improved model and named it as FP-CSO. Furthermore, the performance analysis and the comparative analysis have concluded that the proposed model was effective in DR detection.

In 2019, Selcuk and Alkan [107] have intended for accurate, efficient and automatic detection of microaneurysms that were complex for color fundus image detection in an early stage. For this purpose, ant colony optimization algorithm was used in place of existing image processing models. From the retinal fundus images of DIARETDB1 and MESSIDOR datasets, the structure of retinal vascular was extracted. In the next step the microaneurysm segmentation was performed by ant colony algorithm. For five various image processing and clustering models, the similar process was given for comparing the behavior of the developed model over traditional models. By eye specialist doctor, the manually detected microaneurysm images were employed for computing the conventional models performances. The similarities among microaneurysms that were segmented automatically or manually were experimented by Dice and Jaccard similarity index values. The results have proven that varying performances were seen in the traditional microaneurysm segmentation based on the quality of an image. Consequently, the developed model acquired consistent performance without reducing the brightness of an image. Thus, it was manifested that the developed model has detected microaneurysms effectively even with poor image quality and it helped the ophthalmologists for detecting DR easily

 Sinthanayothin et al. [108] have addressed an automatic DR detection via a window-oriented recursive region growing segmentation algorithm. The hard exudates could only be detected. Hence, an effective technique was needed to overcome the shortcomings of the traditional techniques. Phillips et al [109] recognized the exudates with the help of local and global thresholding. The pre-processing eliminated the photographic non-uniformities and the exudates contrast was then improved. The lesion-oriented sensitivity of this approach was dependent on 14 images. The shortcoming of this approach was that various bright lesions were recognized in the wrong manner. There are several methods available for diabetic retinopathy analysis and they are discussed in [110] to reveal their performance in detecting retinal abnormalities.

6.3 Proposed Methodology

Several attempts have been made in the past years to reduce the complexities in DR detection. However, there have been few faults for disease detection in an early stage with the conventional model. For diagnosing DR effectively, a novel approach is developed in this chapter by performing discrete evaluations. The architectural model of the introduced DR detection method is depicted in Fig. 6.1.
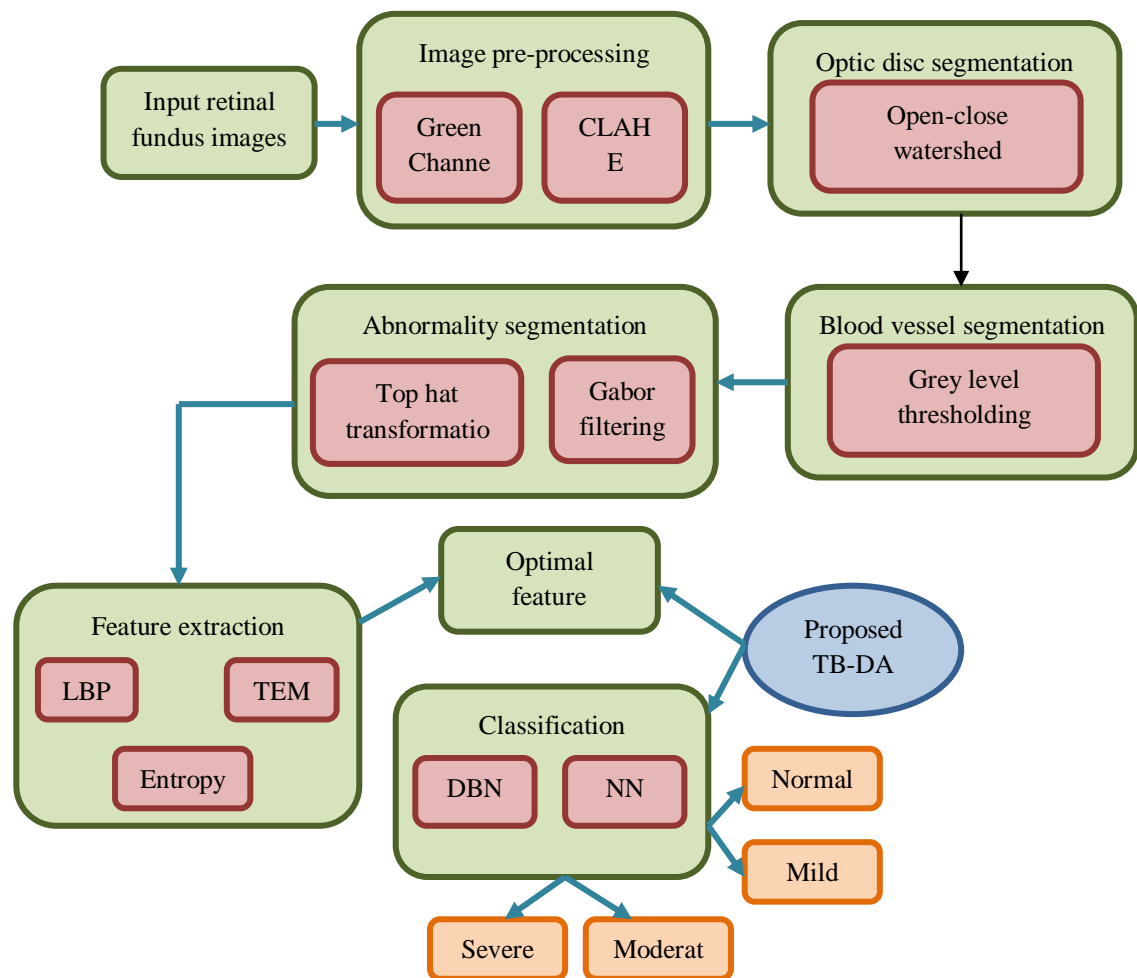
Fig. 6.1: Architecture representation of developed DR detection model

The introduced DR detection model includes many steps like "image pre-processing, optic disc segmentation, blood vessel segmentation, feature extraction, optimal feature selection and classification". During the pre-processing phase, the green channel conversion and CLAHE are accomplished for improving the image's brightness. Using the open-close watershed transform, the segmentation of optic disc is done. This segmentation approach is employed for segmenting the optic disc by using the beneficial concepts of region processing.

Later, the segmentation of blood vessels is done using grey-level thresholding. Furthermore, the abnormality segmentation is performed by "top hat transformation and Gabor filtering approaches". By considering the optic disc, blood vessels and segmented abnormalities such as "hard exudates, hemorrhages, Microaneurysm and soft exudates", this model concentrates on the assessment of DR detection. To extract features like "LBP, TEM and entropy", each segmented image is taken into consideration. The optimal feature selection is done for decreasing the feature-length and this is done by the hybrid TB-DA algorithm. These optimized features are subjected to a machine learning algorithm which is formed by combining "NN and DBN" classifiers. Here, the weight update of both "NN and DBN" is optimized by the proposed TB-DA algorithm, in which the classification of the image is done as "normal, mild, moderate, or severe" on the basis of the analysis of three components. During the optimal feature selection, the major intuition of the proposed TB-DA algorithm is to reduce the correlation among the chosen features, whereas to minimize the error difference among the "forecasted and the actual outcome" during the weight update in the hybrid classifier.

- **Image Description**

Consider Ip_{im} as input retinal fundus image. The term Ip_{pro} represents the pre-processed retinal fundus image. The optic disc removed image is denoted as Ip_{odr} and the blood vessel removed image is denoted as Ip_{bvr}. Likewise, the term Ip_{abn} denotes the abnormality segmented image. From the segmented abnormalities, the input features are given by Ip_{fea}, in which $fea = 1,2,\cdots,nf$, and the count of features are denoted as nf. The optimal feature selection is denoted as Ip_{fea}^*, in which $fea = 1,2,\cdots,nf^*$, and nf^* is the count of optimal features.

- **Objective function**

In the proposed DR diagnosis model, there are two objectives, which are resolved by the developed DR detection method. Initially, the objective is to minimize the correlation among the selected features during the optimal feature selection. This is performed by the proposed TB-DA algorithm. The correlation among two features is defined as c and d and the count of feature pairs is defined as Nfp_e. The minimized correlation function that comes under optimal feature selection is defined in Eq. (5.16) and Eq. (5.18) of section 5.3.5.

In addition, the other objective is to reduce the error difference among the "actual and forecasted output" of both NN and DBN by performing optimal training using the proposed TB-DA. The error function between the actual and the forecasted output is defined in Eq. (6.1). Here, the actual output vector is given by D^d and the forecasted output of both NN and DBN is denoted as E^d. Thus, the objective function of optimal classification is done on the basis of Eq. (6.2).

$$er = D^d - E^d \tag{6.1}$$

$$Mer2 = \underset{\{M_{ne}^{nn}, M_{ne}^{dbn}\}}{\arg\min} (er) \tag{6.2}$$

Therefore, the developed TB-DA is employed for acquiring the better performance on DR detection using "optimal feature selection and classification". Pre-processing, segmentation and features extraction methods are same as discussed in chapter 5.

6.3.1 Optimal Feature Selection

From the given input features Ip_{fea}, the optimal features are chosen by the implemented TB-DA, which is used for selecting optimal features Ip_{fea}^*. Fig. 6.2 shows the solution encoding of optimal feature selection.
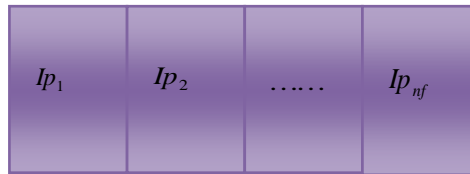
Figure 6.2: Solution encoding for optimal feature selection

The complete description of the conventional Dragonfly Algorithm is given in Section 4.4 of Chapter 4. The conventional ROA is explained in Chapter 5, Section 5.3.4.

6.3.2 Trial Based-Dragonfly Algorithm

The conventional DA is performing well in solving compound optimization issues. However, it has some challenges such as random flight interruption as it has more searching phases and searches space overflow. The concept of ROA is developed for enhancing the LFM of DA. The major benefits of ROA are less expensive and can solve complex tasks. In addition to this, ROA is capable of acquiring the global optimal solutions. Thus, the hybrid model named TB-DA is introduced with the combination of DA and ROA to detect DR effectively. Several

optimization algorithms are merged in the earlier contributions to developing a novel hybridized algorithm. These hybridized algorithms produce the best results for particular search complexities. For attaining the fast convergence rate, this hybrid algorithm employs the benefits of discrete optimization algorithms. The convergence behavior has been provided for being best when compared to conventional algorithms. Based on the trial, the proposed TB-DA is operated that is counted when there is no enhancement in the solution. When the trial is less than or equal to 5, the general update process of DA is done. If the trial is greater than 5, the solution is updated using the bypass rider based on Eq. (6.3). Here, the terms δ and β are the random values that lies in between 0 and 1, and the terms η and ξ indicate the random values ranging from 0 to rd, k is leading rider position. The step-by-step procedure of introduced TB-DA is shown in Algorithm 6.1.

$$\Delta Lo_{itr+1} = \delta\left[Lo_{itr}(\eta,k)*\beta(k) + Lo_{itr}(\xi,k)*\left[1-\beta(k)\right]\right] \tag{6.3}$$

Algorithm 6.1: Proposed TB-DA

Input: Image pixels, feature vectors and weight function of NN and DBN
1. The entire solution of dragonflies X is initialized
2. **while** the final condition is not satisfied
3. **If** $(trial \leq 5)$
4. Update source of food & enemy
5. update δ, se, al, co, af, and de
6. Compute Se, Al, Co, Af, and De
7. Update the radius of neighbours
8. **If** a dragonfly has at least one neighboring dragonfly
9. Update velocity vector
10. Update position vector
11. **Else**
12. Update position vector
13. **end if**
14. **End if**
15. **Else**
16. **If** $(trial > 5)$
17. Update the solution by bypass rider by Eq. (6.3)
18. **End if**
19. Validate the updated solution by fitness evaluation
20. **end while**
Output: Optimized threshold value, feature vector and weight function

---

6.3.3 Hybrid Classifier

In order to detect DR, the hybridization of DBN and NN is employed, where the training algorithm is enhanced by the developed TB-DA. To update the weight of both NN and DBN based on Fig. 6.3, the proposed TB-DA algorithm is used. Here, the weight function of NN and DBN are denoted as M_{ne}^{nn} and M_{ne}^{dbn}, respectively. The description of NN is provided in Chapter 4 and the description of DBN is given in Chapter 5.

$$M_{ne}^{nn} \qquad M_{ne}^{dbn}$$

Fig. 6.3: Optimal classification in solution pattern

6.4 Results and Discussions

The developed DR detection method was programmed using MATLAB 2018a and the analysis was performed. In order to assess the developed model, the dataset named DIARETDB1 is employed. The population size considered for the experiment is 10, whereas the total count of maximum iterations is considered as 100. The performance of the developed TB-DA-based NN+DBN is compared over "WOA-DBN+NN, ROA-DBN+NN, MGS-ROA-DBN+NN, DA-DBN+NN and MLU-DA-DBN+NN" in terms of the performance measures like "accuracy, sensitivity, specificity, precision, FPR, FNR, NPV, FDR, F1-score and MCC".

- **Analysis of Segmentation**

Fig. 6.4 portrays the test results of optic disc, blood vessels and abnormality segmentation.

	Image 1	Image 2	Image 3	Image 4	Image 5
Original Images					
Optic disc segmentation					

| Blood vessel segmentation | | | | | |
| Abnormality segmentation | | | | | |
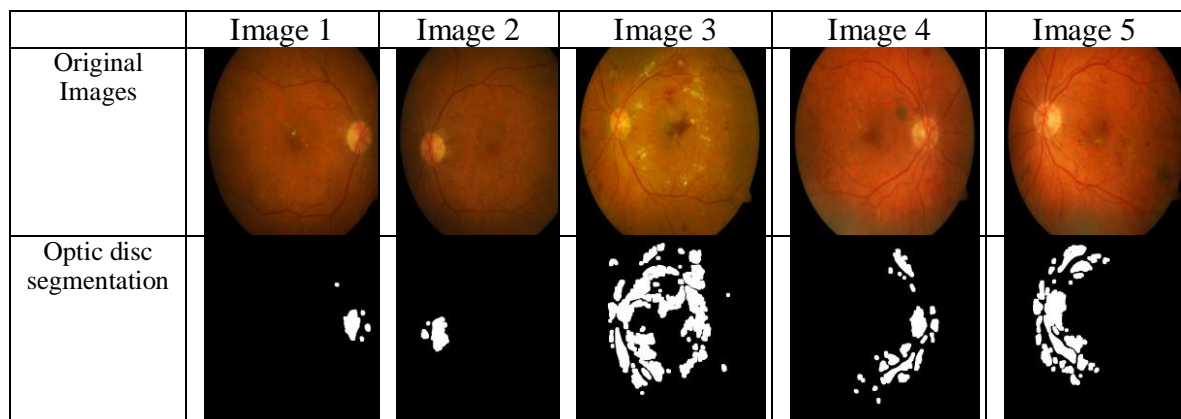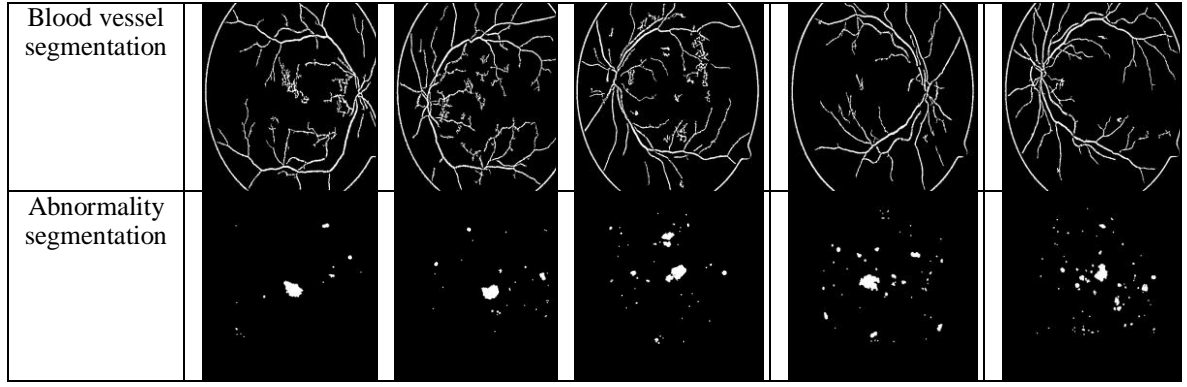
Fig. 6.4: Experimental Results for retina image segmentation

- **Analysis of Performance Measures**

The analysis of optic disc using the developed TB-DA-DBN+NN and the traditional meta-heuristic-based DBN+NN is depicted in Figure 6.5. The accuracy of the labeled TB-DA-DBN+NN is improved when compared over conventional algorithms when considering any of the learning percentages and it is shown in Fig. 6.5 (a). It is 12.5% superior to MLU-DA-DBN+NN, 16.1% advanced than WOA-DBN+NN and 20% advanced than MGS-ROA-DBN+NN at a learning percentage 85. When considering any of the learning percentages in Fig. 6.5 (b), the precision of the implemented TB-DA-DBN+NN is acquiring best performance in DR detection. At learning percentage 85, the precision of the enhanced TB-DA-DBN+NN is 25% better than WOA-DBN+NN, 56% better than DA-DBN+NN, 72% surpassed than ROA-DBN+NN, 76% surpassed than MGS-ROA-DBN+NN and 100% better than MLU-DA-DBN+NN. Moreover, it is confirmed that the remaining measures are also exhibiting the best performance at any of the learning percentages for the proposed TB-DA-DBN+NN. In Table 6.1, the overall performance analysis of the proposed TB-DA-DBN+NN and the existing heuristic algorithms for effective DR detection are tabulated. The accuracy of the proposed TB-DA-DBN+NN is 25.8%, 21.6%, 15.8%, 19.6% and 7.3% advanced than WOA-DBN+NN, ROA-DBN+NN, MGS-ROA-DBN+NN, DA-DBN+NN and MLU-DA-DBN+NN, respectively. In addition, it is proved that the performance of the introduced TB-DA-DBN+NN is well in detecting DR. In Figure 6.6, the classification performance of the developed TB-DA-DBN+NN is compared over traditional classifiers concerning learning percentage for DR detection is shown. The accuracy of TB-DA-DBN+NN is 25% surpassed than DBN+NN, 15.3% surpassed than NN, and 50% surpassed than DBN when taking the learning percentage as 85, which is shown in Fig.6.6 (a). Additionally, the precision of the recommended TB-DA-DBN+NN is acquiring best results when compared over conventional machine learning algorithms and it is displayed in Fig.6.6 (b). At learning percentage 75, the

precision of the developed TB-DA-DBN+NN is 9.4% higher than DBN+NN and NN and 77.1% higher than DBN. The overall performance of the suggested TB-DA-DBN+NN and the traditional classifiers is revealed in Table 6.2. From Table, the accuracy of the proffered TB-DA-DBN+NN is 49% progressed than DBN and 14.1% progressed than NN and DBN+NN, respectively. Therefore, it is confirmed that the recommended TB-DA-DBN+NN has obtained the optimal outcomes in detecting DR.

Fig. 6.5: Analysis of DR detection by segmenting optic disc using three performance metrics like (a) "Accuracy, (b) Precision, and (c) F1 score"

Table 6.1: Analysis on performance metrics for detecting diabetic retinopathy from optic disc using different heuristic-based hybrid classifier

Performance Measures	WOA-DBN+NN [72]	ROA-DBN+NN [97]	MGS-ROA-DBN+NN (73)	DA-DBN+NN [111]	MLU-DA-DBN+NN	TB-DA-DBN+NN (Proposed)
MCC	-0.0463	-0.0300	-0.0781	-0.0216	0.1198	**0.3866**
F1-score	0.1176	0.1250	0.0740	0.1290	0.2307	**0.4444**
FDR	0.9200	0.9130	0.9444	0.9090	0.8235	**0.6666**
NPV	0.7088	0.7341	0.7848	0.7468	0.8227	**0.8481**
FNR	0.7777	0.7777	0.8888	0.7777	0.6666	**0.3333**
FPR	0.2911	0.2658	0.2151	0.2531	0.1772	**0.1519**
Precision	0.0800	0.0869	0.0555	0.0909	0.1764	**0.3333**
Specificity	0.7088	0.7341	0.7848	0.7468	0.8227	**0.8481**
Sensitivity	0.2222	0.2222	0.1111	0.2222	0.3333	**0.6666**
Accuracy	0.6590	0.6818	0.7159	0.6931	0.7727	**0.8295**

(a)

(b)

(c)
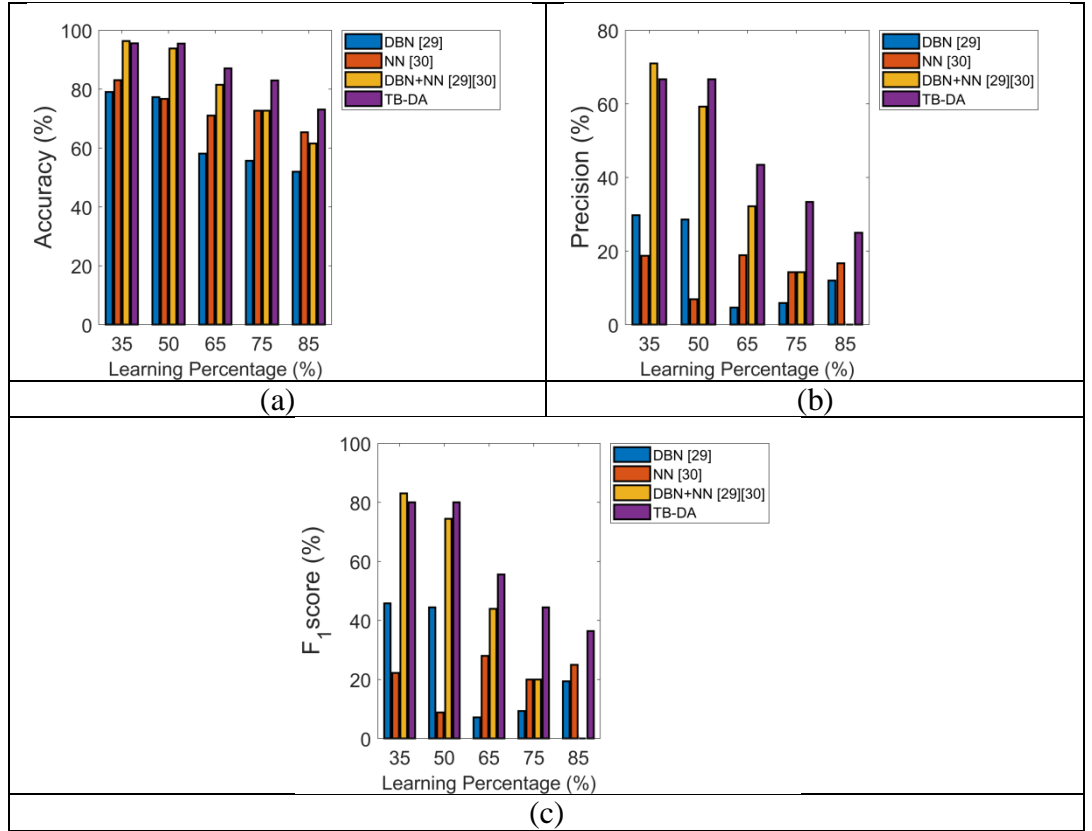
Fig. 6.6: Analysis of DR detection by segmenting optic disc using various conventional classifiers for performance metrics like "(a) Accuracy, (b) Precision, and (c) F1 score"

Table 6.2: Analysis on performance metrics for detecting diabetic retinopathy from optic disc using different existing classifiers

Performance Measures	DBN	NN	DBN+NN	TB-DA-DBN+NN (Proposed)
MCC	-0.1137	0.0749	0.0749	**0.3866**
F1-score	0.0930	0.2000	0.2000	**0.4444**
FDR	0.9411	0.8571	0.8571	**0.6666**
NPV	0.5949	0.7721	0.7721	**0.8481**
FNR	0.7777	0.6666	0.6666	**0.3333**
FPR	0.4050	0.2278	0.2278	**0.1519**
Precision	0.0588	0.1428	0.1428	**0.3333**
Specificity	0.5949	0.7721	0.7721	**0.8481**
Sensitivity	0.2222	0.3333	0.3333	**0.6666**
Accuracy	0.5568	0.7272	0.7272	**0.8295**

Fig. 6.7 shows the performance analysis of the proposed TB-DA-DBN+NN and meta-heuristic-oriented-DBN+NN in terms of learning percentage for detecting DR. From Fig. 6.7 (a), when describing any of the learning percentages, the accuracy of the introduced TB-DA-DBN+NN is attaining best results when compared over remaining algorithms. At learning percentage 85, the accuracy of the presented TB-DA-DBN+NN is 1.1% better than DA, 5.8% better than MGS-ROA, 8.4% advanced than ROA-DBN+NN and 11.1% advanced than MLU-DA-DBN+NN. When considering any of the learning percentages, the precision of the recommended TB-DA-DBN+NN is acquiring optimal performance in detecting DR. It is 1.4% superior to MLU-DA-DBN+NN and 16.6% higher than DA-DBN+NN at learning percentage 50. Table 6.3 shows the overall performance of the introduced TB-DA-DBN+NN and the traditionalheuristic-based-DBN+NN. In Table 6.3, the accuracy of the developed TB-DA-DBN+NN is 6.5% exceeded than WOA-DBN+NN, 3.8% exceed than ROA-DBN+NN, 1.2% exceeded than MGS-ROA-DBN+NN and 2.5% exceeded than MLU-DA-DBN+NN and DA-DBN+NN. Further, the overall analysis of the improved TB-DA-DBN+NN and the traditional machine learning algorithms with respect to learning percentage in detecting DR is depicted in Fig. 6.8. At learning percentage 35, the accuracy of the introduced TB-DA-DBN+NN is 2% progressed than DBN+NN, 41.4% progressed than NN, and 1% progressed than DBN and it is described in Fig. 6.8 (a). From Fig. 6.8 (b), the precision of the suggested TB-DA-DBN+NN at any of the learning percentages is attaining best results. It is 45% more

than DBN+NN, 65.5% more than NN, and 82.7% more than DBN when considering the learning percentage as 85. In Table 6.4, the overall analysis of the proffered TB-DA-DBN+NN and the traditional classifiers is tabulated. The developed TB-DA-DBN+NN's accuracy is 6.5% advanced than DBN+NN, and DBN and 10.9% advanced than NN. Thus, it is demonstrated that the developed TB-DA-DBN+NN are advanced than conventional algorithms in DR detection.
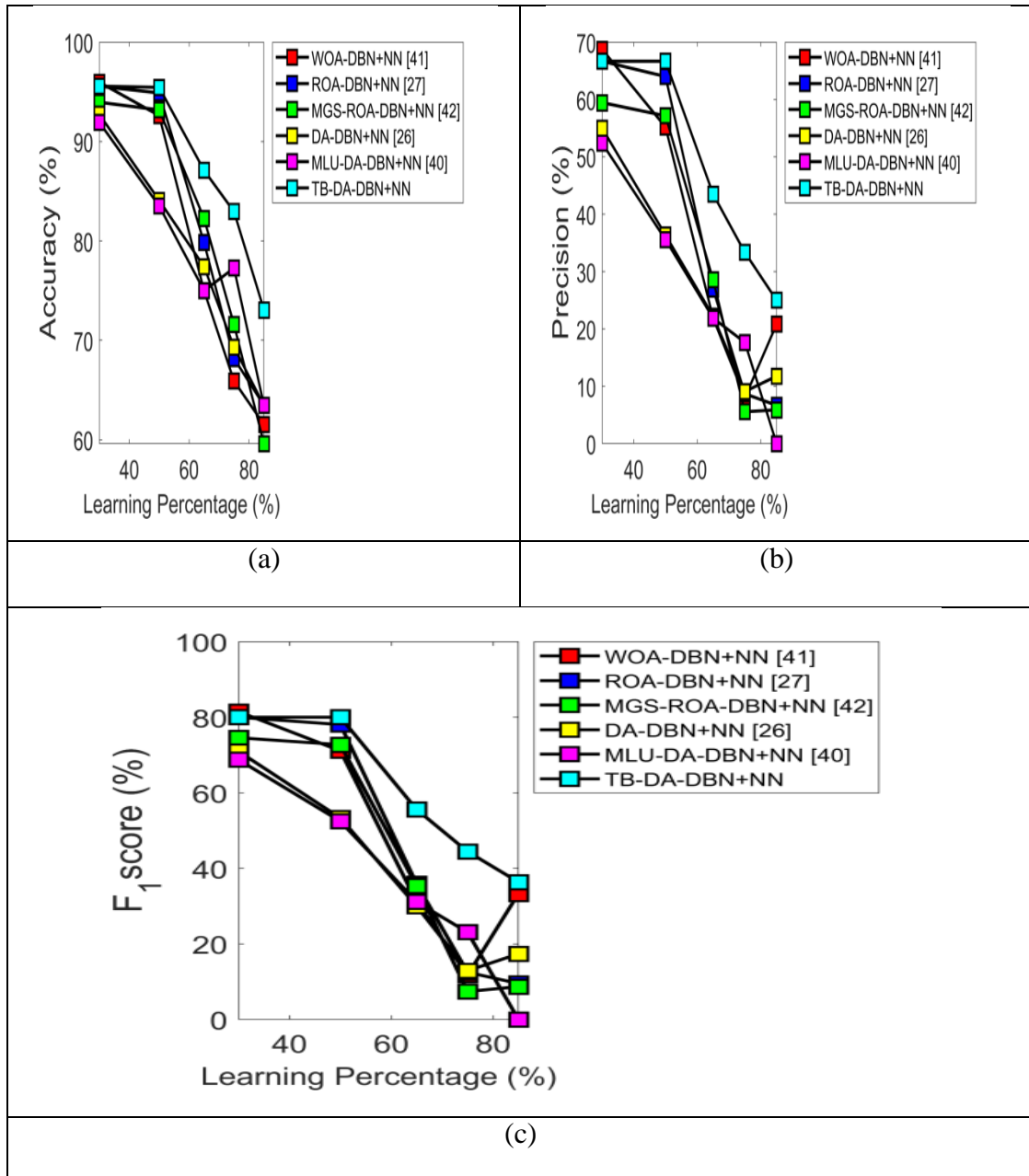

(a)

(b)

(c)
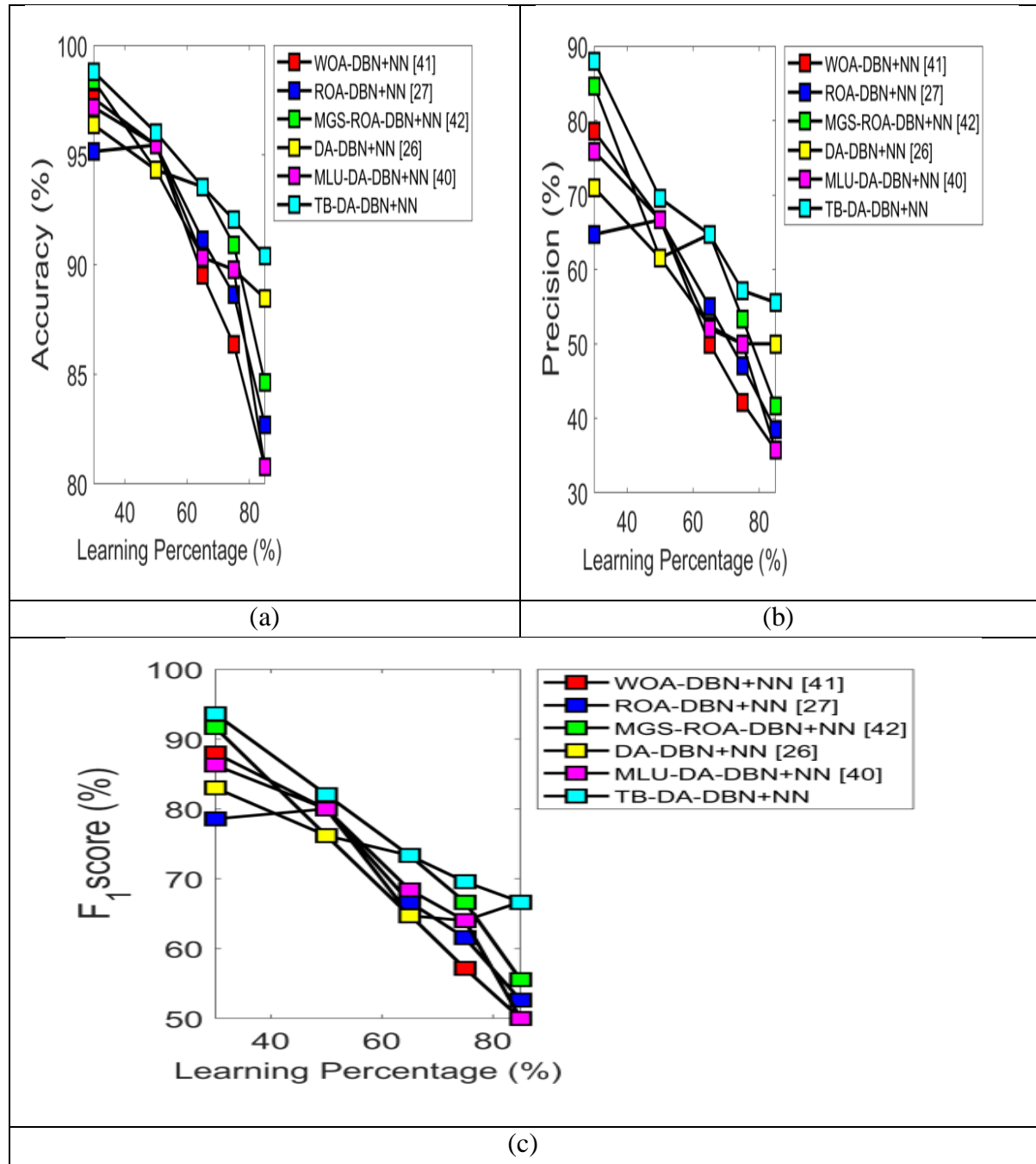
Fig. 6.7: Analysis of DR detection by segmenting blood vessels using three performance metrics like, "(a) Accuracy, (b) Precision, and (c) F1 score"

Table 6.3: Analysis on performance metrics for detecting diabetic retinopathy from blood vessels using different heuristic-based hybrid classifier

| Performance Measures	WOA-DBN+NN [72]	ROA-DBN+NN [97]	MGS-ROA-DBN+NN (73)	DA-DBN+NN [111]	MLU-DA-DBN+NN	TB-DA-DBN+NN (Proposed)
MCC	0.5520	0.5947	0.6448	0.6187	0.6187	**0.6734**
F1-score	0.5714	0.6153	0.6666	0.6400	0.6400	**0.6956**
FDR	0.5789	0.5294	0.4666	0.5000	0.5000	**0.4285**
NPV	0.8607	0.8860	0.9113	0.8987	0.8987	**0.9240**
FNR	0.1111	0.1111	0.1111	0.1111	0.1111	**0.1111**
FPR	0.1392	0.1139	0.0886	0.1012	0.1012	**0.0759**
Precision	0.4210	0.4705	0.5333	0.5000	0.5000	**0.5714**
Specificity	0.8607	0.8860	0.9113	0.8987	0.8987	**0.9240**
Sensitivity	0.8888	0.8888	0.8888	0.8888	0.8888	**0.8888**
Accuracy	0.8636	0.8863	0.9090	0.8977	0.8977	**0.9204**
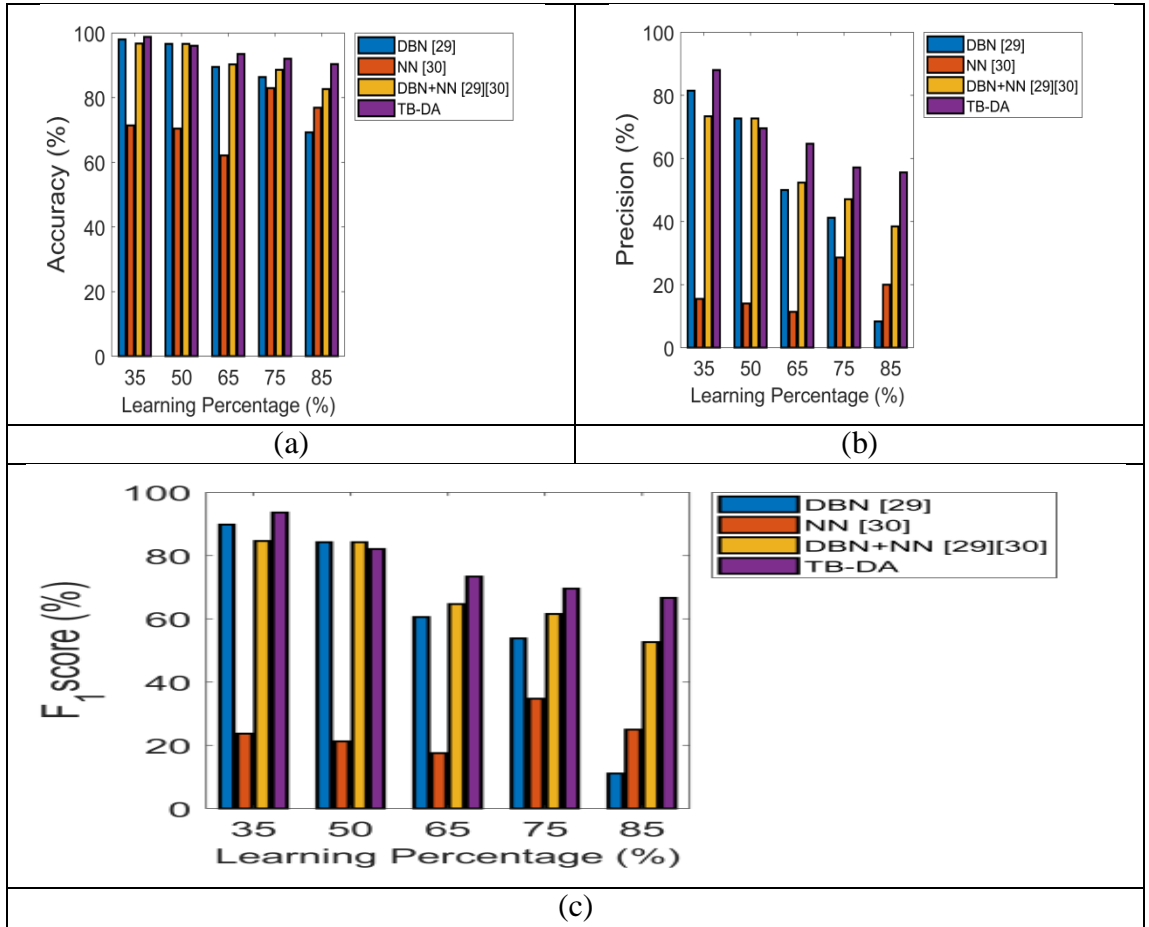
Fig. 6.8: Analysis of DR detection by segmenting blood vessels using various conventional classifiers for performance metrics like, "(a) Accuracy, (b) Precision, and (c) F1 score"

Table 6.4: Analysis on performance metrics for detecting diabetic retinopathy from blood vessels using different existing classifiers

Performance Measures	DBN [106]	NN [95]	DBN+NN [106]	TB-DA-DBN+NN (Proposed)
MCC	0.4998	0.2633	0.5947	**0.6734**
F1-score	0.5384	0.3478	0.6153	**0.6956**
FDR	0.5882	0.7142	0.5294	**0.4285**
NPV	0.8734	0.8734	0.8860	**0.9240**
FNR	0.2222	0.5555	0.1111	**0.1111**
FPR	0.1265	0.1265	0.1139	**0.0759**
Precision	0.4117	0.2857	0.4705	**0.5714**
Specificity	0.8734	0.8734	0.8860	**0.9240**
Sensitivity	0.7777	0.4444	0.8888	**0.8888**
Accuracy	0.8636	0.8295	0.8863	**0.9204**

In Fig. 6.9, the performance of the introduced TB-DA-DBN+NN and the traditionalheuristic-based-DBN+NN algorithms in terms of learning percentages for detecting DR is depicted. The accuracy of the suggested TB-DA-DBN+NN is gaining optimal outcomes in detecting DR at any of the learning percentages is depicted in Fig. 6.9 (a). When considering the learning percentage as 85, the accuracy of the developed TB-DA-DBN+NN is 3.4% improved than MLU-DA-DBN+NN, 5.8% progressed than ROA-DBN+NN, 8.4% progressed than DA-DBN+NN and 11.1% progressed than MGS-ROA-DBN+NN. The precision of the suggested TB-DA-DBN+NN at learning percentage 50 is 5.8% more than DA-DBN+NN, 20% more than MGS-ROA-DBN+NN, 25% more than MLU-DA-DBN+NN, and 50% more than WOA-DBN+NN. Table 6.5 describes the overall performance of the suggested TB-DA-DBN+NN and the existing algorithms for effective DR detection. Further, the accuracy of the introduced TB-DA-DBN+NN is 5% superior to WOA-DBN+NN and ROA-DBN+NN, 9.2% better than MGS-ROA-DBN+NN and 3.7% superior to DA-DBN + NN and MLU-DA-DBN + NN. The classification analysis of the recommended and the traditional classifiers concerning learning percentage for automatic DR detection is diagrammatically represented in Fig. 6.10. At learning percentage 85, the accuracy of the addressed TB-DA-DBN+NN is 13.9% progressed than DBN+NN, 11.1% progressed than NN and 5.8% progressed than DBN, which is shown in Fig. 6.10 (a). The precision of the introduced TB-DA-DBN+NN at learning percentage 85 from Fig. 6.10(b) is 56.7% progressed than DBN+NN, 48.7% progressed than NN and 16% progressed than DBN.

Furthermore, the overall classification analysis of the suggested TB-DA-DBN+NN and existing machine learning algorithms are tabulated in Table 6.6. The accuracy of the labeled TB-DA-DBN+NN is 2.4%, 3.7%, and 9.2% enhanced than DBN, NN, and DBN+NN. Finally, it is concluded that the improved TB-DA-DBN+NN is outperforming the conventional algorithms in DR detection from the retinal abnormalities
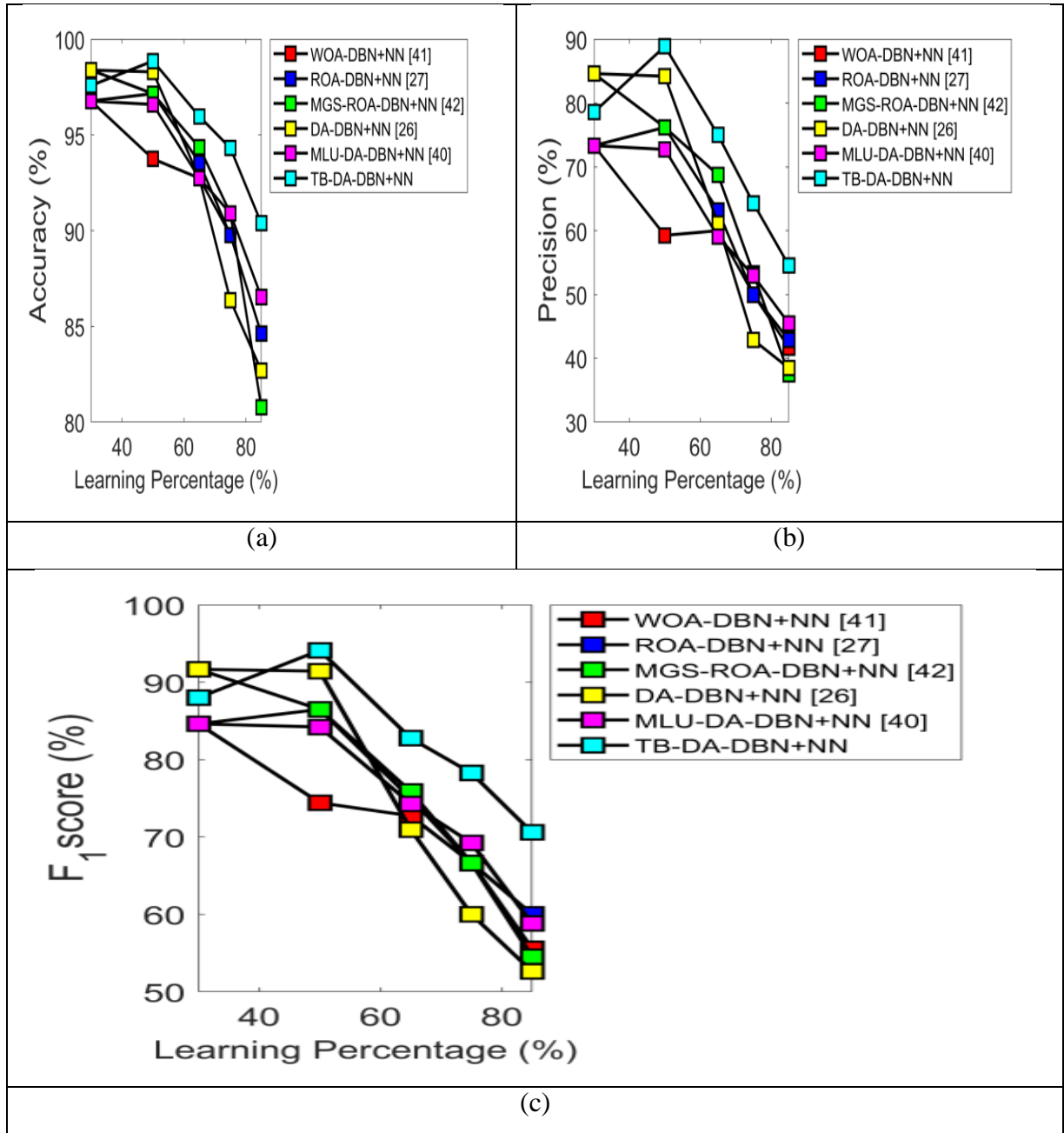
Fig. 6.9: Analysis of DR detection by segmenting retinal abnormalities using three performance metrics like, "(a) Accuracy, (b) Precision, and (c) F1 score"

Table 6.5: Analysis of performance metrics for detecting diabetic retinopathy from retinal abnormalities using different heuristic-based hybrid classifier

| Performance Measures	WOA-DBN+NN [91]	ROA-DBN+NN [106]	MGS-ROA-DBN+NN (95)	DA-DBN+NN [81]	MLU-DA-DBN+NN (80)	TB-DA-DBN+NN (Proposed)
MCC	0.6656	0.6656	0.6028	0.6448	0.6897	**0.7760**
F1-score	0.6666	0.6666	0.6000	0.6666	0.6923	**0.7826**
FDR	0.5000	0.5000	0.5714	0.4666	0.4705	**0.3571**
NPV	0.8860	0.8860	0.8481	0.9113	0.8987	**0.9367**
FNR	0.0000	0.0000	0.0000	0.1111	0.0000	**0.0000**
FPR	0.1139	0.1139	0.1519	0.0886	0.1012	**0.0632**
Precision	0.5000	0.5000	0.4285	0.5333	0.5294	**0.6428**
Specificity	0.8860	0.8860	0.8481	0.9113	0.8987	**0.9367**
Sensitivity	1.0000	1.0000	1.0000	0.8888	1.0000	**1.0000**
Accuracy	0.8977	0.8977	0.8636	0.9090	0.9090	**0.9431**
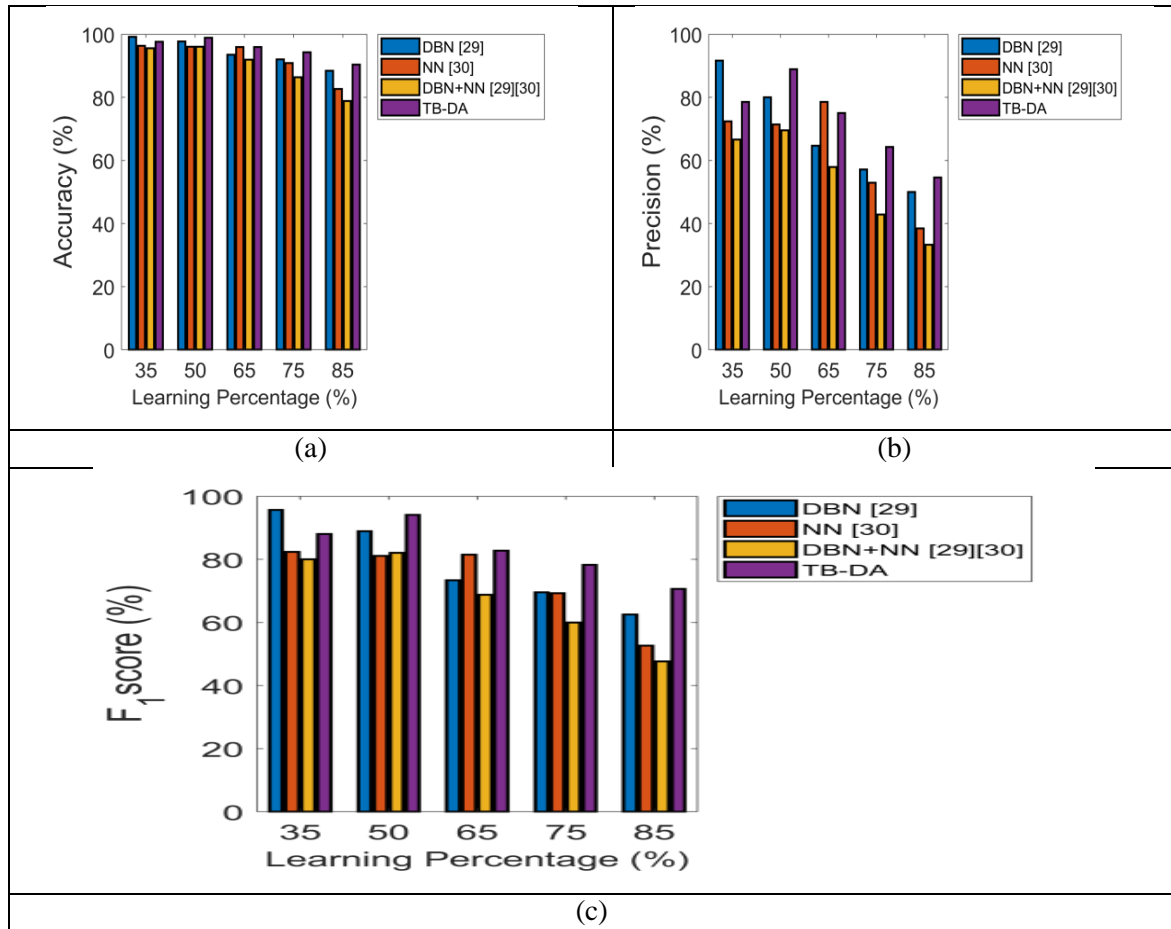
Fig. 6.10: Analysis of DR detection by segmenting retinal abnormalities using various conventional classifiers for performance metrics like, "(a) Accuracy, (b) Precision, and (c) F1 score"

Table 6.6: Analysis on performance metrics for detecting diabetic retinopathy from retinal abnormalities using different existing classifiers

Performance Measures	DBN [106]	NN [95]	DBN+NN [106]	TB-DA-DBN+NN (Proposed)
MCC	0.6734	0.6897	0.6028	**0.7760**
F1-score	0.6956	0.6923	0.6000	**0.7826**
FDR	0.4285	0.4705	0.5714	**0.3571**
NPV	0.9240	0.8987	0.8481	**0.9367**
FNR	0.1111	0.0000	0.0000	**0.0000**
FPR	0.0759	0.1012	0.1519	**0.0632**
Precision	0.5714	0.5294	0.4285	**0.6428**
Specificity	0.9240	0.8987	0.8481	**0.9367**
Sensitivity	0.8888	1.0000	1.0000	**1.0000**
Accuracy	0.9204	0.9090	0.8636	**0.9431**

6.5 Summary

The developed DR detection has included three analysis models that were relied on "optic disc, blood vessels and abnormalities of the retina". In the initial step, for the input images, the green channel conversion and the CLAHE operations are performed. By using open-close watershed transformations, the optic disc is segmented. Using the grey level thresholding, the blood vessels were segmented. The abnormality segmentation is performed using "top-hat transformation and Gabor filtering". From the segmented image, the features such as "LBP, TEM and Entropy features" are extracted. From the extracted features, the optimal features are chosen as the length of features seems to be high. This optimal feature selection is accomplished by the proposed TB-DA algorithm. These optimal features are given to the hybrid classifier named NN+DBN using the new training algorithm named TB-DA algorithm. Finally, the performance analysis is done based on optic disc, blood vessels and abnormalities using many performance measures. From the performance measure indicators, it is observed that the developed DR detection methodology provides very good results when compared with many existing algorithms.

Chapter 7

Conclusion and Future Scope

The research work towards the detection of Diabetic Retinopathy is carried out with different approaches. This research work has analyzed the retinal fundus images to show the efficient diagnosis of DR by intelligent approaches. The detection of DR is carried out in various phases. The conclusion with respect to the research work is summarized below.

7.1 Conclusion

- Firstly, the blood vessels, optic disc and exudates are analyzed by various methods. For the detection of optic disc, the wavelet transform is employed on the DIARETDB1 dataset. The morphological operations and DWT is used to detect the exudates and the classification is performed to classify images into "normal and abnormal images". In the analysis of blood vessels, filtering, image enhancement and morphological operations are used for the DRIVE database. The morphological operation, filtering, DWT and computation of PSNR and MSE are applied for the CHASE_DBI and DRIVE databases. GLCM features are extracted and classification is performed by SVM and distance measures. For the first contribution, better performance analysis is achieved for CHASE_DBI and DRIVE databases. The sensitivity of the suggested method is 26% and 0.38% advanced than Azzopardi and Fraz *et al.* respectively

- Secondly, the research work has utilized the wavelet transform for the "segmentation and classification" of the retinal images. Once the images are pre-processed, then the image segmentation is done by the two-level DWT with mathematical morphology. Thresholding is performed for segmenting optic disc and exudates. Spatial density is computed to differentiate between optic disc and exudates. For the second contribution, the proposed method has achieved better classification accuracy, which is 13% and 30% superior to Meindert Niemeije*r et al.* and K. Narasimha*n et al*.

- Thirdly, this research work has continued with the blood vessel segmentation and analysis for the detection of DR. The pre-processing is performed by the mixture of "CLAHE and average filter". The blood vessel segmentation is done by the optimized Gray level thresholding and the feature extraction is performed by the "LBP, TEM, Shanon's entropy and Kapur's entropy". Later, the images are classified using the optimally trained

NN. A new algorithm implemented called MLU-DA is used to improve the performance of segmentation and classification for the images as "normal and abnormal images".

- At the fourth phase, from the retinal fundus images, the DR diagnosis is done by the segmentation and analysis of the abnormalities in the retina such as "Microaneurysm, hemorrhages, hard exudates and soft exudates". Once the image enhancement is accomplished by the CLAHE, "the optic disc and the blood vessels" are removed using the open-close watershed transformation and Grey Level thresholding, respectively. Further, the retinal abnormalities are segmented by the "Top hat transformation and Gabor filtering". The resulting segmented abnormalities were subjected to the feature extraction process by "LBP, TEM, Shanon's and Kapur's entropy" and the obtained features are subjected to the optimal feature selection method by MGS-ROA. Then, the optimized DBN is employed to classify the images into normal, severe, moderate and earlier stages of DR. Here, the DBN weights are updated by the MGS-ROA and the DIARETDB1 image dataset is used for the experimentation. For the fourth contribution, the proposed MGS-ROA-DBN has shown better accuracy and it is 32.2%, 30.1%, and 17.1% superior to KNN, NN, DBN and SVM, respectively.

- The final contribution of the research work mainly focused on the analysis of "blood vessels, optic disc and retinal abnormalities" for the DR diagnosis. The optic disc and the blood vessels are segmented using the open-close watershed transformation and Grey Level thresholding, respectively. The "top hat transform and Gabor filtering" are used to segment the abnormalities such as Microaneurysm, hemorrhages, hard exudates and soft exudates. From the segmented optic disc, blood vessels and abnormalities, the features are extracted using methods like "LBP, TEM, Shanon's and Kapur's entropy". The proposed TB-DA is applied to execute the optimal feature selection process. The images are classified with the hybridization of NN and DBN, where the TB-DA is used for the training and classification of the images using the DIARETDB1 dataset. For the fifth contribution, better accuracy is achieved by the implemented TB-DA-DBN+NN than the conventional algorithms. It is 20%, 16.1%, and 12.5% superior to MGS-ROA, WOA and MLU-DA-based DBN+NN, respectively. The proposed TB-DA-DBN+NN shown the better accuracy than the conventional methods for segmenting blood vessels. It is 11.1%, 1.1%, 8.4% and 5.8% improved than MLU-DA, DA, ROA and MGS-ROA-based-DBN+NN, respectively. The proposed TB-DA-DBN+NN are compared with the other existing algorithms and it has shown better accuracy for the retinal abnormalities. It is

11.1%, 8.4%, 5.8% and 3.4% superior to MGS-ROA, DA, ROA and MLU-DA based-DBN+NN, respectively.

7.2 Future Scope

This research can be further extended by considering the below-mentioned points.

- The developed approach can be improved by adopting various classifiers along with more optimal feature sets for reducing the probability of errors. For the segmented images, the post-processing methods can be utilized to improve the results.

- The automatic screening can be further developed for predicting the abnormalities. This can assist the medical experts and patients for proper medical assistance.

- In the future, some more abnormalities such as fibrous proliferation, maculopathy, traction drusen, retinal detachment, macular edema, spot, etc can also be considered.

- For the segmentation of the blood vessels and other abnormalities, several algorithms can be applied further to validate the performance of the DR detection.

- The experiments can be done by the various other standard databases. As an improvement, the real-time DR images can also be experimented.

- In future, it is required to encourage the latest intelligent models from computer vision for categorizing the diverse stages of DR

Author's Publications

Journal Publications:

1. A.S.Jadhav and Pushpa B.Patil, "Classification of diabetes retina images using blood vessel area," *International Journal on Cybernetics & Informatics (IJCI),* vol. 4, no. 2, pp. 251-257, April 2015.

2. A. S. Jadhav, Pushpa B. Patil and Dr. Sunil Biradar "Computer Aided Diabetic Retinopathy Diagnostic Model using Optimal Thresholding Merged with Neural Network," *International Journal of Intelligent Computing & cybernetics*, vol.13, no.3, pp.283-310, July 2020

3. A. S. Jadhav and Pushpa B. Patil and Dr. Sunil Biradar "Optimal Feature Selection-based Diabetic Retinopathy Detection using Improved Rider Optimization Algorithm Enabled with Deep Learning," *Evolutionary Intelligence,*pp. 1-18, Aprl 2020

4. A. S. Jadhav, Pushpa B. Patil and Dr. Sunil Biradar, "Analysis of Diagnosing Diabetic Retinopathy by segmenting Blood vessels, Optic disc and retinal abnormalities," *Journal of Medical engineering and Technology*, vol.44, no.6, pp. 299-316, July 2020.

5. A. S. Jadhav, Pushpa B. Patil, "Algorithmic Analysis on Modified Gear and Steering-based Rider Optimization for Diagnosing Diabetic Retinopathy," Communicated to the *Journal of Multimedia Tools and Applications.*

Conference Publications:

1. A.S.Jadhav and Pushpa B.Patil, "Detection of Optic Disc from Retinal Images using Wavelet Transform", *In proceedings of international Conference on Signal processing, Communication, Power and Embedded System (SCOPES), Paralakhemundi*, pp.178-181, October 2016.

2. A.S.Jadhav and Pushpa B.Patil, "Detection of Exudates for Diabetic Retinopathy using Wavelet Transform", *In proceedings of international Conference Power, Control, Signal and Instrumentation Engineering (ICPCSI), Chennai*, pp.568-571, September 2017.

3. A.S.Jadhav and Pushpa B.Patil, "Detection of Blood vessels in Retinal images for diagnosis of Diabetics," *In proceedings of international and Conference on Inventive Systems and Control (ICISC), Coimbatore*, pp.888-891, Janaury 2018.

4. A. S. Jadhav and Pushpa B. Patil, "Preprocessing and Segmentation of Retina Images for Blood Vessel Extraction," *In proceedings of international conference on Recent Trends in Image Processing and Pattern Recognition (RTIP2R-2018), Solapu*r, pp. 341-348, December 2018.

5. A.S.Jadhav and Pushpa B.Patil, "Segmentation and Classification of Retina Images using SVD Features", 5th IEEE International conference ICEECCOT-2021 held on 10th to 11th Dec.2021 at Mysore.

Book chapters:

[1] A.S. Jadhav and Pushpa B. Patil, "Blood Vessel Segmentation using Wavelet transform and Grading of Retina images using Distance Measures," *In Book Advances in Biometrics, Modern Methods and Implementation Strategies,* pp. 157-182, November 2019.

References

[1] Md Mohaimenul Islam, Hsuan ChiaYang, Tahmina NasrinPoly and Wen-ShanJianeYu-Chuan, "Deep learning algorithms for detection of diabetic retinopathy in retinal fundus photographs: A systematic review and meta-analysis," *Computer Methods and Programs in Biomedicine*, vol. 191, pp.1-16, July 2020.

[2] K. A. Goatman, A. D. Fleming, S. Philip, G. J. Williams, J. A. Olson and P. F. Sharp, "Detection of New Vessels on the Optic Disc Using Retinal Photographs," *IEEE Transactions on Medical Imaging*, vol. 30, no. 4, pp. 972-979, April 2011.

[3] Qiwei Xie, Yanfei Liu, Hui Huang, Bei Hong, Jinxin Wang, Hua Han, and Yue Liu, "An innovative method for screening and evaluating the degree of diabetic retinopathy and drug treatment based on artificial intelligence algorithms," *Pharmacological Research*, vol. 159, pp.1-9, September 2020.

[4] Yulan Dai, Chengzhang Zhu, Xi Shan, Zhenzhen Cheng, and Beiji Zou, "A Survey on Intelligent Screening for Diabetic Retinopathy," *Chinese Medical Sciences Journal*, vol. 34, no. 2, pp. 120-132, June 2019.

[5] S. Safia, T. Anam, M.U. A., "A comparison and evaluation of computerized methods for blood vessel enhancement and segmentation in retinal images," *International Journal of Future Computer Communication,* vol. 2, no. 6, pp. 600–603, December 2013.

[6] R.S. Biyani and B.M.Patre, "Algorithms for red lesion detection in Diabetic Retinopathy: A review," *Biomedicine & Pharmacotherapy*, vol. 107, pp. 681-688, November 2018.

[7] Y. Sun and D. Zhang, "Diagnosis and Analysis of Diabetic Retinopathy Based on Electronic Health Records," *IEEE Access*, vol. 7, pp. 86115-86120, May 2019.

[8] K. Jaspreet, H.P.Sinha. Dr, "Automated detection of retinal blood vessels in diabetic retinopathy using Gabor filter," *International Journal of Computer Science Network Secuity,* vol. 12, no. 4, pp. 109–116, April 2012.

[9] A. Osareh, B. Shadgar and R. Markham, "A Computational-Intelligence-Based Approach for Detection of Exudates in Diabetic Retinopathy Images," *IEEE*

Transactions on Information Technology in Biomedicine, vol. 13, no. 4, pp. 535-545, July 2009.

[10]   A.S.Jadhav and Pushpa B. Patil, "Classification of diabetes retina images using blood vessel area," *International Journal on Cybernetics & Informatics (IJCI),* Vol. 4, No. 2, pp. 251-257, April 2015.

[11]   A.S.Jadhav and Pushpa B. Patil, "Preprocessing and Segmentation of Retina Images for Blood Vessel Extraction," I*n Proc.Int.Conf.on Recent Trends in Image Processing and Pattern Recognition (RTIP2R-2018),* Solapur, pp. 341-348, 2018

[12]   A.S.Jadhav and Pushpa B. Patil, "Detection of Blood vessels in Retinal images for diagnosis of Diabetics," *In Proc. Int.Conf. on Inventive Systems and Control (ICISC),* Coimbatore, pp.888-891, 2018

[13]   Jiawei Xu, Xiaoqin Zhang, Huiling Chen, Jing Li, Jin Zhang, Ling Shao and Gang Wang, "Automatic Analysis of Microaneurysms Turnover to Diagnose the Progression of Diabetic Retinopathy," *IEEE Access*, vol. 6, pp. 9632-9642, Febraury 2018.

[14]   Akara Sopharak, Bunyarit Uyyanonvara and Sarah Barman, "Simple hybrid method for fine microaneurysm detection from non-dilated diabetic retinopathy retinal images," *Computerized Medical Imaging and Graphics,* vol. 37, no.s 5–6, pp. 394-402, July–September 2013.

[15]   Tao Li, Yingqi Gao, Kai Wang, Song Guo, HanruoLiu and Hong Kang, "Diagnostic assessment of deep learning algorithms for diabetic retinopathy screening," *Information Sciences*, vol.501, pp.511-522, October 2019.

[16]   Hugo Aguirre-Ramos, Juan GabrielAvina-Cervantes, IvanCruz-Aceves, JoséRuiz-Pinales, and SergioLedesma, "Blood vessel segmentation in retinal fundus images using Gabor filters, fractional derivatives and Expectation Maximization," *Applied Mathematics and Computation*, vol.339, pp.568-587, December 2018.

[17]   J. Wang, Y. Bai and B. Xia, "Feasibility of Diagnosing Both Severity and Features of Diabetic Retinopathy in Fundus Photography*," IEEE Access*, vol. 7, pp. 102589-102597, July 2019.

[18] W. Zhou, C. Wu, D. Chen, Y. Yi and W. Du, "Automatic Microaneurysm Detection Using the Sparse Principal Component Analysis-Based Unsupervised Classification Method," *IEEE Access, vol.* 5, pp. 2563-2572, February 2017.

[19] D. Kumar, G. W. Taylor and A. Wong, "Discovery Radiomics with CLEAR-DR: Interpretable Computer Aided Diagnosis of Diabetic Retinopathy," *IEEE Access,* vol. 7, pp. 25891-25896, January 2019.

[20] Fahimuddin Shaik, Anil Kumar Sharma and Syed Musthak Ahmed, "Hybrid model for analysis of abnormalities in diabetic cardiomyopathy and diabetic retinopathy related images," *Springer Plus*, vol. 5, pp.1-17, April 2016.

[21] C. Agurto, Victor Murray, Eduardo Barriga, Sergio Murillo, Marios Pattichis, Herbert Davis, Stephen Russell, Michael Abràmoff and Peter Soliz, "Multiscale AM-FM Methods for Diabetic Retinopathy Lesion Detection," *IEEE Transactions on Medical Imaging*, vol. 29, no. 2, pp. 502-512, February 2010.

[22] L. Zhou, Y. Zhao, J. Yang, Q. Yu and X. Xu, "Deep multiple instance learning for automatic detection of diabetic retinopathy in retinal images," *IET Image Processing*, vol. 12, no. 4, pp. 563-571, April 2018.

[23] P. Costa, A. Galdran, A. Smailagic and A. Campilho, "A Weakly-Supervised Framework for Interpretable Diabetic Retinopathy Detection on Retinal Images," *IEEE Access*, vol. 6, pp. 18747-18758, March 2018.

[24] B. Dashtbozorg, J. Zhang, F. Huang and B. M. ter Haar Romeny, "Retinal Microaneurysms Detection Using Local Convergence Index Features," *IEEE Transactions on Image Processing*, vol. 27, no. 7, pp. 3300-3315, July 2018.

[25] L. Seoud, T. Hurtut, J. Chelbi, F. Cheriet and J. M. P. Langlois, "Red Lesion Detection Using Dynamic Shape Features for Diabetic Retinopathy Screening," *IEEE Transactions on Medical Imaging*, vol. 35, no. 4, pp. 1116-1126, April 2016.

[26] Ruikar D.D., Santosh K.C. and Hegadi R.S., "Segmentation and analysis of CT images for bone fracture detection and labelling," *in: Medical Imaging: Artificial Intelligence, Image Recognition, and Machine Learning Techniques*, New York, Taylor & Francis Group, 2020, Ch. 7, PP.131-154.

[27] Hegadi, R.S., Navale, D.I., Pawar, T.D., Ruikar, D.D, "Multi feature-based classification of osteoarthritis in knee joint X-ray images," *in Medical Imaging: Artificial Intelligence, Image Recognition and Machine Learning Techniques*, New York, Taylor & Francis Group, 2020, Ch. 5, PP. 75-96.

[28] G.Azzopardi, N. Strisciuglio, M. Vento and N. Petkov, "Trainable COSFIRE filters for vessel delineation with application to retinal images," *Medical Image Analysis*, vol. 19, pp. 46-57, January 2015.

[29] Fraz, M., Remagnino, P., Hoppe, A., Uyyanonvara, B., Rudnicka, A., Owen, C., Barman, S., "An ensemble classification-based approach applied to retinal blood vessel segmentation," *IEEE Transactions on Biomedical Engineering*, vol. 59, pp. 2538-2548, June 2012.

[30] Deepa Thomas, Dr.Jubilant and Shabana, "Segmentation of the Blood Vessel and Optic Disc in Retinal Images Using EM Algorithm," *IOSR Journal of Computer Engineering (IOSR-JCE)*, vol. 17, no. 6, pp. 102-112, December 2015.

[31] Lam, Gao and Liew, "General retinal vessel segmentation using Regularization based multiconcavity modeling," *IEEE Transactions on Medical Imaging*, vo. 29, no.7, pp. 1369-1381, July 2010.

[32] A.M. Mendonca and A. Campilho, "Segmentation of retinal blood vessels by combining the detection of centerlines and morphological reconstruction," *IEEE Transactions on Medical Imaging*, vol. 25, no. 9, pp. 1200-1213, September 2006.

[33] Santosh Nagnath Randive, Amol D. Rahulkar and Ranjan K. Senapati1, "LVP extraction and triplet-based segmentation for diabetic retinopathy recognition," *Evolutionary Intelligence,* vol. 11, pp.117–129, June 2018.

[34] Ambaji S. Jadhav and Pushpa B. Patil, "Blood Vessel Segmentation using Wavelet transform and Grading of Retina images using Distance Measures," *in Advances in Biometrics, Modern Methods and Implementation Strategies,* Springer, Cham, 2019, Ch.8, pp. 157-182.

[35] M. Niemeijer, M. D. Abramoff and B. van Ginneken, "Information Fusion for Diabetic Retinopathy CAD in Digital Color Fundus Photographs," *IEEE Transactions on Medical Imaging,* vol. 28, no. 5, pp. 775-785, May 2009.

[36] H. Narasimha-Iyer et al., "Robust detection and classification of longitudinal changes in color retinal fundus images for monitoring diabetic retinopathy," *IEEE Transactions on Biomedical Engineering,* vol. 53, no. 6, pp. 1084-1098, June 2006.

[37] A.S. Jadhav and Pushpa B. Patil, "Detection of Optic Disc from Retinal Images using Wavelet Transform," in Proc. Int. Conf. of Signal processing, Communication, Power and Embedded System (SCOPES), Paralakhemundi, pp. 178-181, 2016

[38] A.S.Jadhav and Pushpa B. Patil, "Detection of Exudates for Diabetic Retinopathy using Wavelet Transform," *in Proc.of Int. Conf. of Power, Control, Signal and Instrumentation Engineering (ICPCSI),* Chennai, pp.568-571, 2017.

[39] B. Antal and A. Hajdu, "An Ensemble-Based System for Microaneurysm Detection and Diabetic Retinopathy Grading," *IEEE Transactions on Biomedical Engineering*, vol. 59, no. 6, pp. 1720-1726, June 2012.

[40]   R. Pires, S. Avila, H. F. Jelinek, J. Wainer, E. Valle and A. Rocha, "Beyond Lesion-Based Diabetic Retinopathy: A Direct Approach for Referral," *IEEE Journal of Biomedical and Health Informatics*, vol. 21, no. 1, pp. 193-200, Janaury. 2017.

[41] S. Sil Kar and S. P. Maity, "Gradation of diabetic retinopathy on reconstructed image using compressed sensing," *IET Image Processing*, vol. 12, no. 11, pp. 1956-1963, November 2018.

[42] Eydis Olafsdottir, Dan K. G. Andersson, Inger Dedorsson, Kurt Svärdsudd, Stefan P. O. Jansson, and Einar Stefánsson,"Early detection of type 2 diabetes mellitus and screening for retinopathy are associated with reduced prevalence and severity of retinopathy," vol. 94, no. 3, pp. 232-239, May 2016.

[43] S.S. Basha and K.S. Prasad, "Automatic detection of hard exudates in diabetic retinopathy using morphological segmentation and fuzzy logic," *International Journal of Computer Science and Network Security*, vol. 8, no. 12, pp. 211-218, December 2008.

[44] A. B. Mansoor, Z. Khan, A. Khan and S. A. Khan, "Enhancement of exudates for the diagnosis of diabetic retinopathy using Fuzzy Morphology," *in Proc.Int.Conf. on Multitopic*, Karachi, pp. 128-131, 2008

[45] H. Das, A. Saha and S. Deb, "An expert system to distinguish a defective eye from a normal eye," *in Proc. Int. Conf. on Issues and Challenges in Intelligent Computing Techniques (ICICT),* Ghaziabad, pp. 155-158, 2014

[46] R. Bhattacharjee and M. Chakraborty, "Exudates, retinal and statistical features detection from diabetic retinopathy and normal fundus images: An automated comparative approach," *in Proc. Int. Conf. on Computing and Communication Systems*, Durgapur, pp. 1-6, 2012

[47] A. Osareh, M. Mirmehdi, B. Thomas and R. Markham, "Automated identification of diabetic retinal exudates in digital colour images," *British Journal of Ophthalmology*, vol. 87, 1220–1223, September 2003.

[48] N. G. Ranamuka and R. G. N. Meegama, "Detection of hard exudates from diabetic retinopathy images using fuzzy logic," *IET Image Processing*, vol. 7, no. 2, pp. 121-130, March 2013.

[49] Keeffe J, Taylor HR, Fotis K, Pesudovs K, Flaxman SR, Jonas JB, J Leasher, K Naidoo, H Price, R A White, T Y Wong, S Resnikoff and R. A. Bourne, "Prevalence and causes of vision loss in Southeast Asia and Oceania: 1990–2010," *British Journal of Ophthalmol*, vol. 98, pp. 586-591, August 2014.

[50] Resnikoff S, Pascolini D, Etya'ale D, Kocur I, Pararajasegaram R, Pokharel GP and Silvio P. Mariotti, "Global data on visual impairment in the year 2002," *Bull World Health Organization,* vol. 82, pp. 844-851, November 2004.

[51] Yoon KC, Mun GH, Kim SD, Kim SH, Kim CY, Park KH, Young Jeung Park, Seung-Hee Baek, Su Jeong Song, Jae Pil Shin, Suk-Woo Yang, Seung-Young Yu, Jong Soo Lee, Key Hwan Lim, Hye-Jin Park, Eun-Young Pyo, Ji-Eun Yang, Young-Taek Kim, Kyung-Won Oh and Se Woong Kang, "Prevalence of Eye Diseases in South Korea: Data From the Korea National Health and Nutrition Examination Survey 2008-2009," *Korean Journal of Ophthalmol*, vol. 25, no. 6, pp. 421-433, December 2011

[52] Ie Byung Park et al., "Diabetes Epidemics in Korea: Reappraise Nationwide Survey of Diabetes: Diabetes in Korea 2007," *Diabetes Metab Journal*, vol. 37, no. 4, pp. 233-239, August 2013.

[53] H. K. Kim, C. H. Kim, S. W. Kim, J. Y. Park, S. K. Hong, Y. H. Yoon and K. U. Lee, "Development and Progression of Diabetic Retinopathy in Koreans With NIDDM," *Diabetes Care*, vol. 21, no. 1, pp. 134-138, Janaury 1998.

[54] Yoon Jeon Kim, June-Gone Kim, Joo Yong Lee, Kyoung Sub Lee, Soo Geun Joe, Joong-Yeol Park, Min-Seon Kim and Young Hee Yoon, "Development and Progression of Diabetic Retinopathy and Associated Risk Factors in Korean Patients With Type 2 Diabetes: The Experience of a Tertiary Center," *Journal of Korean Medical Science*, vol. 29, no. 12, pp. 1699-1705, December 2014.

[55] Ahmed Wasif Raza C. Esswaran. Kaharudin Dimyati, "Diagnosis of diabetic retinopathy: Automatic extraction of optic disc and exudates from retinal images using marker control watershed transformation," *Journal of medical sysyems*, vol. 35, pp. 1491-1501, Janaury 2011.

[56] Walter,T., Klein, J.C., Massin, P. and Erginary, A, "A contribution of image processing to the diagnosis of diabetic retinopathy-Detection of exudates in color fundus images of the human retina," *IEEE Transactions in Medical Imaging*, vol. 21, no. 10, pp. 1236-1243, October 2002.

[57] Ambaji S. Jadhav and Pushpa B. Patil, "Computer Aided Diabetic Retinopathy Diagnostic Model using Optimal Thresholding Merged with Neural Network," *International Journal of Intelligent Computing & cybernetics*, vol.13, no.3, pp.283-310, July 2020

[58] Sabyasachi Chakraborty, Gopal Chandra Jana, Divya Kumari, and Aleena Swetapadma, "An improved method using supervised learning technique for diabetic retinopathy detection," *International Journal of Information Technology*, vol.13, no.3, pp.283-310, July 2019

[59] M. Leeza and H. Farooq, "Detection of severity level of diabetic retinopathy using Bag of features model," *IET Computer Vision*, vol. 13, no. 5, pp. 523-530, August 2019.

[60] S.W. Franklin, and S.E. Rajan, "Diagnosis of diabetic retinopathy by employing image processing technique to detect exudates in retinal images," *IET Image Procesing*, vol. 8, no.10, pp. 601–609, November 2013.

[61] D. Marín, A. Aquino, M. E. Gegundez-Arias and J. M. Bravo, "A New Supervised Method for Blood Vessel Segmentation in Retinal Images by Using Gray-Level and Moment Invariants-Based Features," *IEEE Transactions on Medical Imaging*, vol. 30, no. 1, pp. 146-158, Jan. 2011.

[62] Javeria Amin, Muhammad Sharif, Amjad Rehman, Mudassar Raza, and Muhammad Rafiq Mufti, "Diabetic retinopathy detection and classification using hybrid feature set," *Special Section: Light Sheet Fluorescence Illumination Microscopy*, vol. 81, no. 9, pp.990-996, September 2018.

[63] Shailesh Kumar, Abhinav Adarsh, Basant Kumar and Amit Kumar Singh, "An automated early diabetic retinopathy detection through improved blood vessel and optic disc segmentation," *Optics and Laser Technology*, vol. 121, pp. 1-11, January 2020.

[64] F. Amel, M. Mohammed and B. Abdelhafid, "Improvement of the hard exudates detection method used for computer-aided diagnosis of diabetic retinopathy," *International Journal of Image, Graphics and Signal Processing (IJIGSP)*, vol.4, no.4, pp. 19–27, May 2012.

[65] A Osareh, M Mirmehdi, B Thomas and R Markham, "Automated identification of diabetic retinal exudates in digital colour images," *British journal of ophthalmology vol.* 87, no.10, pp.1220-1223, January 2003.

[66] Akara Sopharak, Bunyarit Uyyanonvara and Sarah Barman, "Simple hybrid method for fine microaneurysm detection from non-dilated diabetic retinopathy retinal images," *Computerized Medical Imaging and Graphics*, vol. 37, no.s 5–6, pp. 394-402, July–September 2013.

[67] G.G. Rajput and Preethi N. Patil, "Detection and Classification of Exudates using k-Means Clustering in color Retinal Images," *in Proc. Int. Conf. on Signal and Image Processing,* Bangalore, pp.126-130, 2014

[68] Frank A Sloan, Arseniy P Yashkin, and Yiqun Chen, "Gaps in Receipt of Regular Eye Examinations Among Medicare Beneficiaries Diagnosed With Diabetes or Chronic Eye Diseases," *Ophthalmology*, vol. 121, no. 12, pp. 2452-2460, December 2014.

[69] N. P. Nirmala Sreedharan, B. Ganesan, R. Raveendran, P. Sarala, B. Dennis, and R. Boothalingam R., "Grey Wolf optimisation-based feature selection and classification for facial emotion recognition," *IET Biometrics*, vol. 7, no. 5, pp. 490-499, September 2018.

[70] S. Liao, M. W. K. Law and A. C. S. Chung, "Dominant Local Binary Patterns for Texture Classification," *IEEE Transactions on Image Processing*, vol. 18, no. 5, pp. 1107-1118, May 2009.

[71] Gupta R. and Undrill P.E., "The use of texture analysis to delineate suspicious masses in mammography," *Physics in Medicine Biology*, vol.40, pp. 835–855, May 1995.

[72] M.E.H.Pedersen, and A.J.Chipperfield, "Simplifying Particle Swarm Optimization," *Applied Soft Computing*, vol.10, no.2, pp.618-628, March 2010

[73] F. Fernández-Navarro, M. Carbonero-Ruz, D. Becerra Alonso and M. Torres-Jiménez, "Global Sensitivity Estimates for Neural Network Classifiers," *IEEE Transactions on Neural Networks and Learning Systems*, vol. 28, no. 11, pp. 2592-2604, November 2017.

[74] Seyedali Mirjalili and Andrew Lewis, "The Whale Optimization Algorithm," *Advances in Engineering Software* vol.95, pp.51-67, May 2016.

[75] Seyedali Mirjalili, Seyed Mohammad Mirjalili and Andrew Lewis, "Grey Wolf Optimizer," *Advances in Engineering Software*, vol.69, pp.46-61, March 2014.

[76] Ambaji S. Jadhav and Pushpa B. Patil, "Optimal Feature Selection-based Diabetic Retinopathy Detection using Improved Rider Optimization Algorithm Enabled with Deep Learning," *Evolutionary Intelligence,* pp. 1-18, April 2020

[77] Chen Y, Hu X, Fan W, Shen L, Zhang Z, Liu X, Du J, Li H, Chen Y, Li H., "Fast density peak clustering for large scale data based on kNN," *Knowl-Based Syst*, Available online July 2019.

[78] Sundararaj Wilfred Franklin and Samuelnadar Edward Rajan, "Diagnosis of diabetic retinopathy by employing image processing technique to detect exudates in retinal images," *IET Image Processing,* vol. 8, no. 10, pp. 601–609, October 2014.

[79] Gerald S. and Edmond L., "An investigation into neural network for detection of exudates in retinal images," *Applications of Soft Computing (ASC),* vol. 52, pp. 169–177, October 2009.

[80] C. Jayakumari and T. Santhanam, "An intelligent approach to detect hard and soft exudates using echo state neural network," *Information Technology Journal*, vol. 7, no. 2, pp. 386–395, January 2008.

[81] S. N. Sangeetha and P. Uma Maheswari, "An Intelligent Model for Blood Vessel Segmentation in Diagnosing DR Using CNN," *Journal of Medical Systems*, vol.42, no.175, pp.1-10, October 2018.

[82] Shaohua Wan, Yan Liang and Yin Zhang, "Deep convolutional neural networks for diabetic retinopathy detection by image classification," *Computers and Electrical Engineering*, vol.72, pp.274-282, November 2018.

[83] D. Jude Hemanth, Omer Deperlioglu and Utku Kose, "An enhanced diabetic retinopathy detection and classification approach using deep convolutional neural network," *Neural Computing and Applications*, vol. 32, pp.1–15, January 2019.

[84] X. Zeng, H. Chen, Y. Luo and W. Ye, "Automated Diabetic Retinopathy Detection Based on Binocular Siamese-Like Convolutional Neural Network," vol. 7, pp. 30744-30753, March 2019.

[85] Sehrish Qummar, Fiaz Gul Khan, Sajid Shah, Ahmad Khan, Shahaboddin Shamshirband, Zia Ur Rehman, Iftikhar Ahmed Khan and Waqas Jadoon, " A Deep Learning Ensemble Approach for Diabetic Retinopathy Detection," *IEEE Access*, vol. 7, pp. 150530-150539, October 2019.

[86] Y. Sun, "The Neural Network of One-Dimensional Convolution-An Example of the Diagnosis of Diabetic Retinopathy," *IEEE Access*, vol. 7, pp. 69657-69666, May 2019.

[87] Z. Gao, J. Li, J. Guo, Y. Chen, Z. Yi and J. Zhong, "Diagnosis of Diabetic Retinopathy Using Deep Neural Networks," *IEEE Access*, vol. 7, pp. 3360-3370, December 2019.

[88] M. Ghazal, S. S. Ali, A. H. Mahmoud, A. M. Shalaby and A. El-Baz, "Accurate Detection of Non-Proliferative Diabetic Retinopathy in Optical Coherence Tomography Images Using Convolutional Neural Networks," *IEEE Access*, vol. 8, pp. 34387-34397, February 2020

[89] Murat Seçkin Ayhan, Laura Kühlewein, Gulnar Aliyeva, Werner Inhoffen, Focke Ziemssen and Philipp Berens, "Expert-validated estimation of diagnostic uncertainty for deep neural networks in diabetic retinopathy detection," *Medical Image Analysis*, vol. 64, pp.1-13, August 2020.

[90] Gabriel Tozatto Zago, Rodrigo Varejão Andreão, Bernadette Dorizzi and Evandro Ottoni Teatini Salles, "Diabetic retinopathy detection using red lesion localization and convolutional neural networks," *Computers in Biology and Medicine*, vol. 116, pp. 1-12, January 2020.

[91] Tahira Nazir, Aun Irtaza, Zain Shabbir, Ali Javed, Usman Akram and Muhammad Tariq Mahmood, "Diabetic retinopathy detection through novel tetragonal local octa patterns and extreme learning machines," *Artificial Intelligence in Medicine*, vol. 99, pp. 1-10, August 2019.

[92] Sonali, Sima Sahu, Amit Kumar Singh, S.P.Ghrera and Mohamed Elhoseny, "An approach for de-noising and contrast enhancement of retinal fundus image using CLAHE," *Optics and Laser Technology*, vol.110, pp.87-98, February 2019

[93] S. Madhumitha and M. Manikandan, "Quantitative analysis of marker-based watershed image segmentation," *Department of Electronics Engineering, Madras Institute of Technology, Anna University*, vol. 114, no. 5, 10 March 2018.

[94] Ali Abdullah Yahya, Jieqing Tan and Min Hu, "A Novel Model of Image Segmentation Based on Watershed Algorithm," *Advances in Multimedia (Report)*, Publisher: Hindawi Limited, August 2013.

[95] Shihab Hamad Khaleefah, Salama A.Mostafa, Aida Mustapha and Mohammad Faidzul Nasrudin, "The ideal effect of Gabor filters and Uniform Local Binary Pattern combinations on deformed scanned paper images," *Journal of King Saud University - Computer and Information Sciences*, vol.4, pp. 1-12, July 2019

[96] D. Binu and B. S Kariyappa, " RideNN: A New Rider Optimization Algorithm-Based Neural Network for Fault Diagnosis in Analog Circuits," *IEEE Transactions on Instrumentation and Measurement,* vol.68, no.1, pp. 2-26, January 2019.

[97] Yumin Liu, Haofei Zhou, Fugee Tsung and Shuai Zhang, "Real-time quality monitoring and diagnosis for manufacturing process profiles based on deep belief networks," *Computers and Industrial Engineering,* vol.136, pp.494-503, October 2019.

[98] K.Shankar, Abdul Rahaman WahabSait, Deepak Gupta, S.K.Lakshmanaprabu, Ashish Khanna, and Hari Mohan Pandey, "Automated detection and classification of fundus diabetic retinopathy images using synergic deep learning model," *Pattern Recognition Letters,* vol. 133, pp. 210-216, May 2020

[99] Ambaji S. Jadhav and Pushpa B. Patil, "Computer Aided Diabetic Retinopathy Diagnostic Model using Optimal Thresholding Merged with Neural Network, "Analysis of Diagnosing Diabetic Retinopathy by segmenting Blood vessels, Optic disc and retinal abnormalities" *Journal of Medical engineering and Technology*, vol.44, no.6, pp. 299-316, July 2020.

[100] Li Xuechen, Shen Linlin, Shen Meixiao, TanFan and Qiu Connor S, "Deep learning based early stage diabetic retinopathy detection using optical coherence tomography," *Neurocomputing*, vol. 369, pp. 134-144, December 2019.

[101] Hui Wang, Guohui Yuan, Xuegong Zhao, Lingbing Peng, Zhuoran Wang, Yanmin He, Chao Qu and Zhenming Peng, "Hard exudate detection based on deep model learned information and multi-feature joint representation for diabetic retinopathy screening," *Computer Methods and Programs in Biomedicine*, vol. 191, pp. 1-16, July 2020.

[102] Sundararaj, Wilfred, Franklin, Samuelnadar and Edward Rajan, "Diagnosis of diabetic retinopathy by employing image processing techniquesto detect exudates in retinalimages," *IET image processing,* vol. 8, no.10, pp. 601-609. October 2014.

[103] A. Sopharak, M. N. Dailey, B. Uyyanonvara, S. Barman, T. Williamson, K. T. Nwe and Y. A. Moe, "Machine learning approach to automatic exudate detection in retinal images from diabetic patients," *Journal of Modern Optics*, vol. 57, no. 2, pp. 124–135, August 2010.

[104] S. S. Kar and S. P. Maity, "Automatic Detection of Retinal Lesions for Screening of Diabetic Retinopathy," *IEEE Transactions on Biomedical Engineering*, vol. 65, no. 3, pp. 608-618, March 2018.

[105] I. Usman and K. A. Almejalli, "Intelligent Automated Detection of Microaneurysms in Fundus Images Using Feature-Set Tuning," *IEEE Access*, vol. 8, pp. 65187-65196, April 2020.

[106] TV Roshini, Ranjith V Ravi, A Reema Mathew, Anoop Balakrishnan Kadan, and Perumal Sankar Subbian, "Automatic diagnosis of diabetic retinopathy with the aid of adaptive average filtering with optimized deep convolutional neural network," *International Journal of Imaging systems and technology*, vol. 1, pp. 1-21, April 2020.

[107] Turab Selçuk and Ahmet Alkan, "Detection of microaneurysms using ant colony algorithm in the early diagnosis of diabetic retinopathy," *Medical Hypotheses,* vol. 129, pp.1-14, August 2019.

[108] C. Sinthanayothin, J. Boyce, T. Williamson, H. Cook, E. Mensah, S. Lal and D. Usher, "Automated detection of diabetic retinopathy on digital fundus images," *Diabetic Medicine*, vol. 19, no. 2, pp. 105–112, March 2002.

[109] Fleming A.D., Philips S., Goatman K.A., Williams G.J., Olson J.A. and Sharp P.F., "Automated detection of exudates for diabetic retinopathy screening," *Physics in Medicine and Biology*, vol. 52, no. 24, pp. 7385–7396, December 2007.

[110] NikosTsiknakis, Dimitris Theodoropoulos, Georgios Manikis, Emmanouil Ktistakis, Ourania Boutsora, Alexa Berto, Fabio Scarpa, Alberto Scarpa, Dimitrios I. Fotiadis, Kostas Marias, "Deep learning for diabetic retinopathy detection and classification based on fundus images: A review", *Computers in Biology and Medicine,* vol.135, pp. 1-19, 2021

[111] Jafari M, Bayati Chaleshtari MH. Using dragonfly algorithm for optimization of orthotropic infinite plates with a quasi-triangular cut-out. Eur J Mech A: Solids. Vol. 66, pp. 1-14, May 2017.

[112] R. F. Mansour, "Evolutionary Computing Enriched Computer-Aided Diagnosis System for Diabetic Retinopathy: A Survey," *IEEE Reviews in Biomedical Engineering*, vol. 10, pp. 334-349, May 2017.

[113] K.C.Santosh, S Antani, D S Guru, and N Dey, Medical Imaging, Artificial Intelligence, Image Recognition, and Machine Learning Techniques, CRC, ISBN 978-036-71-3961-2, (2019) DOI: 10.1201/9780429029417

[114] K.C.Santosh, N Das, and Ghosh: Deep Learning Models for Medical Image, Elsevier Academic Press, ISBN. 9780128236505, 2020